Remediation by steam injection

Ph.D. Thesis, October 2003

Jacob Gudbjerg
Environment & Resources DTU
Technical University of Denmark

Preface

The present report "Remediation by steam injection" has been submitted as a part of the requirements for the Ph.D. degree at the Technical University of Denmark. The study has been performed at Environment & Resources DTU in the period April 2000 to July 2003, with Karsten Høgh Jensen and Torben Obel Sonnenborg as supervisors.

The report consists of a review followed by four journal papers where the first one has been published and the last three have been submitted for publication. Reinhard Schmidt performed the experimental work in the first paper and part of the numerical work was performed during my master's project. Oliver Trötschler and Arne Färber performed the 2-D experiments in the third paper.

The review will mainly focus on the issues I have worked with during my study and as such should not be regarded as a complete review of all the research that has been performed concerning steam injection.

In chronological order I would like to thank the following people. First of all, Kent Udell for starting my interest in steam injection. Since his very inspiring lecture at the Technical University of Denmark in the autumn of 1998 not a single day has passed where I have not thought about steam injection. Hopefully, that is going to change. I want to thank Reinhard Schmidt for letting me use his excellent data sets and for the good cooperation we had during the making of our paper. I am grateful to the people at the VEGAS-facility at the University of Stuttgart for letting me use their excellent experimental facilities and for the technical support they provided during my stay there. I also want to thank Gorm and Tom Heron, Thomas Hauerberg Larsen, Jarl Dall Jepsen, Torben Højbjerg Jørgensen and Hans Skou for keeping me in contact with real-life applications of steam injection. That has kept me focused on the important issues and prevented me from getting lost in unimportant details.

The following institutions provided the necessary funding for the study:

Danish Environmental Protection Agency, Programme for Development of Technology - Soil and Groundwater Contamination

Groundwater Research Center, DTU

Danish Energy Authority, Energy Research Programme.

Lyngby, October 2003

Jacob Gudbjerg

Abstract

Chemical spills have created a large number of contaminated sites where toxic compounds are present as nonaqueous phase liquids (NAPL). These sites have proved difficult to remediate and aggressive technologies are needed. Remediation by steam injection is such a technology and it may be the optimal technology at heavily contaminated sites. Steam injection involves the injection of steam into the subsurface and simultaneous recovery of fluids from extraction wells. The injected steam heats the soil and creates a steam zone that expands from the injection wells as more steam is injected. The physical-chemical properties of typical contaminants change with temperature and this makes them easier to extract. In particular the increase in vapor pressure is important. Additionally, two immiscible liquid phases will boil when the sum of their vapor pressures equals the surrounding pressure and this phenomenon proves very important for the contaminant mass transfer.

The objectives of this study have been to further our understanding of the dominant processes and mechanisms involved in steam injection through the use of numerical modeling, laboratory experiments and field-scale data. The focus has been on the following four issues that have been reported separately:

1. Removal of NAPLs from the unsaturated zone using steam: prevention of downward migration by injecting mixtures of steam and air

Steam injection for remediation of porous media contaminated by non-aqueous phase liquids has been shown to be a potentially efficient technology. There is, however, concern that the technique may lead to downward migration of separate phase contaminant. In this work a modification of the steam injection technology is presented where a mixture of steam and air was injected. In two-dimensional experiments with unsaturated porous medium contaminated with non-aqueous phase liquids it was demonstrated how injection of pure steam lead to severe downward migration. Similar experiments where steam and air were injected simultaneously resulted in practically no downward migration and still rapid cleanup was achieved. The processes responsible for the prevention of downward migration when injecting steam-air mixtures were analyzed using a non-isothermal multiphase flow and transport model. Hereby, three mechanisms were identified and it was demonstrated how the effectiveness of these mechanisms depended on the air to steam mixing ratio.

2. Remediation of NAPL below the water table by steam induced heat conduction

Previous experimental studies have shown that NAPL will be removed when it is contacted by steam. However, in full-scale operations steam may not contact the NAPL directly and this is the situation addressed in this study. A two-dimensional intermediate scale sand box experiment was performed where an organic contaminant was emplaced below the water table at the interface between a coarse and a fine sand layer. Steam was injected above the water table and after an initial heating period the contaminant was recovered at the outlet. The experiment was successfully modeled using the numerical code T2VOC and the dominant removal mechanism was identified to be heat conduction induced boiling of the separate phase contaminant. Subsequent numerical modeling showed that this mechanism was insensitive to the

porous medium properties and that it could be evaluated by considering only one-dimensional heat conduction.

3. On spurious water flow during numerical simulation of steam injection into water saturated soil

Numerical simulation of steam injection into a water saturated porous medium may be hindered by unphysical behavior causing the model to slow down. We show how spurious water flow may arise on the boundary between a steam zone and a saturated zone, giving rise to dramatic pressure drops. This is caused by the discretization of the temperature gradient coupled with the direct relation between pressure and temperature in the steam zone. The problem may be a severe limitation to numerical modeling. A solution is presented where the spurious water flow is blocked and this widely enhances the performance of the model. This new method is applied to a previously reported example exhibiting numerical problems. Furthermore, it is applied to the simulation of 2-D sand box experiments where LNAPL is remediated from a smearing zone by steam injection. These experiments would have been difficult to analyze numerically without the adjustment to prevent spurious flow. The simulation proves to be very sensitive to the type of relative permeability model. The LNAPL is removed by a combination of vaporization and flow. Based on the numerical results it is argued that it is necessary for the steam to contact the NAPL directly to achieve clean-up at field-scale.

4. Three-dimensional numerical modeling of steam override observed at a full-scale remediation of an unconfined aquifer

Steam injected below the water table tends to move upwards because of buoyancy. This limits the horizontal steam zone development, which determines the optimal spacing between injection wells. In this study, observations indicating steam override at a full-scale remediation of an unconfined aquifer are analyzed by numerical modeling using the code T2VOC. A simplified 3-D numerical model is set up, which qualitatively shows the same mechanisms as observed at the site. By means of the model it is found that it will be possible to achieve a larger horizontal extent of the steam zone in a layered geology compared to the homogeneous case. In the homogeneous case the steam injection rate increases dramatically when the injection pressure is increased, which is necessary to achieve a larger horizontal development. The development of the steam zone under unconfined conditions is found to be a complex function of the geologic layering, the ground water table at steady-state extraction and the injection/extraction system. Because of this complexity it will be difficult to predict steam behavior without 3-D numerical modeling.

Resume

Spild af kemikalier har skabt et stort antal forurenede grunde, hvor toksiske forbindelser er til stede som fri fase. Det har vist sig vanskeligt at oprense disse grunde, og det er nødvendigt at benytte aggressive oprensningsteknologier. Oprensning ved dampinjektion er en sådan teknologi, og det kan være den optimale teknologi ved kraftigt forurenede grunde. Ved dampinjektion injiceres damp i undergrunden samtidig med, at der oppumpes i ekstraktionsbrønde. Den injicerede damp opvarmer jorden og skaber en dampzone, som ekspanderer væk fra injektionsbrønden, efterhånden som mere damp injiceres. De fysisk-kemiske egenskaber for typiske forureningsstoffer ændrer sig med temperaturen, og det gør dem lettere at ekstrahere. Specielt er stigningen i damptryk meget vigtig. Ydermere vil to ikke-blandbare væsker koge, når summen af deres damptryk svarer til omgivelsernes tryk, og dette fænomen vises sig at være meget vigtigt for transporten af forurening.

Formålet med dette projekt har været at øge forståelsen af de dominerende processer og mekanismer i dampinjektion gennem numerisk modellering, laboratorieforsøg og data fra en oprensning på felt-skala. Fokus har været på de følgende fire emner som er blevet afrapporteret særskilt:

1. Fjernelse af fri fase fra den umættede zone ved hjælp af damp: forhindring af nedadrettet transport ved injektion af damp-luft blandinger

Dampinjektion til oprensning af porøse medier forurenet med ikke-vandig fri fase har vist sig at være en potentiel effektiv teknologi. Der er dog bekymring for, at teknikken kan føre til nedadrettet transport af forurening på fri fase. I dette projekt præsenteres en modifikation af teknikken, hvor en blanding af damp og luft blev injiceret. I to-dimensionale eksperimenter med umættet porøst medium forurenet med fri fase blev det demonstreret, hvordan injektion af ren damp førte til nedadrettet transport. Tilsvarende eksperimenter, hvor damp og luft blev injiceret samtidig viste stort set ingen nedadrettet transport, og stadigvæk blev hurtig oprensning opnået. De dominerende processer for forhindringen af nedadrettet transport ved damp-luft injektion blev analyseret ved hjælp af en ikke-isoterm flerfasestrømning og transport model. Herved blev tre mekanismer identificeret, og det blev vist hvordan effektiviteten af disse mekanismer afhang af damp-luft blandingsforholdet.

2. Oprensning af fri fase under grundvandsspejlet ved damp-induceret varmeledning

Tidligere eksperimentelle studier har vist, at fri fase bliver fjernet, når den kommer i kontakt med damp. I oprensninger på fuld skala kan damp dog ikke altid komme i direkte kontakt med den fri fase, og den situation er emnet for dette projekt. Et to-dimensionalt forsøg i en kasse med sand blev udført, hvor en organisk forurening blev placeret under grundvandsspejlet på grænsefladen mellem et groft og et fint sandlag. Damp blev injiceret over grundvandsspejlet og efter en initial opvarmningsperiode blev forureningen ekstraheret ved udløbet. Forsøget blev simuleret tilfredsstillende ved hjælp af den numeriske model T2VOC og den dominerende fjernelsesmekanisme blev identificeret som kogning af den frie fase forårsaget af varmeledning. Efterfølgende numerisk modellering viste, at denne

mekanisme ikke var sensitiv over for det porøse mediums egenskaber, og at den kunne evalueres ved kun at betragte en-dimensional varmeledning.

3. Om falsk vandstrømning ved numerisk simulering af dampinjektion i vandmættet jord

Numerisk modellering af dampinjektion i vandmættet porøst medium kan blive hæmmet af ufysisk opførsel, som får modellen til at køre langsomt. Vi viser, hvordan falsk vandstrømning kan opstå på grænsen mellem en dampzone og en mættet zone, hvilket giver anledning til dramatiske trykfald. Det er forårsaget af diskretiseringen af temperaturgradienten sammenholdt med den direkte relation mellem tryk og temperatur i en dampzone. Problemet kan være en alvorlig begrænsning for numerisk modellering. En løsning bliver præsenteret, hvor den uægte vandstrømning blokeres, hvilket øger modellens ydelse betragteligt. Denne nye metode bliver anvendt på et tidligere afrapporteret eksempel, der udviste numeriske problemer. Ydermere bliver den anvendt til at simulere to-dimensionale eksperimenter, hvor fri fase blev oprenset ved dampinjektion. Disse eksperimenter ville have været svære at analysere numerisk uden justeringen til at forhindre falsk vandstrømning. Simuleringen viser sig at være meget sensitiv over for typen af relativ permeabilitetsmodel. Den frie fase blev fjernet ved en kombination af fordampning og strømning. Baseret på de numeriske resultater argumenteres der for, at det er nødvendigt med direkte kontakt mellem damp og den frie fase for at kunne oprense på fuld skala.

4. Tre-dimensional numerisk modellering af dampoverløb observeret ved en fuld-skala oprensning af et frit grundvandsmagasin.

Damp injiceret under grundvandsspejlet vil bevæge sig opad på grund af opdrift. Det begrænser den horisontale udbredelse af dampzone, som bestemmer den optimale afstand mellem injektionsboringerne. I dette projekt bliver observationer, der indikerer dampoverløb ved en fuld-skala oprensning af et frit grundvandsmagasin analyseret ved numerisk modellering med modellen T2VOC. En forsimplet tre-dimensional model bliver opsat, som kvalitativt viser de mekanismer, der blev observeret på grunden. Ved hjælp af modellen findes det, at det vil muligt at opnå en større horisontal udbredelse af dampzonen i en lagdelt geologi sammenlignet med det homogene tilfælde. I det homogene tilfælde stiger dampinjektionsraten dramatisk, når injektionstrykket øges, hvilket er nødvendigt for at opnå større horisontal udbredelse. Udviklingen af dampzonen i et frit magasin er en kompleks funktion af den geologiske lagdeling, grundvandsspejlet ved oppumpning og injektions/ekstraktionssystemet. På grund af den kompleksitet vil det være vanskeligt at forudse dampens opførsel uden tre-dimensional numerisk modellering.

Table of contents

1. Introduction

Industrial activities during the last four to five decades have created a large number of sites where chemical spills have contaminated the subsurface. It is estimated that 14,000 sites in Denmark are contaminated due to spills (Danish EPA 1999). Contamination is basically found where chemicals have been used in large amounts and typically below old gas stations, dry cleaners, military bases, gas works etc. Typical contaminants are chlorinated solvents, gasoline/fuels, coal tar and creosote. These contaminants are almost immiscible with water and will often be present as nonaqueous phase liquids (NAPL).

Mercer and Cohen (1990) provide the following description of NAPL transport in subsurface. When spilled into the unsaturated zone the NAPL migrates downward due to gravity. The NAPL may spread horizontally due to capillary forces and heterogeneities and furthermore some of the NAPL may be immobilized as residual. If the spill is large enough the NAPL eventually reaches the saturated zone where it floats in the top of the capillary fringe if it is lighter than water (LNAPL) and migrates further downwards if it is denser than water (DNAPL). Low permeable layers in the saturated zone may arrest the downward migration and divert the flow horizontally or pools may form in depressions. Entrapment will also occur in the saturated zone and usually at a higher saturation than in the unsaturated zone. LNAPL may also become entrapped in the saturated zone due to water table fluctuations during which an LNAPL smearing zone is formed. The transport of NAPL is influenced by heterogeneities at all scales and therefore extremely difficult to predict and furthermore the heterogeneous distribution makes it difficult to detect and quantify a given spill.

The NAPL in the subsurface may evaporate into the gas phase and spread in the unsaturated zone and dissolved components will spread with the water phase. Even though the solubility is low it is much higher than common drinking water standards. This means that even a small spill can potentially contaminate large groundwater resources and it may take very long time before the NAPL is completely dissolved. In addition to the contamination of the groundwater, chemicals in the gas phase may migrate into housing. Because of the risk of human exposure to these chemicals combined with their toxicity it may be necessary to remediate a contaminated site. This is most often done by excavating the contaminated soil and treating it off site. However, at some sites the volume of contaminated soil might be too large or there might be buildings that make it impossible to excavate. Therefore remediation has to take place in situ without disturbing the soil. Traditional in situ remediation technologies are pump-and-treat in saturated zone and soil vapor extraction in the unsaturated zone. Unfortunately, these technologies have shown to be very inefficient at NAPL sites. The mass transfer rate from the heterogeneously distributed NAPL becomes diffusion-limited and large volumes need to be flushed to achieve clean-up. Furthermore, Sale and McWhorther (2001) showed that near-complete removal of NAPL is necessary to reduce the short-term groundwater concentration. At heavily contaminated sites the clean-up time may be in the order of decades with these technologies.

Consequently, there is a need for more aggressive technologies that can address these sites effectively. Innovative technologies have been proposed such as surfactant flooding, alcohol flooding, chemical oxidation and air sparging; however, these

technologies may also be limited by diffusion and the efficiency can be strongly influenced by heterogeneities. Thermal technologies provide a means to overcome these limitations and may in some case be able to achieve clean-up goals rapidly. With thermal technologies the contaminated soil is heated and this strongly affects the physical-chemical properties of the contaminants in most cases to the benefit of the recovery process. This is the fundamental basis of thermal technologies and the most important temperature effects will be briefly described here.

1.1. Temperature effect on physical-chemical properties

The vapor pressure increases dramatically with temperature (Fig. 1) and this is the most important reason why thermal technologies are effective. As the vapor pressure increases the contaminant will vaporize into the gas phase, where it is much easier to remove than in the water phase or as a NAPL.

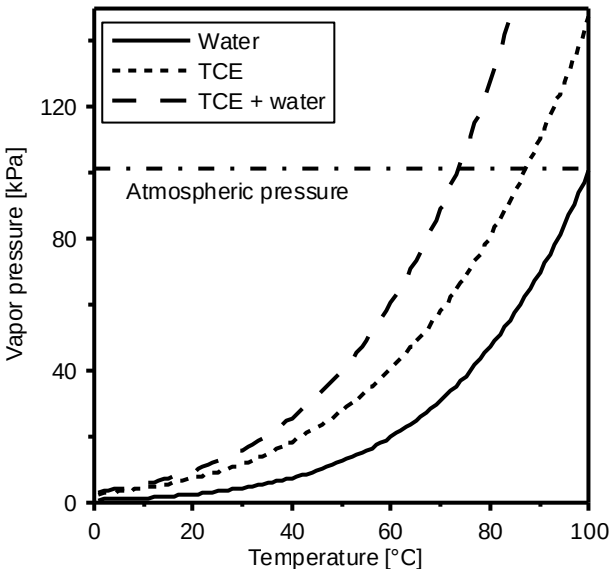

Fig. 1. Vapor pressure as a function of temperature for water, TCE and the sum (Reid et al. 1983).

At 100 °C the vapor pressure of water is equal to the atmospheric pressure, which is marked by the horizontal line in Fig. 1. This is by definition the normal boiling point. When two immiscible liquids are present their vapor pressures will be independent and the liquids will boil when their summed vapor pressure equals the atmospheric pressure (Atkins, 1996). Thus, the boiling point for two immiscible liquids will be lower than both their individual boiling points. This intuitively surprising result will show to be extremely important for the mass transfer from the NAPL phase.

The viscosity decreases with temperature making NAPL flow more rapid; however, remediation rarely relies on NAPL flow alone and the viscosity reduction is therefore of little importance. Flow of NAPL will always leave a residual phase behind and a reduction in ground water concentration will only be achieved at the very long term.

The density of NAPL and water decreases slightly with temperature but not enough to significantly affect the flow processes.

The solubility of contaminants generally increases with temperature. Heron et al. (1998) found a 15 % increase in the solubility of TCE from 7 °C to 71 °C. This, of course, makes it easier to extract contaminant in the water phase; however, removal in the water phase will still be extremely slow.

Sorption decreases with increasing temperature (Sleep and McClure 2001b) and where the removal is limited by sorption this may be significant. Still, only little contaminant mass can be sorbed compared to the mass present as NAPL. Thus, the increased mass removal because of a decrease in sorption is not expected to justify a full-scale steam thermal operation.

Diffusion increases with temperature but still diffusion will not affect the mass removal significantly.

Generally speaking the temperature effect on the physical-chemical properties make the contaminants more mobile and thereby easier to remove; however, it is the effect on the vapor pressure that justifies the use of thermal technologies for remediation.

1.2. Steam injection

Steam injection is the most commonly used thermal remediation technology. It involves the injection of steam into subsurface combined with extraction in the water, gas and NAPL phases. As previously stated it is the increase in vapor pressure that is important in thermal technologies and therefore contaminants will mainly be extracted in the gas phase. Extraction of the water phase is mostly performed to avoid spreading of contaminant. When steam contacts the soil it condenses and heats the soil. A zone with steam temperature is formed, which expands as more steam is injected. This process and the actual contaminant removal mechanisms will be addressed later.

Steam injection was originally developed as an enhanced oil recovery technology where it was the reduction in viscosity that was most important. Oil in reservoirs has a much lower viscosity than typical contaminants and often the vapor pressure is too low to be considered. Therefore the scope has been somewhat different and in this particular study steam injection as an oil recovery technique will not be addressed or very much referenced. That being said, it is obvious that much of the pioneering work on steam injection as a remediation technology was based on the experiences from steam injection as an enhanced oil recovery technique.

The technology is expensive and difficult to implement and should only be used in highly contaminated source zones where rapid remediation is required.

2. Objectives

The overall objectives of this study have been to further our understanding of the dominant mechanisms involved in remediation by steam injection. An increased understanding will help us to apply the technology in the most optimal way. The approach has been to use numerical modeling combined with laboratory experiments and data from field-scale applications. This has resulted in four journal papers, which addresses different aspects as reflected by their titles:

1) Removal of NAPLs from the unsaturated zone using steam: prevention of downward migration by injecting mixtures of steam and air

2) Remediation of NAPL below the water table by steam induced heat conduction

3) On spurious water flow during numerical simulation of steam injection into water saturated soil

4) Three-dimensional numerical modeling of steam override observed at a full-scale remediation of an unconfined aquifer

The first part of the thesis presents a brief review of the current status of steam injection as a remediation technology. This is not a comprehensive review of all the work that has been done within this field but rather a review of the current understanding of the dominant processes and mechanisms. Thus, only key studies that illustrate these processes and mechanisms are referenced. A second objective of this document is to provide a more thorough description of the numerical model, as this has been the most essential tool in this study. In that description some of the preliminary considerations that lead to the approaches taken in the papers are described.

3. Numerical modeling

The numerical code used in this study T2VOC (Falta et al., 1995) is a member of the TOUGH family of codes developed to simulate multidimensional, non-isothermal, multiphase flow and transport in porous media (Pruess, 1987; Pruess, 1991).

3.1. Governing equations

This section briefly describes the governing equations of the T2VOC code. The description is largely based on the T2VOC User's Guide (Falta et al., 1995). The model considers gas, water and NAPL as separate phases. These phases consist of the three components *air, water* and *chemical*. As an example a gas phase may be a mixture of *air, water* and *chemical* or in the case of pure steam it would be only *water*. Note the difference between *water* as a component and water as a phase. In non-isothermal mode *heat* is considered a fourth component. For each of the components a balance equation is formulated:

$$\frac{d}{dt}\int_{V_n} M^k \, dV_n = \int_{A_n} F^k \cdot n \, dA_n + \int_{V_n} q^k \, dV_n \qquad \textbf{(1)}$$

where M is the mass or energy of component κ (*air, water, chemical* or *heat*) per unit porous medium volume V_n, F^κ is the flux of κ through the surface area A_n of V_n and q^κ is the mass or heat generation per unit volume.

The mass/energy term is calculated as a sum of the contributions from the separate phases:

$$M^k = f \sum_b S_b \, r_b \, X_b^k \qquad \textbf{(2)}$$

where ϕ is porosity, S is saturation and ρ is density of phase β and X is the mass fraction of component κ in phase β. For the component *heat* the mass fraction is replaced by the specific internal energy and the specific internal energy of the soil grains is added. For the *chemical* an additional term may be added to include sorption.

The flux term is calculated as the sum of advection/convection and diffusion/conduction where the former is calculated by a multiphase extension of Darcy's law:

$$F^k_{advection/convection} = \sum_b - X_b^k \; k \frac{k_{rb} \, r_b}{m_b} \left(\nabla P_b - r_b \, g \right) \qquad \textbf{(3)}$$

where k is the intrinsic permeability, $k_{r\beta}$ is the relative permeability to phase β, ρ is the density, μ is the viscosity, P is the pressure and g is the gravitational acceleration vector. In the case of heat flux the mass fraction is once again replaced by the specific internal energy.

Mass flux by diffusion is included in the gas and water phase through Fick's law:

$$F^k_{diffusion} = \sum_b - f S_b \, D_b^k \, r_b \nabla X_b^k \qquad \textbf{(4)}$$

where D_b^k is the molecular diffusion coefficient of κ in the β phase.

Diffusion in the water phase is actually not described in the T2VOC User's manual and has not been included in the presented simulations. However, it is now part of the new release of T2VOC.

Heat flux by conduction is calculated from Fourier's law:

$$F_{conduction} = -K\nabla T \qquad \textbf{(5)}$$

where K is the overall heat conductivity coefficient of the porous medium.

The mass/ heat generation term q in equation (**1**) may represent various forms of sinks and sources such as fluid injection or withdrawal.

The model assumes equilibrium among the phases within each gridblock and the component distribution is calculated from functions relating vapor pressure and solubility to temperature. Water dissolved in the NAPL phase is not accounted for.

The set of equations are discretized by integral finite difference technique, which is illustrated in Fig. 2.

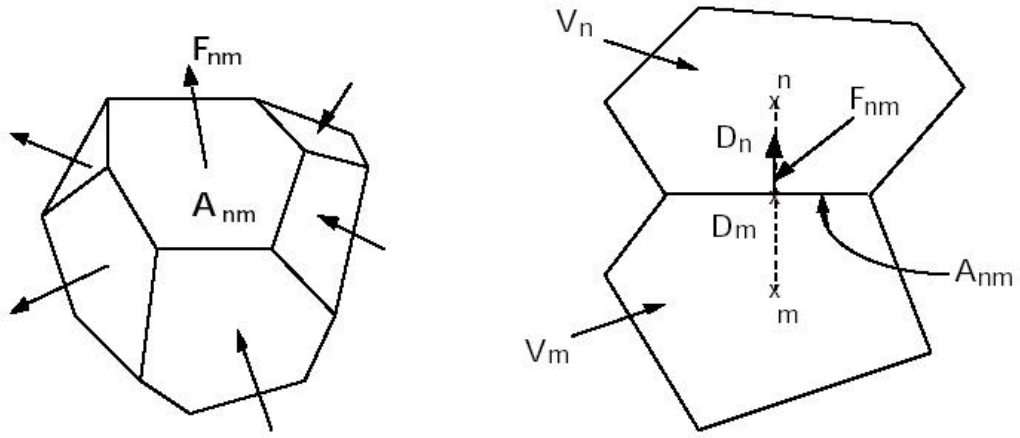

Fig. 2. Integral finite difference discretization. From Falta et al. (1995).

F_{nm} is the flux from gridblock m with the volume V_m across the interface A_{nm} into gridblock n with the volume V_n. The flux is calculated from the finite differences between for instance phase pressures in the gridblocks and the distance $D_m + D_n$. Thus, a gridblock is defined by a volume and the connections to other gridblocks. The connections are again defined by a contact area and a distance from the center to the contact area. In this type of discretization the gridblocks can have any size and any shape and do not have to be related to any physical position. Generally, upstream weighting is used except that the heat conductivity coefficient is harmonically weighted and the density in the calculation of the gravity contribution is arithmetically averaged. Other weighting schemes may be applied and for instance Gudbjerg et al. (2003a) changed the upstream weighting factor for the density of the water phase to $\rho_{ij} = 0.98\rho_i + 0.02\rho_j$, where i is the upstream gridblock This greatly improved the stability of the model when a NAPL phase had just disappeared from a gridblock.

The non-linear algebraic equations are solved by Newton-Raphson iteration and the linear equations arising from this are solved by iterative preconditioned conjugate gradient techniques.

The four mass balance equations are solved for four independent primary variables. Since the three phases may not be present in all gridblocks at all times it is necessary to switch between different sets of primary variables for each phase

combination. The model assumes that the water phase is always present and consequently there are four possible phase combinations as listed in Table 1.

Table 1. Phase combinations and primary variables.

Phases	Primary variables			
Water	P_{water}	$X_{air\text{-}water}$	$\chi_{chemical\text{-}water}$	T
Water, NAPL	P_{NAPL}	S_{water}	$X_{air\text{-}water}$	T
Water, gas	P_{gas}	S_{water}	$\chi_{chemical\text{-}gas}$	T
Water, NAPL, gas	P_{gas}	S_{water}	S_{gas}	T

where $X_{air\text{-}water}$ is the mass fraction of air in the water phase and $\chi_{chemical\text{-}water}$ is the mole fraction of chemical in the water phase.

In every iteration it is checked whether a phase appears or disappears in a gridblock and if so a switch of primary variables is made corresponding to the new phase combination. From these four primary variables a set of secondary variables (density, viscosity, enthalpy etc.) can be calculated that fully describe the thermodynamic properties of the system. The relative permeability/capillary pressure-saturation relationships belong to this set of secondary variables. These relationships are somewhat special because they are soil specific and very fundamental in multiphase flow. Additionally there is a lot more uncertainty concerning these relations compared to other properties such as density and viscosity. Therefore they will be discussed here and again with emphasis on the model applications in the journal papers.

3.2. Capillary pressure

The individual phase pressures are related through the capillary pressures in the following way:

$$P_{gas} = P_{NAPL} + P_{c,gas-NAPL} = P_{aqueous} + P_{c,gas-aqueous} \qquad \textbf{(6)}$$

where P_c is the capillary pressure between two phases. Water is normally the wetting phase, NAPL the intermediate wetting phase and gas the non-wetting phase. This makes the capillary pressures positive; however, this is not a prerequisite in the model.

In soil sciences the most commonly used parametric models to describe the capillary pressure-saturation relationship are the van Genuchten (1980) and the Brooks and Corey (1966) models. These models were originally formulated for two-phase systems, however, following the scaling approach of Lenhard and Parker (1987b) they can be extended to describe three-phase systems:

van Genuchten (VG):

$$P_{c,gas-NAPL} = \frac{1}{b_{gn}a}\left(\overline{S}_l^{\frac{-1}{m}} - 1\right)^{\frac{1}{n}}, \quad P_{c,NAPL-water} = \frac{1}{b_{nw}a}\left(\overline{S}_w^{\frac{-1}{m}} - 1\right)^{\frac{1}{n}}, \quad m = 1 - \frac{1}{n} \qquad \textbf{(7)}$$

Brooks and Corey (BC):

$$P_{c,gas-NAPL} = \frac{P_e}{b_{gn}}\frac{1}{\overline{S}_l^{\frac{1}{l}}}, \quad P_{c,NAPl-water} = \frac{P_e}{b_{nw}}\frac{1}{\overline{S}_w^{\frac{1}{l}}} \qquad \textbf{(8)}$$

where α and n in the VG-model and P_e and λ in the BC-model can be considered as fitting parameters. Yet, P_e has a more physical meaning as it represents the gas entry pressure in a water saturated medium. The effective saturations are defined as follows:

$$\bar{S}_w = \frac{S_w - S_{wr}}{1 - S_{wr}}, \quad \bar{S}_l = \frac{S_w + S_n - S_{wr}}{1 - S_{wr}} \qquad \textbf{(9)}$$

The scaling parameters are calculated from the interfacial tension:

$$b_{gn} = \frac{s_{gas-water}}{s_{gas-NAPL}}, \quad b_{nw} = \frac{s_{gas-water}}{s_{NAPL-water}} \qquad \textbf{(10)}$$

In a gas-water system the capillary pressure is calculated from:

$$P_{c,gas-water} = P_{c,gas-NAPL} + P_{c,NAPL-water} \qquad \textbf{(11)}$$

For this to correctly reduce to the two-phase capillary pressure it is required that:

$$b_{nw} = \frac{1}{1 - \frac{1}{b_{gn}}} \qquad \textbf{(12)}$$

which is the same as:

$$s_{gas-water} = s_{gas-NAPL} + s_{NAPL-water} \qquad \textbf{(13)}$$

In these models the capillary pressure in a given soil type is only a function of saturation and the fluid-dependent scaling parameter. The scaling parameter is a constant based on the surface tensions; however, it is well known that surface tension may vary with the concentration of dissolved components and temperature. Thus, it would be more correct to include a variable scaling parameter, which is equivalent to saying that the capillary pressure is also a function of temperature and composition of the phase instead of just saturation. However, as will be illustrated in the next section the temperature dependence of the capillary pressure is uncertain and therefore not straightforward to include in simulations.

3.2.1. Temperature dependence of capillary pressure

The capillary pressure is known to decrease with increasing temperature as illustrated in Fig. 3 showing capillary pressure curves measured at two temperatures.

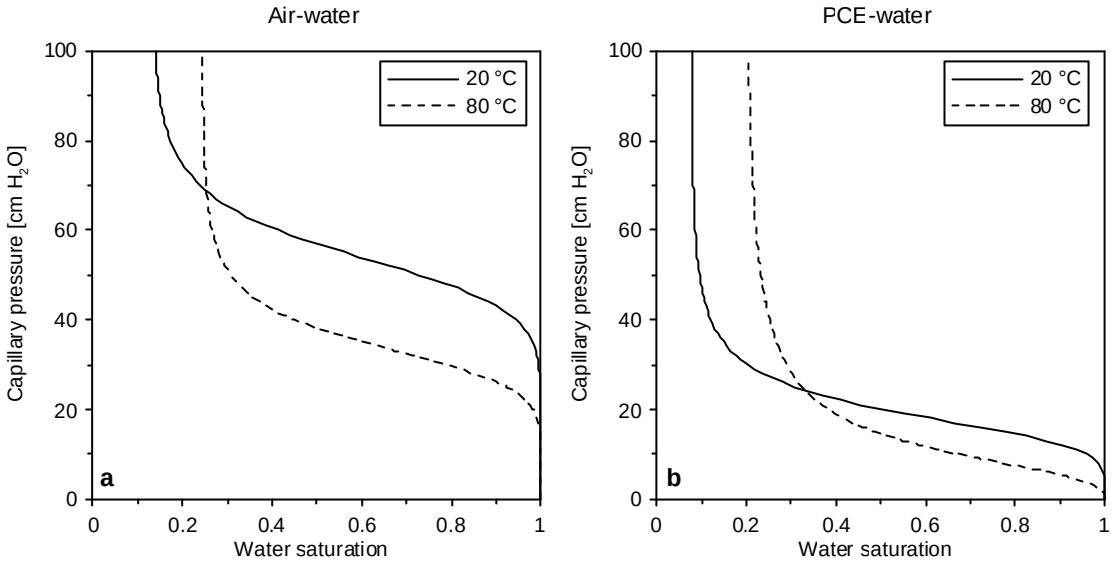

Fig. 3. Primary drainage curves for air-water (a) and PCE-water (b) measured at two temperatures. Fitted data from She and Sleep (1998).

Both for the air-water and the PCE-water system the capillary pressure for the same effective saturation is lower at higher temperature. It appears that the residual water content is also influenced by temperature but from the available experimental data it is difficult to deduce a general trend. It should also be noted that the residual water content is inherently difficult to measure and may be very much affected by small-scale heterogeneity in the sand packing (Mortensen et al., 2001).

The capillary pressure is not a physical-chemical property of a fluid but it is a lumped property describing the interaction between two fluids and possibly a solid. Consequently, it is relevant to describe the temperature dependence of the capillary pressure by considering the temperature dependence of the underlying properties. In a circular tube the capillary pressure between two fluids can be described by the following equation (Bear 1988):

$$P_c = \frac{2s\cos q}{r} \qquad \textbf{(14)}$$

where σ is the interfacial tension between the two fluids, θ is the contact angle of the fluid-fluid interface with the solid surface and r is radius of the tube. From Youngs equation the definition of the contact angle is (Dullien 1992):

$$\cos q = \frac{s_{sn} - s_{ws}}{s_{wn}} \qquad \textbf{(15)}$$

where subscripts s, n and w refer to solid, non-wetting and wetting respectively. Thus, the contact angle is a relative measure of the attractive forces between and within the three phases. When considering capillary pressure in soil it is often assumed that the water phase perfectly wets the solid phase. This means that there will be no three-phase points and the cosine of the contact angle will be unity. Using this assumption Philip and de Vries (1957) provided the first equation relating the capillary pressure to temperature:

$$\left(\frac{\partial P_c(S_w)}{\partial T}\right)_{S_w} = \frac{P_c(S_w)}{s_{wn}}\frac{\partial s_{wn}}{\partial T} \qquad \textbf{(16)}$$

In this equation the capillary pressure scales with the change in interfacial tension in the same way scaling between different fluid pairs have been performed. However, subsequent experimental work has shown consistently that the change in capillary pressure with temperature is larger than what would be expected from the interfacial tension alone (e.g. Davis (1994); She and Sleep (1998)). According to Grant (2003) the typical relative decrease in capillary pressure at 298 K is about five times the relative decrease in interfacial tension. This made Grant and Salehzadeh (1996) include the temperature dependence of the contact angle and derived the following equation:

$$\left(\frac{\partial P_c(S_w)}{\partial T}\right)_{S_w} = \frac{P_c(S_w)}{s_{wn}}\frac{\partial s_{wn}}{\partial T} + \frac{P_c(S_w)}{\cos q}\frac{\partial \cos q}{\partial T} \qquad \textbf{(17)}$$

By further assuming that the dependence of the interfacial tension and the contact angle with temperature could be described linearly the following relation was obtained:

$$P_{cf} = P_{cr}\left(\frac{b + T_f}{b + T_r}\right) \qquad \textbf{(18)}$$

where P_{cf} and P_{cr} are the capillary pressure at temperature T_f and T_r respectively and β is a constant describing the lumped temperature dependence of the interfacial tension and contact angle. She and Sleep (1998) successfully fitted this equation to air-water and PCE-water capillary pressure curves measured at 20°, 40°, 60° and 80 °C. However, they concluded that the fitted value of β implied unrealistic changes in the contact angle. It also appears contradictory that the entire drainage curve should have a relation to the contact angle, which by definition is a three-phase point. As long as water wets the soil grains there is no contact angle. It could be argued that a contact angle exists at large capillary pressures when water is only present in pendular rings but in the beginning of the drainage process it does not seem appropriate to relate the capillary pressure to the contact angle. For imbibition curves it would seem more relevant to include the contact angle.

Liu and Dane (1993) suggested that the total water content should be divided into isolated water and continuous water where the latter controlled the capillary pressure. The amount of isolated water would be temperature dependent, which would lead to a larger temperature effect on the capillary pressure curve. The argument was based on measurements showing a decrease in residual water content with increasing temperature. However, this theory can only explain increased temperature effects at low saturations and the available experimental data show temperature effects over the entire saturation span. Furthermore, a decrease in residual water with higher temperatures could not be confirmed by the results of She and Sleep (1998) or Davis (1994).

Other researchers, as referenced in Liu and Dane (1998), have referred the temperature effect to the presence of entrapped air. However, no air is entrapped on the primary drainage curve that shows the largest temperature effect in She and Sleep (1998).

Thus, at present there is no fulfilling explanation to what exactly causes the observed temperature effect on the capillary pressure. Consequently it is not feasible to include this effect in simulations unless direct measurements are available for the actual fluid pair and porous medium. Additionally, no information has been found on

the temperature effect on three-phase capillary pressure curves. Therefore the temperature effect on the capillary pressure has not been accounted for in the simulations performed in the journal papers.

3.3. Relative permeability

In soil science the two most commonly used relative permeability models are that of Burdine (1953):

$$k_{rw}(\overline{S}_w) = \overline{S}_w^2 \frac{\int_0^{\overline{S}_w} \frac{1}{P_c^2(x)} dx}{\int_0^1 \frac{1}{P_c^2(x)} dx} \quad \textbf{(19)}$$

and that of Mualem (1976):

$$k_{rw}(\overline{S}_w) = \overline{S}_w^{½} \left(\frac{\int_0^{\overline{S}_w} \frac{1}{P_c(x)} dx}{\int_0^1 \frac{1}{P_c(x)} dx} \right)^2 \quad \textbf{(20)}$$

These models were derived through theoretical considerations and calibrated to experimental data. When combining these equations with the parametric BC and VG models for the capillary pressure-saturation relationship closed form expressions can be derived, which relates the relative permeability directly to saturation. Parker et al. (1987) extended the two-phase relations to three phases resulting in the following set of equations (See White and Oostrom 1996 for an overview):

VG-Mualem:

$$k_{rw} = \overline{S}_w^{½} \cdot \left(1 - \left(1 - \overline{S}_w^{\frac{1}{m}}\right)^m\right)^2, \; k_{rn} = \overline{S}_n^{½} \left(\left(1 - \overline{S}_w^{\frac{1}{m}}\right)^m - \left(1 - \overline{S}_l^{\frac{1}{m}}\right)^m \right)^2, \; k_{rg} = \overline{S}_g^{½} \cdot \left(1 - \overline{S}_l^{\frac{1}{m}}\right)^{2m} \quad \textbf{(21)}$$

VG-Burdine:

$$k_{rw} = \overline{S}_w^2 \cdot \left(1 - \left(1 - \overline{S}_w^{\frac{1}{m}}\right)^m\right), \quad k_{rn} = \overline{S}_n^2 \left(\left(1 - \overline{S}_w^{\frac{1}{m}}\right)^m - \left(1 - \overline{S}_l^{\frac{1}{m}}\right)^m \right), \quad k_{rg} = \overline{S}_g^2 \cdot \left(1 - \overline{S}_l^{\frac{1}{m}}\right)^m \quad \textbf{(22)}$$

BC-Mualem:

$$k_{rw} = \overline{S}_w^{\frac{4+5\lambda}{2\lambda}}, \quad k_{rn} = \overline{S}_n^{½} \left(\overline{S}_l^{\frac{1+\lambda}{\lambda}} - \overline{S}_w^{\frac{1+\lambda}{\lambda}} \right)^2, \quad k_{rg} = \overline{S}_g^{½} \left(1 - \overline{S}_l^{\frac{1+\lambda}{\lambda}}\right)^2 \quad \textbf{(23)}$$

BC-Burdine:

$$k_{rw} = \overline{S}_w^{\frac{2+3\lambda}{\lambda}}, \quad k_{rn} = \overline{S}_n^2 \left(\overline{S}_l^{\frac{2+\lambda}{\lambda}} - \overline{S}_w^{\frac{2+\lambda}{\lambda}} \right), \quad k_{rg} = \overline{S}_g^2 \left(1 - \overline{S}_l^{\frac{2+\lambda}{\lambda}}\right) \quad \textbf{(24)}$$

where the effective phase saturation are calculated from:

$$\overline{S}_w = \frac{S_w - S_{wr}}{1 - S_{wr}}, \quad \overline{S}_g = \frac{S_g}{1 - S_{wr}}, \quad \overline{S}_n = \frac{S_n}{1 - S_{wr}}, \quad \overline{S}_l = \frac{S_o + S_w - S_{wr}}{1 - S_{wr}} \quad \textbf{(25)}$$

In Fig. 4 the two models are compared for a two-phase system calculated from the BC-formulation with $\lambda = 1.3$.

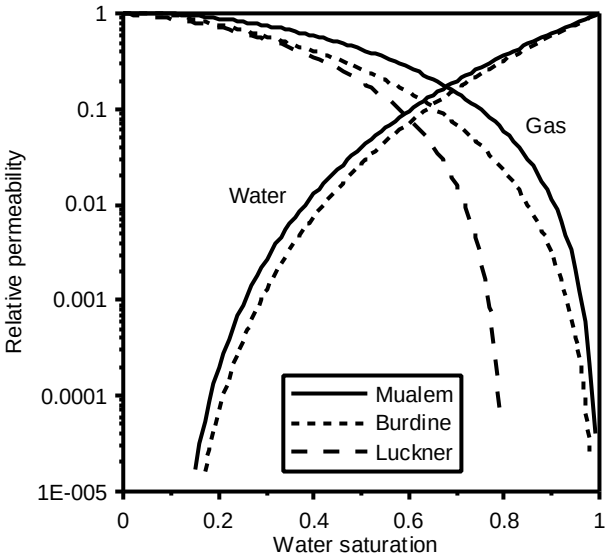

Fig. 4. Relative permeability-saturation with different models.

The Burdine model predicts a lower relative permeability than the Mualem model especially for the non-wetting phase. Also in a three-phase system will the Burdine model give lower relative permeability (Oostrom and Lenhard 1998). As pointed out by Gudbjerg et al. (2003b) this difference will significantly influence the simulated pressure during constant rate steam injection in a water-saturated medium. For two-phase systems Luckner et al. (1987) extended the models by introducing residual non-wetting phase saturation in the calculation of the effective saturation. This approach was validated by Dury et al. (1999) for the air permeability in air-water systems. Even on the main drainage path it was necessary to include residual non-wetting phase saturation, so this is not a hysteresis phenomenon. It also seems logical that the non-wetting phase needs to be at a certain saturation to be able to flow. Furthermore, it has been shown that drainage of a NAPL in an unsaturated zone may cease at a saturation larger than zero contrarily to the prediction of the relative permeability models (Hofstee et al. 1997). This was the case in Schmidt et al. (2002) where it was necessary to include a residual NAPL saturation in the relative permeability model. Also in this case the non-wetting phase residual saturation is not a result of hysteresis as it occurred on the main drainage path.

This reveals that there is a rather large uncertainty regarding which relative permeability model is most appropriate. Therefore different approaches have been taken in this thesis depending on which features were in focus.

In the soil science literature no information has been found on the temperature effect on the relative permeability. In the petroleum literature some studies have been made but the results are somewhat inconclusive. Also since in theory the relative permeability only depends on the porous medium and not on the fluids one would not expect a temperature dependency.

3.4. Hysteresis

Parker and Lenhard (1987) and Lenhard and Parker (1987a) presented rather comprehensive capillary pressure/relative permeability models that describe hysteresis. These models predict history-dependent effective saturations and interpolate between main drainage and imbibition capillary pressure curves. They introduce a series of residual saturations that need to be determined experimentally. However, it would not be straightforward to incorporate these hysteretic functions in T2VOC as it would require more primary variable switches. Furthermore, neither of the mechanisms causing residual non-wetting phase saturation described above would be accounted for by these models. Instead a simpler approach was used in Gudbjerg et al. (2003b) where it was necessary to account for hysteresis. Non-wetting phase residual saturation was not introduced in the capillary pressure model but only in the relative permeability model following the approach of Luckner et al. (1987). When an imbibition capillary pressure curve is determined experimentally it appears that a residual non-wetting phase saturation should be included; however, this is because the capillary pressure is measured between the water phase and the atmospheric pressure. In the model the gas phase pressure will be the pressure within the entrapped gas bubbles. Even at maximum water saturation on the imbibition path there will be a capillary pressure and the gas phase pressure will become higher than atmospheric. Thus, there is a difference between the sample scale capillary pressure curve that can be measured and the small-scale capillary pressure curve used in the model. This approach ensures that the correct gas phase pressure is used when calculating vaporization and re-entry of gas in a saturated sample.

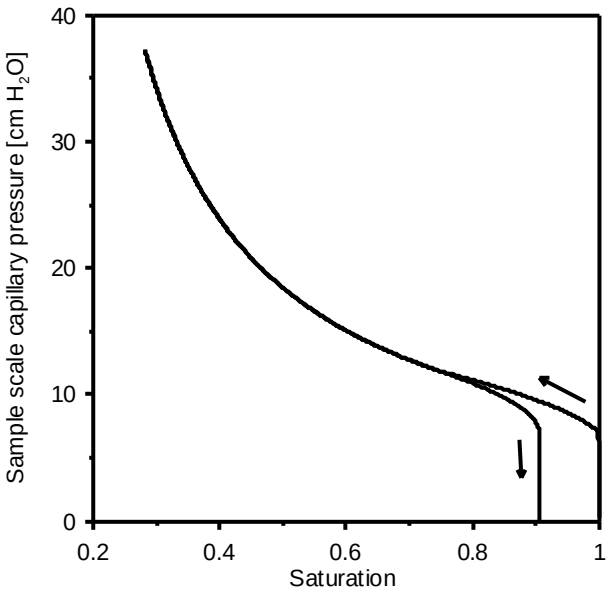

Fig. 5. Simulated capillary pressure experiment.

To illustrate this, a simulation has been performed of a pressure cell experiment to determine the capillary pressure-saturation curve following the approach of Wildenschild et al. (1997). Water is extracted at a slow rate from the bottom of a water-saturated sample to establish the main drainage path. When a certain capillary

pressure has been reached the flow direction is reversed and the primary imbibition curve is obtained. The capillary pressure is determined as the atmospheric pressure minus the pressure in the water phase and represents the capillary pressure at sample scale. As Fig. 5 shows gas will be entrapped and the simulated sample scale capillary pressure curve appears realistic even though gas phase entrapment is only included in the relative permeability model. The capillary pressure model used in the simulation corresponds to the main drainage curve. Note that this approach can only simulate entrapment and does not account for the generally lower capillary pressure observed during imbibition.

3.5. Implementation of the BC capillary pressure-saturation model

The BC model has a conceptual advantage over the VG model because it has a distinct entry pressure, which seems more physically realistic. This is especially true in situations where boiling occurs in coarse homogeneous sand as described in Gudbjerg et al. (2003a). In the original formulation the T2VOC code assumes a continuous transition from the water pressure at full saturation to the gas pressure at unsaturated conditions. Actually a variable switch is made from water pressure to gas pressure when a gas phase appears but the numerical value of the pressure is not changed. To be able to use the BC model it is necessary to change the pressure when the gas phase appears because of the distinct entry pressure. The entry pressure is the pressure difference between the water pressure and the gas pressure at infinitesimal gas saturation in a two-phase system. The code has been altered in the equation-of-state module and in the module calculating the flow. In the original equation-of-state a gas phase appears when the pressure of the would-be gas phase exceeds the water pressure. With the new formulation the air entry pressure is added to the water pressure. Thus, for an air-water simulation a gas phase appears when:

$$P_{air} + P_{sat,water} > P_{aqueous} + P_e$$

where P_{air} is the partial pressure of the dissolved air, $P_{sat,\ water}$ is the saturated vapor pressure of water, P_{water} is the pressure in the water phase and P_e is the gas-water entry pressure calculated for a gas saturation of 10^{-6}, which is the lowest possible gas saturation.

When a gas phase appears a variable switch is made by adding the entry pressure to the water pressure and the new variable is the gas pressure. Furthermore, in the flow module the entry pressure is also taken into account when calculating gas flow into a water-saturated gridblock. The pressure gradient is calculated from the gas phase pressure in the unsaturated gridblock and the water pressure + the entry pressure in the saturated gridblock. This ensures that gas can only flow into a water-saturated gridblock if the entry pressure is exceeded (Again the entry pressure is found by calling the capillary pressure routine with a gas saturation of 10^{-6}). The table below summarizes the changes made in the equation-of-state module.

Table 2. Implementation of BC in the equation-of-state module. The bold P is the primary variable.

	$S_g = 0$	Gas appears if:	$S_g = 10^{-6}$
Old	$\mathbf{P} = P_{water,\,1}$	$P_{air} + P_{sat,water} > \mathbf{P}$	$\mathbf{P} = P_g = P_{water,1}$
			$P_{water,2} = \mathbf{P} - P_c(S_g)$
New	$\mathbf{P} = P_{water,\,1}$	$P_{air} + P_{sat,water} > \mathbf{P} + P_c(Sg=10^{-6})$	$\mathbf{P} = P_g = P_{water,1} + P_c(S_g)$
			$P_{water,\,2} = P_{water,\,1}$

Indices 1 and 2 on the P_{water} refer to before and after the gas phase appears.

These changes can also be used with other capillary pressure models even though they do not have a distinct entry pressure. Actually since the minimum gas saturation is 10^{-6} all models will have an entry pressure and the code can therefore be expected to run smoother using this formulation.

Three-phase combinations are handled in a similar way using either the gas-NAPL or the NAPL-water entry pressure.

3.5.1. Verification

To verify the implementation a gravity drainage example has been simulated where a column drains from full saturation to a fixed water table using the VG and the BC model. The column is 0.5 m high and resolved by 100 gridblocks. The bottom pressure is fixed at 101.7 kPa and the atmospheric pressure at the upper boundary is set to 100 kPa. The capillary pressure data have been determined experimentally and the parameters for the VG and the BC model have been found by curve fitting. The soil properties are given in the table below.

Table 3. Soil properties.

Parameter	Value
Intrinsic permeability	$1.8 \cdot 10^{-9} m^2$
Porosity	0.41
BC pore distribution index	5.4
BC air entry pressure	0.041 m
VG α	21.7 m^{-1}
VG n	7.9
Residual water saturation	0.05

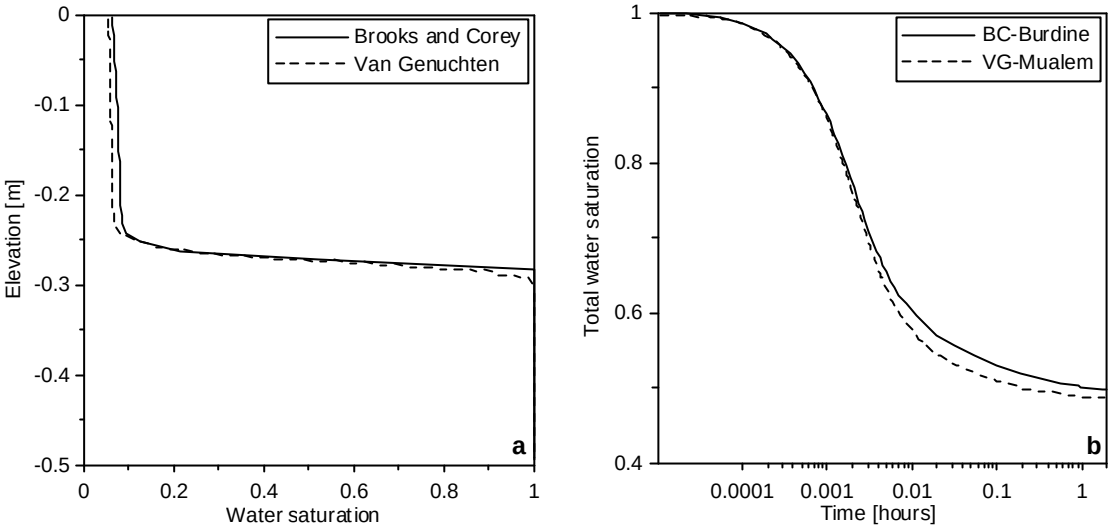

Fig. 6. Simulated water saturation after two hours of drainage (a) and the total water saturation of the column as a function of time (b). Note that the x-axis is logarithmic in (b).

As shown in Fig. 6a the resulting water saturation is almost similar for the two models. Close to saturation they differ slightly which is to be expected from the shape of the capillary pressure curves. Fig. 6b shows the total water saturation as a function of time and it is seen that also the temporal behavior is similar for the two models. The difference between the models is caused by the difference in the relative permeability models. When the Mualem-model is used with the BC model there is no discernible difference on the curves and vice versa with the Burdine model. Several other verification examples have been performed, including test of three phases, and they have documented that the BC model has been implemented correctly.

In Schmidt et al. (2002) it was found necessary to use a linearization close to saturation with the VG-model to avoid oscillating behavior and small time steps. This may be avoided by using the new formulation where the variable switch is more correctly accounted for. The drainage example has been simulated for different values of the VG-parameter n and the corresponding BC-parameter λ. Fig. 7a illustrates the effect of the VG-n parameter on the shape of the capillary pressure curve and Fig. 7b shows the number of time steps necessary to simulate the drainage example.

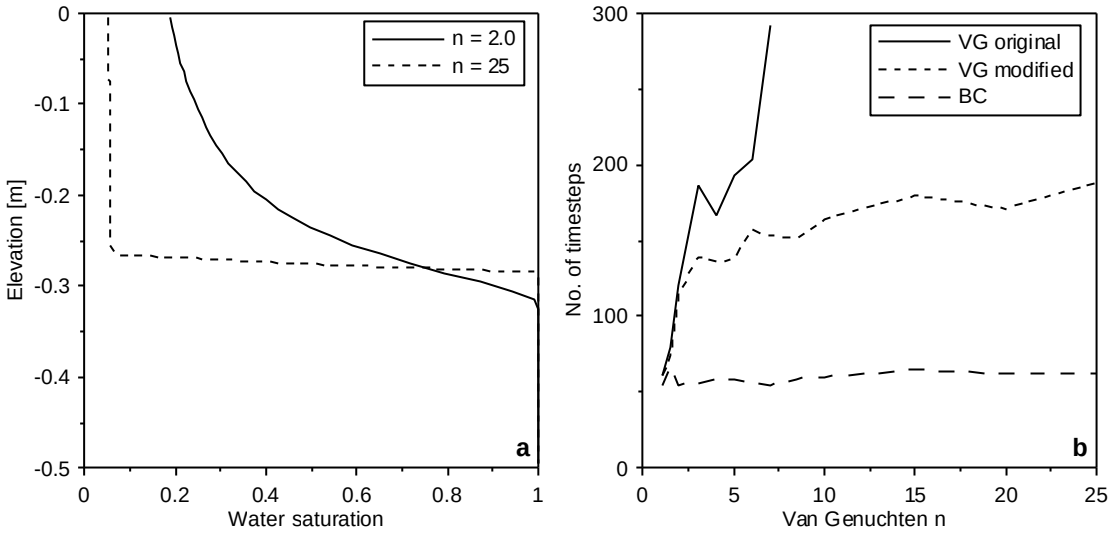

Fig. 7. Water saturation with depth (a) and no. of time steps (b) for different values of VG-n. and corresponding BC-1.

With the original formulation the number of time steps increases dramatically with n and for n larger than 7 it is not possible to complete the simulation, whereas with the modified formulation the VG-model does not exhibit the same problem. This is because the original formulation gives rise to a discontinuity in water pressure when the gas phase appears. The gas pressure is set equal to the previous value of the water pressure and since the new water pressure is equal to gas pressure minus the capillary pressure the water pressure necessarily decreases. Consequently, the new formulation is considered more physically correct. It is not possible to see any difference on the curves in Fig. 6 or Fig. 7a with the two different formulations.

The BC model is faster in all cases which is probably caused by the vertical asymptote in the VG model close to saturation where a very small change in saturation gives a large change in capillary pressure, thus making it necessary to use small time steps.

3.6. Unphysical simulation results

Inaccuracies will necessarily arise when the governing equations are solved numerically and this is inherent to all kinds of numerical modeling. In some special cases the results obtained with the model will be completely unphysical and the model may fail to perform the desired simulation. To truly benefit from the models it is important to understand these cases. Furthermore, since modeling of steam injection is computationally demanding it is important that the simulation behaves as efficiently as possible. In modeling of steam injection at least two cases have been found where the model produces results not in accordance with the physical reality. Falta et al. (1992) showed how steam injection into a water saturated column would give rise to a fluctuating behavior. This example has been repeated using a gridblock size of 1.82 cm, which was used by Falta et al. (1992) and a ten times finer discretization. Fig. 8a shows the pressure in the first gridblock and the peaks arise every time the steam front advances one gridblock.

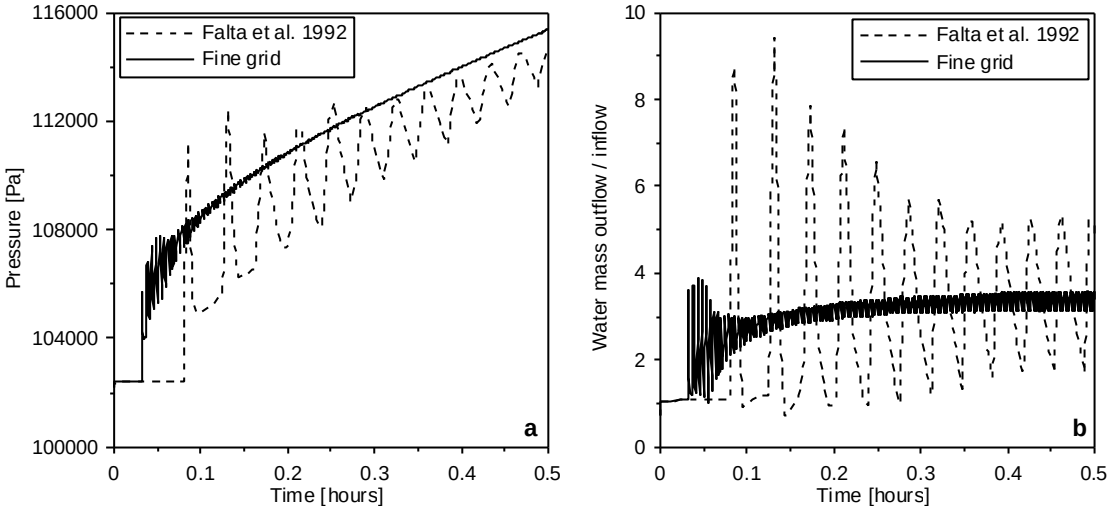

Fig. 8. Injection pressure (a) and relative outflow of water (b) with two different grids.

When steam flows into a gridblock it condenses, which increases the temperature of the gridblock. When the gridblock reaches steam temperature the steam no longer condenses but displaces water and drains the gridblock. Thus, the outflow from the column will increase. This is illustrated in Fig. 8b showing the mass of water flowing out divided by the constant steam injection rate. These peaks in outflow will necessarily be accompanied by peaks in pressure as Fig. 8a shows. In between the pressure peaks the water outflow corresponds to the inflow, which means that all the steam condenses. Draining from a gridblock decreases as soon as steam can flow into the next gridblock and this is essentially determined by the saturation dependent relative permeability. With the fine grid the fluctuations are smaller and it is seen that the coarse grid tends to fluctuate around the fine grid. This shows that the fluctuations cannot be avoided with a finer grid and that the coarse grid only gives uncertain but not directly incorrect results. In reality the steam front will move continuously and not in finite steps and the injection pressure and the water outflow curve will be smooth functions. This phenomenon limits the accuracy by which an injection pressure can be simulated with a certain grid size. Additionally, the time step will necessarily decrease with the sudden increases in pressure and if it were possible to simulate a smooth pressure the time step could probably be larger. These pressure fluctuations are not by themselves a hindrance to practical steam simulations but they may trigger other problems as shown by Gudbjerg et al. (2003b).

In 1-D simulations it was shown how spurious water flow could arise on the boundary between a steam zone and a saturated zone due to the discretization of the temperature gradient. When water flowed from the cold saturated zone into the steam zone, steam would condense, which would cause the pressure to drop. This occurred because pressure and temperature in a steam zone is directly related via the saturated vapor pressure of water. The drop in pressure would cause more water to flow in to the steam zone gridblock until the gridblock was completely saturated. This self-enhancing process occurred very rapidly and caused the time step to decrease dramatically. These findings were further examined in two dimensions where steam was injected at a constant rate into a variably saturated porous medium. Fig. 9 shows the simulated steam zone after 1.2 hours and the steam injection pressure as a function of time.

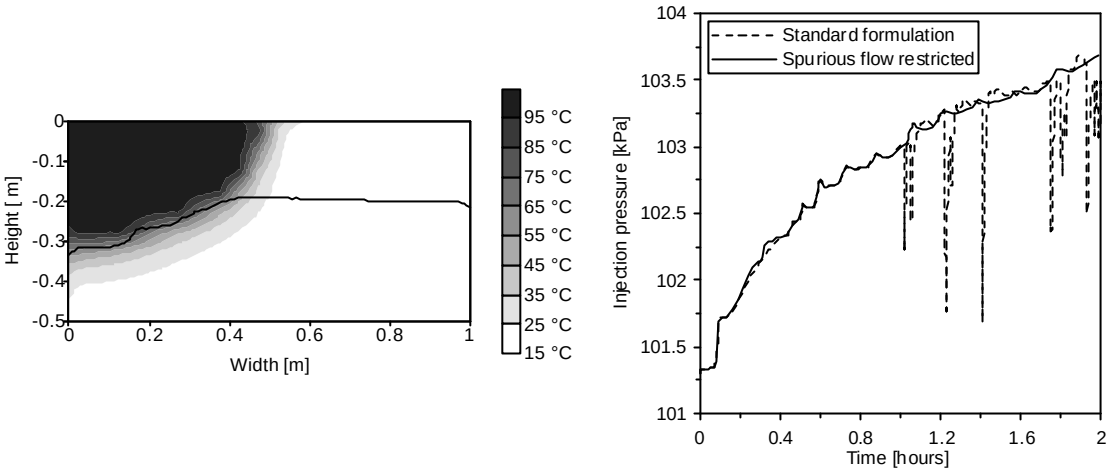

Fig. 9. Simulated temperature zone after 1.2 hours (left) and steam injection pressure (right).

The large drops in pressure are obviously unphysical and they arise because of spurious water flow on the boundary between the unsaturated steam zone and the saturated zone. As Fig. 10 shows the water saturation suddenly increases to almost one in a gridblock located on the boundary. Simultaneously, the pressure and the temperature decrease and that is the cause of the global pressure drops observed on the injection pressure.

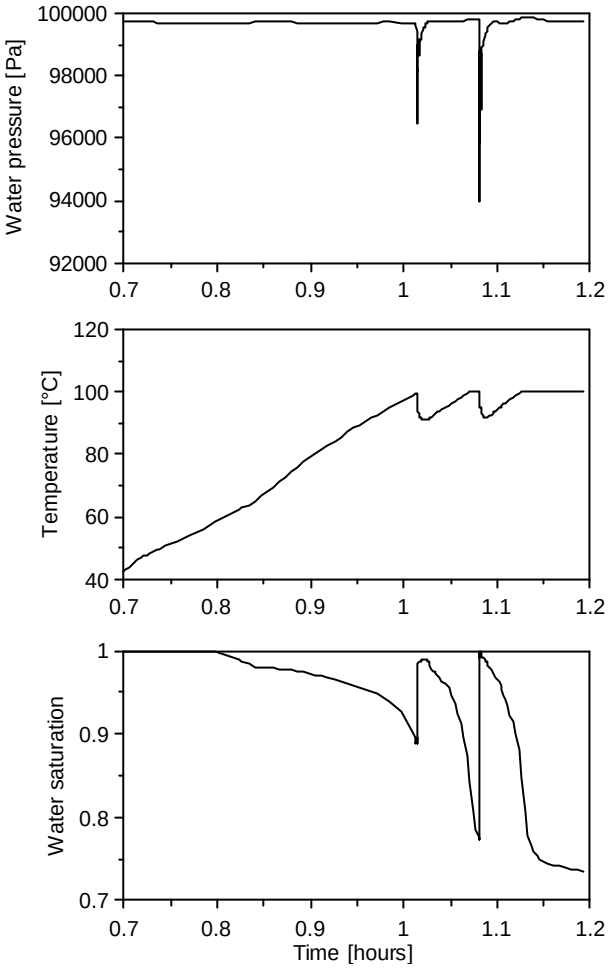

Fig. 10. Temporal development in a steam zone gridblock on the boundary to the saturated zone.

In this case there is no physical reason for the water to flow from the saturated zone into the steam zone, since the injection rate is constant. However, since the steam pressure may fluctuate as illustrated by the Falta et al. (1992)-example the pressure gradient may reverse and water may flow from the saturated zone into the steam zone. Contrarily to the issue reported by Falta et al. (1992) these fluctuations strongly limits the performance of the model and some situations are simply impossible to simulate. Consequently, it was necessary to address the problem. A solution was developed in which the flow of cold water into a steam zone was limited depending on the temperature gradient. The steam zone was detected by the partial pressure of air. With this method the spurious water flow was avoided and the injection pressure remained smooth as illustrated by Fig. 9. The method did not introduce convergence or stability problems and it was assumed to give more physically correct results. The simulations in Gudbjerg et al. (2003c) could not have been performed without this method.

4. Removal mechanisms

One of the strengths of steam injection is that several different mechanisms may be active in the removal of contaminant from the subsurface. Because of this the technology is very versatile and can be used for highly heterogeneous geologic environments and remediation both above and below the water table.

4.1. Frontal removal

Hunt et al. (1988b) presented the first experiments illustrating how steam injection could be used for remediation of contaminated soil. TCE was injected in a water-saturated column and flushed with water before steam was injected. These experiments were subsequently simulated numerically by Falta et al. (1992) and they illustrate how a steam front efficiently removes NAPL.

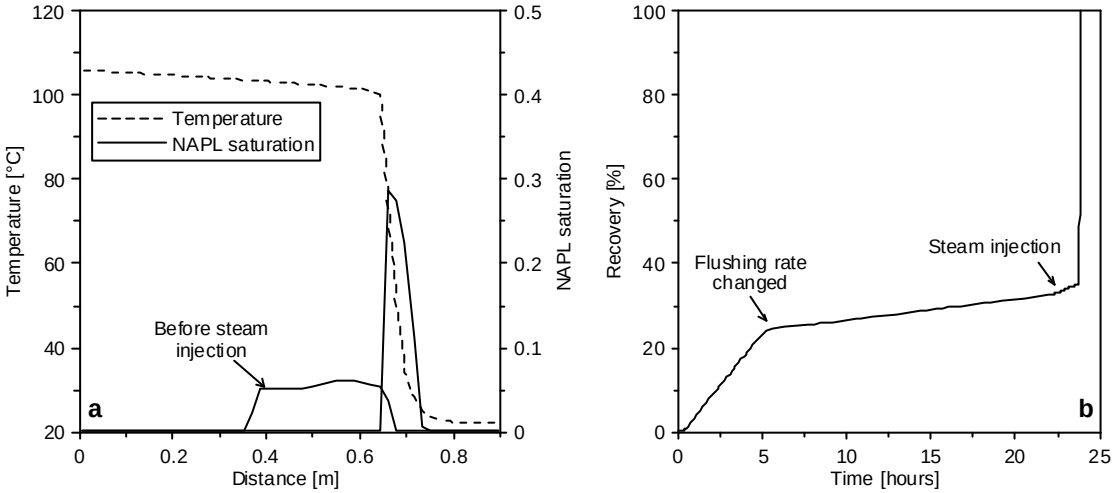

Fig. 11. Temperature profile and NAPL distribution during steam injection (a) and NAPL recovery in % of injected (b). Adapted from Falta et al. (1992b).

Fig. 11a shows that a zone of residual NAPL was present in the column before steam was injected and that this NAPL was pushed ahead of the steam front. The initial water flush recovers some of the NAPL as illustrated in Fig. 11b showing the recovery as a function of time. After 5 hours the flushing rate was reduced by a factor 10 and this reduced the removal rate. Steam broke through at the extraction side after approximately 24 hours and the remaining NAPL was almost immediately recovered. Thus, the recovery rate during steam injection is orders of magnitude larger than during water flushing.

Even though the NAPL appears to be pushed ahead of the steam front the removal mechanism is not displacement but continuous vaporization and condensation. The NAPL was at residual saturation and could not be displaced, since it had zero relative permeability. As soon as the steam contacts the NAPL it will start to vaporize. At thermodynamic equilibrium the partial pressure of the contaminant in the gas phase is equal to vapor pressure of the contaminant at the actual temperature. Subsequently the contaminant condenses downstream in colder areas with the steam. In the numerical model this process will occur over two gridblocks. When the first

gridblock reaches steam temperature NAPL will vaporize and be transported to the next gridblock. In reality this is probably a pore-scale process.

If the NAPL has a low vapor pressure the velocity of the moving NAPL vaporization front may be lower than that of the steam front and then only a part of the NAPL mass will be pushed ahead of the steam front. Falta et al. (1992) derived an expression showing that if the normal boiling point of the NAPL exceeded 175 °C complete frontal removal of NAPL would not occur for the experimental conditions in Hunt et al. (1988). The analysis assumed that NAPL would not accumulate in a concentration larger than residual so this is probably not a conservative estimate. Complete frontal removal is not a requirement for remediation by steam injection. On the contrary it may actually be beneficial if frontal removal could be avoided because the accumulation of NAPL on the front may pose problems as will be discussed in section 6.

This frontal removal mechanism is very rapid and it can often be assumed that all volatile contaminants will be removed from the steam zone and condense on the boundaries. However, Sleep and McClure (2001a) showed in a similar 1-D setup using natural, contaminated soil that the removal may eventually become rate-limited and even after flushing of several pore volumes the soil may still be contaminated. Similar results were obtained by van der Ham and Brouwers (1998) in which the removal rate of low volatile NAPL (normal boiling point: 527 °C) decreased with the NAPL-gas interfacial area. This shows that in some cases steam injection may be subject to the same mass transfer limitation as low temperature flushing. However, due to the mechanism described in the next section this is not expected to be the case for volatile NAPLs such as TCE.

4.2. Conduction-induced boiling

Steam injected in soil will flow preferentially in high permeable areas and bypass low permeable lenses that may be contaminated. Preferential flow in high permeable layers is a major problem for all flow-dependent remediation technologies because the mass transfer in and out of low permeable areas will be dominated by diffusion, which is a very slow process. Mass transfer limitation due to heterogeneities is the main reason why the remediation time to reach desired clean up levels in many cases becomes unacceptably long. In steam injection bypass of contaminated areas may also occur when steam is injected below the water table where buoyancy causes the steam zone to move upwards or if downwards migrating LNAPL gets trapped between the steam zone and the saturated zone.

The area outside the steam zone will, however, be heated by conduction. If NAPL is present in this area, boiling will initiate when the temperature reaches the common boiling point of water and NAPL. As stated in section 1.1 all NAPLs will boil in the presence of water at a temperature below the normal boiling point of water. In the steam zone the temperature will correspond to the normal boiling point of water and in principle the steam zone will always be able to heat the contaminated area to the boiling point by conduction. This mechanism has been illustrated in 2-D sand box experiments by Schmidt (2001) and Gudbjerg et al. (2003a). Schmidt (2001) emplaced NAPL in a low permeable lens and injected steam in surrounding, unsaturated, high permeable sand layers. Gudbjerg et al. (2003a) emplaced NAPL on top of a low permeable layer below the water table and injected steam in the

unsaturated zone above. Thus, in neither case could steam access the contaminated area directly.

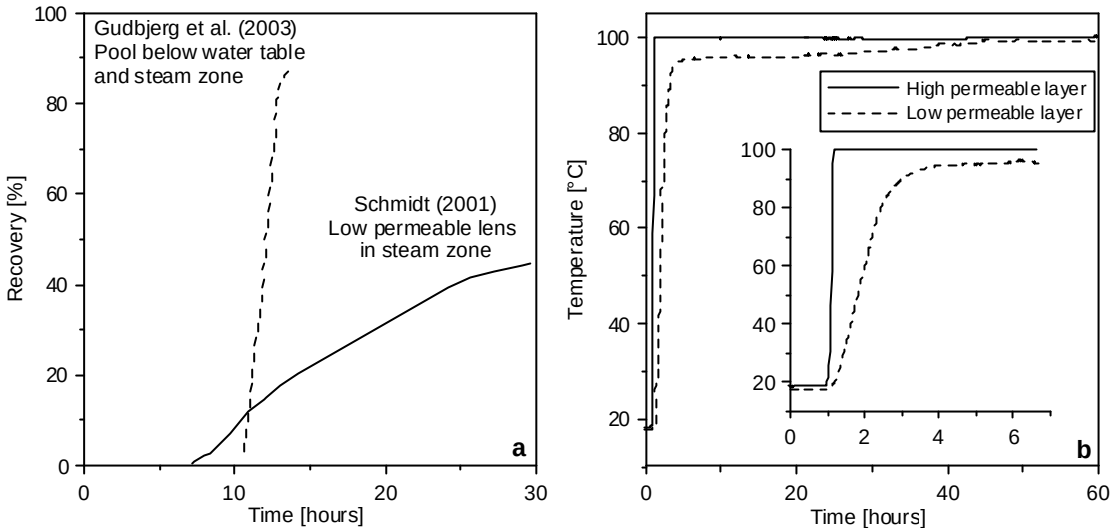

Fig. 12. Recovery by steam induced heat conduction (a) and temperature inside and outside low permeable lens (b) (Schmidt 2001). Insert zooms on early time.

Fig. 12a shows the recovery curve observed in the two experiments. In both experiments steam broke through at the extraction side after 2-3 hours; however, no NAPL was recovered until after 8-10 hours. Recovery initiated when the contaminated area was heated to the common boiling point of water NAPL by heat conduction. This is illustrated in Fig. 12b showing the temperature measured in the high permeable layer and in the low permeable contaminated layer from Schmidt (2001). As the insert shows the temperature increases rapidly and linearly in the high permeable layer indicating a convection-dominated process whereas the increase is slower in the low permeable layer indicating a more conduction-dominated process. During the recovery period the temperature remains constant in the low permeable layer because of boiling. When the NAPL has been removed the temperature increases again, however slowly, which is probably because the area around the thermocouple is still affected by NAPL boiling further inside the low permeable lens. After approximately 60 hours the temperature increases to the boiling point of water and no more contaminant is recovered.

The mechanism was further clarified in Gudbjerg et al. (2003a) by means of numerical modeling. Fig. 13a shows the gas saturation during the contaminant recovery period and it can be noted that an unsaturated zone has been created above the contaminant pool due to gas created by boiling.

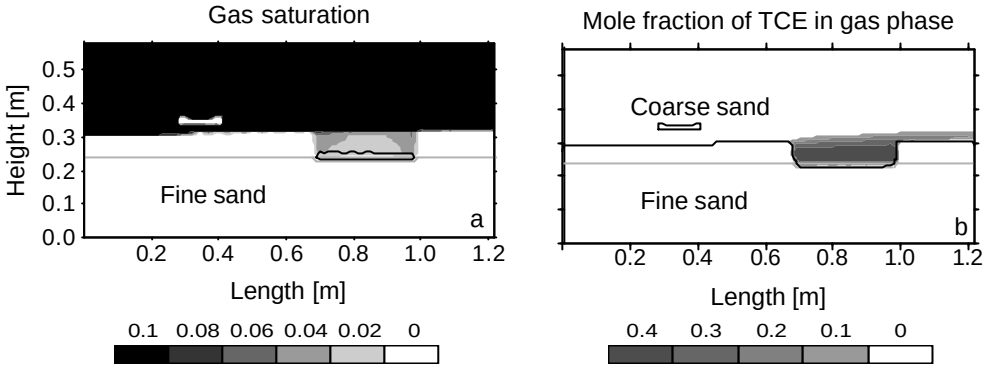

Fig. 13. Simulated gas saturation (a) and the mole fraction of TCE in the gas phase (b) after 12 hours. The gray line indicates the boundary between the fine and the coarse sand. On (a) the black line indicates the NAPL contaminated area and on (b) it indicates the boundary between saturated and unsaturated conditions.

When the contaminant vapor reaches the steam zone it is transported with the steam flow towards the extraction well as illustrated by Fig. 13b that shows the mole fraction of TCE in the gas phase. By means of 1-D numerical modeling it was further shown that the boiling process would be relatively insensitive to porous media properties. Within a range of porous media properties where the presence of separate phase contaminant is possible the clean-up time was dominated by the time to heat the contaminated area to the common boiling point by heat conduction. Thus, it was proposed that clean-up time could be estimated by considering heat conduction alone.

As seen in Fig. 12a there is a difference in recovery rate between the two experiments. This may be explained by the difference in the common boiling point of the NAPLs used in the experiments. The common boiling point for the NAPL used by Schmidt (2001) was approximately 98°C compared to 74°C in the experiment by Gudbjerg et al. (2003a). Thus, in the latter case the heat transfer, which controls the boiling rate would be larger due to the larger temperature gradient. The recovery rate will also be influenced by the distance to the steam zone; however, in both experiments the maximum distance was approximately 10 cm.

The effectiveness of the boiling mechanism can be illustrated by comparing with isothermal experiments where other flushing technologies were used. MacKinnon and Thomson (2002) presented an experiment where a pool of PCE on top of a low permeable layer in a 2-D sand box was remediated by an initial water flush followed by a permanganate flush. The dimensions of the sand box were 2.5 x 0.15 x 0.45 m and 700 g of PCE was emplaced in a pool. After 90 days of water flush 1.4 % of the initial mass had been removed and after 146 days of permanganate flushing 46 % of the initial mass had been destroyed. Oostrom et al. (1999) presented a 2-D sand box experiment (1.67 x 0.05 x 1m) where 837 g of TCE were infiltrated in coarse sand with lenses of low permeable sand. The TCE spread on top of the low permeable lenses and the bulk of the TCE pooled in low permeable depression at the bottom of the box. During a 140-day water flushing period where surfactants were added occasionally 60 % of the emplaced TCE was removed from the sand box. The remaining TCE had migrated into the low permeable sand and could not be removed. These experiments are comparable to the experiment of Gudbjerg et al. (2003a) where a pool of TCE was removed by steam injection within 12 hours. In experiments using flushing technologies remediation was limited by dissolution and diffusion whereas

steam remediation was limited by heat conduction, which results in much faster source removal.

It has been observed at low temperature (Wilkins et al., 1995) that the vaporization of NAPL will decrease with the NAPL-air interfacial area. As previously described this was also observed at high temperature with a semivolatile NAPL (van der Ham and Brouwers, 1998). It is speculated that this is not a general problem in steam injection where vaporization is controlled by boiling and not by a concentration gradient. Except for very low volatile components the heat transfer to the NAPL will be so fast that removal will not appear rate limited.

4.3. NAPL flow

In some cases the direct flow of NAPL may be more important as a recovery mechanism than the vaporization and subsequent transport in the gas phase.

In the 2-D experiment simulated by Gudbjerg et al. (2003b) NAPL recovery could not be simulated when a residual NAPL saturation was included in the relative permeability model. Based on this it was concluded that NAPL flow was more important than vaporization. The NAPL flow was driven by the pressure gradient in the steam zone and as such can be compared to isothermal dual-phase extraction in which pumping takes place in both the gas and NAPL phase. However, this is not expected to be the case at field-scale since the vaporization mechanism will be independent of the areal extent, which is in contrast to the direct flow of NAPL. In any case there will be little advantage in using steam to drive NAPL flow. Note that NAPL flow in general may be very important for the performance of a clean-up by steam injection but as a recovery mechanism it is probably surpassed by the vaporization-mechanisms.

In the petroleum industry NAPL flow has been the dominant recovery mechanism when applying steam injection. This difference arise because the NAPL saturation is much higher and generally has a much lower viscosity, thus making it advantageous to increase the temperature and thereby the flow.

4.4. Additional mechanisms

When steam injection is performed in the unsaturated zone soil vapor extraction is normally performed simultaneously. This induces flow of non-condensable air that may also remove significant mass of contaminant. Even though this is not strictly related to the injection of steam it is an important removal mechanism during remediation. Furthermore in some cases air is co-injected with steam to prevent downward migration and in those cases the removal with the air phase is very important (Schmidt et al., 2002).

In most cases groundwater extraction is also performed during steam injection and consequently some contaminant mass will be removed in the water phase. However, due to the low solubility of most contaminants this will be an insignificant part of the total mass removed.

5. Steam zone development

The most essential issue when designing a steam injection operation is to ensure that the steam targets the contaminated area and consequently it is important to understand how a steam zone develops.

5.1. 1-D steam zone development

The experiments of Hunt et al. (1988) demonstrated how a steam zone develops in one dimension. When steam contacts soil with a temperature below steam temperature it immediately condenses and heats the soil. Eventually the soil reaches steam temperature and the steam zone expands. As illustrated in Fig. 11a, the temperature gradient on the steam front is very steep. Note also that most of the water is displaced from the steam zone and it is therefore not necessary to heat all the water to steam temperature. A simple energy balance could describe the development of the steam zone and the velocity of the steam front was equal to the injected enthalpy per time divided by the enthalpy required to heat the porous medium to steam temperature.

5.2. 3-D steam zone development

In three dimensions the steam zone develops in a similar way, however it is much more complicated to predict the shape of the steam zone. Therefore it is rarely possible to use a simple energy balance approach. Generally speaking, the steam zone will develop in the direction of the steam flow, which is controlled by Darcy's law. Furthermore, the heat loss will depend on the surface area of the steam zone and the fluid flow along that surface. Thus, there are a lot of interacting processes and only in very special cases will it be possible to use a simple model approach. Gudbjerg et al. (2003c) performed a modeling study of steam injection in a saturated zone using a setup simplified by symmetry considerations. The setup was based on observations from a field-scale clean-up.

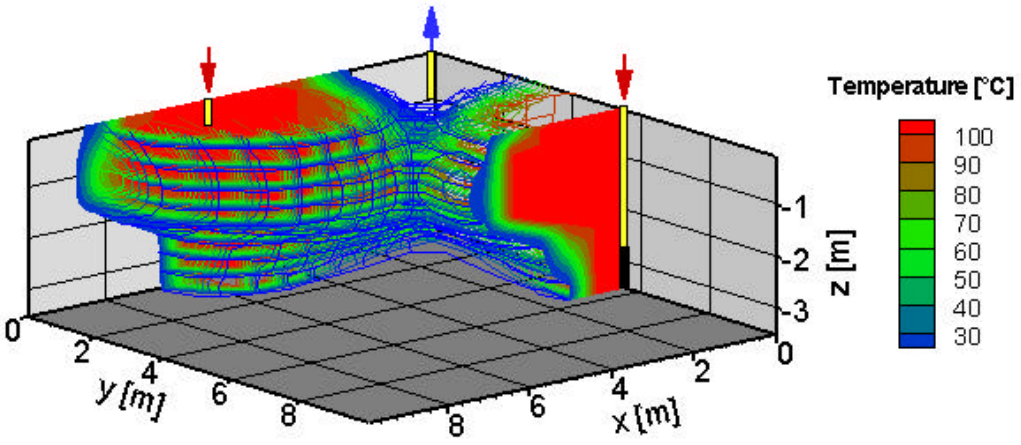

Fig. 14. A 3-D plot of the simulated steady-state temperature viewed from the outer boundary towards the extraction well. The plot corresponds to twice the simulated volume and is symmetric around x = y. The temperature outside the contoured volume is below 20 °C

As illustrated in Fig. 14 the steam zone rises above the saturated zone due to buoyancy and mainly develops in the unsaturated zone. This means that the bottom area between the wells is not heated and it is unlikely to be cleaned up. Using this setup the impact on the steam zone development of various parameters was examined. It was not possible to provide general recommendations on the optimal distribution of wells and instead it was recommended to make a site-specific simulation in each particular case.

5.2.1. Unsaturated zone

In the unsaturated zone the steam zone development is somewhat easier to predict, since buoyancy and water flow are no longer important factors. This means that steam zone development is mainly controlled by permeability contrasts and the cooling effect of the gas flow induced by the simultaneous soil vapor extraction. A simulation has been performed using the same setup as reported in Gudbjerg et al. (2003c) except the water table has been lowered to the bottom of the model grid.

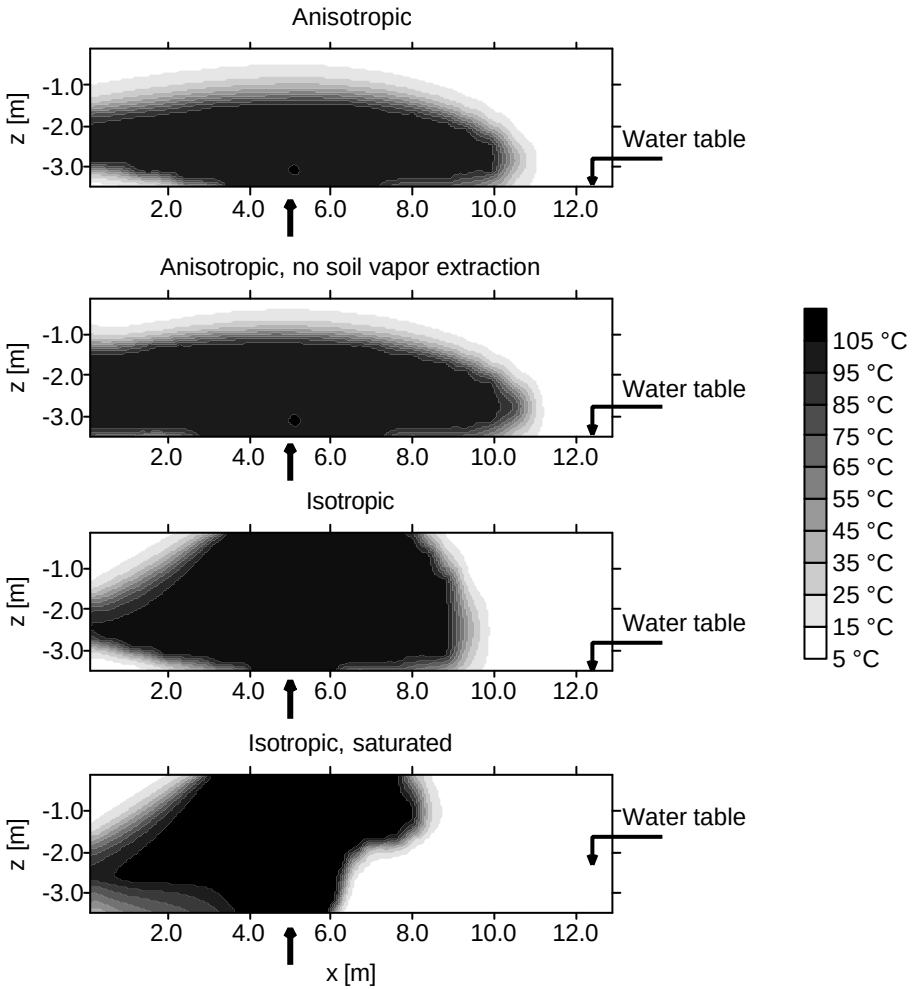

Fig. 15. Contour plots of temperature between injection and extraction well from 3-D setup. Black arrow indicates injection. Extraction occurs at x = 0m.

The injection well is located at x = 5 m and it is seen that the steam zone is almost symmetric around this point in the upper three plots in Fig. 15. This can be compared to the lower plot derived from the saturated model (Fig. 14) where the steam zone is strongly dragged towards the extraction well. Thus, under unsaturated conditions the steam zone is less controlled by the extraction system but is still dependent on the geology. It is not possible to control the direction of the steam flow by means of an extraction well; however, the development of the steam zone may be hindered by the cooling induced by the vapor flow.

6. Downward migration

One of the major concerns when applying steam injection is that it may lead to downward migration of NAPL. This may occur because the capillary pressure is reduced with increasing temperature, thus facilitating entry of NAPL into low permeable layers and migration of capillary entrapped droplets. However, more important is the accumulation of NAPL on the steam front, which in the unsaturated zone may lead to severe downward migration. This was demonstrated by Schmidt et al. (2002) using 2-D sand box experiments and numerical modeling. When the injected steam was mixed with air downward migration could be prevented. This is illustrated in Fig. 16 showing the experimental and the modeled temperature zones.

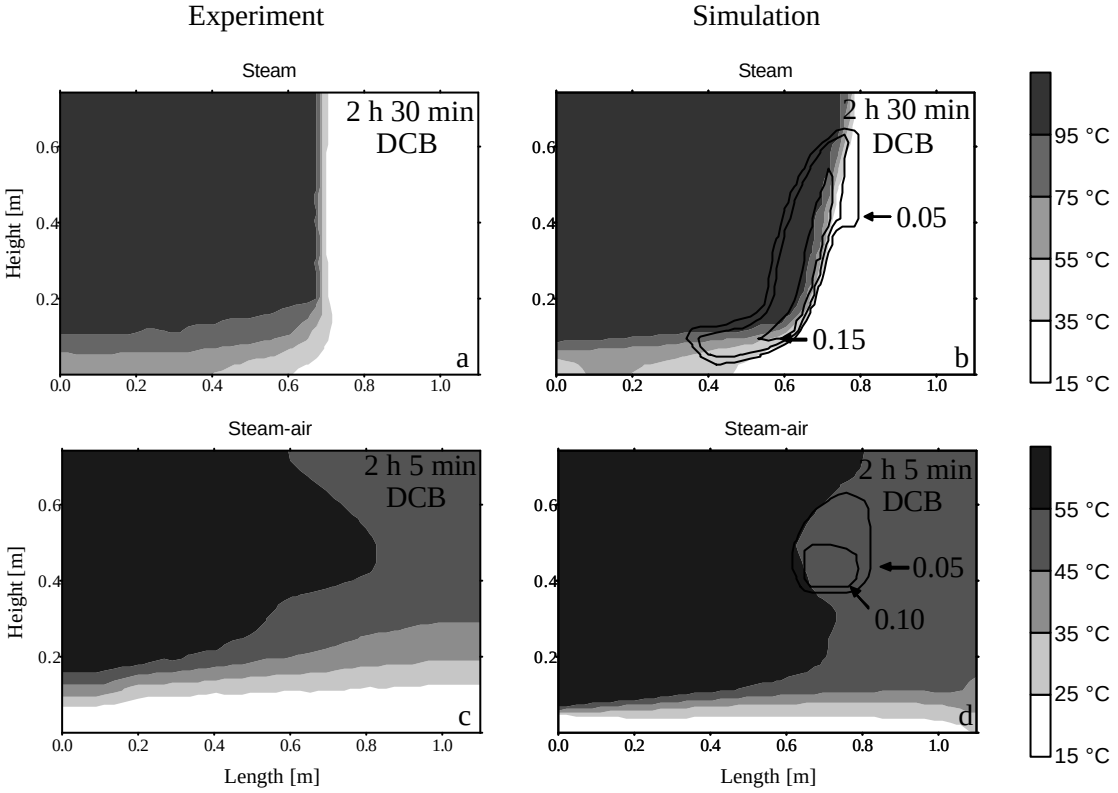

Fig. 16. Experimental and numerical heat zones for steam (a,b) and steam-air (c, d) injection. 0.05 intervals on NAPL saturation contours.

When pure steam is injected the NAPL accumulates on the steam front and migrates downward, which may be detrimental to a clean-up. Contrarily when a steam-air mixture is injected the contaminant is continuously removed and only very limited downward migration occur. By means of the numerical model three mechanisms that prevented downward migration were identified:

1) Removal with the non-condensable air
2) Less steep temperature gradient at heat front
3) Lower velocity of evaporation front compared to heat front

The effectiveness of these mechanisms depended on the air to steam mixing ratio. Unfortunately, it is not possible to provide an optimal mixing ratio without pore-scale knowledge, which will never be available.

Even though these experiments showed almost complete downward migration of the emplaced contaminant it cannot be concluded that steam injection in the unsaturated zone should be avoided. They represent a worst-case situation since the NAPL was at residual saturation and the sand was completely homogeneous. Instead it is recommended to perform soil vapor extraction before beginning steam injection, which will remove the easiest accessible contaminant and thereby reduce the risk of downward migration.

7. Future research areas

Even though steam injection is no longer a new technology there are still areas where we need more knowledge. In this section I provide the three issues I find most important to do future scientific research in. Apart from these issues there are of course practical and economical problems that would be important to address about where and when steam injection will be the optimal technology compared to other remediation technologies.

7.1. Cyclic injection

In the well-documented clean-up at the LLNL-site (Newmark et al., 1994) it was reported that once the site had been heated the contaminant removal rate would increase immediately after a stop in steam injection (Udell 1994). Thus, it was argued that operating the injection in a cyclic manner would remove contaminant faster than continuous steam injection. At the site described in Gudbjerg et al (2003b) cyclic steam injection was performed during the last part of the clean-up. Variations in concentration in the effluent gas phase could clearly be registered; however, it was difficult to quantify and even more difficult to explain the effect.

There is no experimental evidence that cyclic injection has a beneficial effect. Nevertheless it is routinely applied at clean-up operations and beneficial effects are often reported. As long as the basic mechanisms are not understood, optimal injection strategies cannot be developed. It may be difficult to obtain the necessary insight from field-scale results due to many uncontrollable factors and instead it is suggested to investigate the mechanism through numerical modeling. It is likely that cyclic injection only has an effect in special configurations and consequently it cannot be recommended to perform laboratory experiments before a suggestion of a mechanism is available.

7.2. Steam injection in fractured systems

Very little research has been performed on remediation of fractured systems by steam injection and already the first field-scale pilot-tests have been performed. Thus, there is an interest in applying steam injection in fractured systems. Numerical modeling could provide an initial insight on steam zone development in fractured systems and the potential contaminant removal. As for porous media it should be emphasized that steam injection should only be used to recover separate phase contaminants. It can probably not be expected that steam injection would be efficient in removing dissolved contaminant diffused into a low-permeable matrix.

7.3. Temperature effect on capillary pressure

As pointed out the temperature dependence of the capillary pressure has been demonstrated but the exact mechanisms have not been identified. Consequently, it is difficult to take the temperature effect into account in numerical modeling. This may not have a dominant effect on the overall understanding of steam injection but it is dissatisfying that we cannot provide a proper explanation. In general there are unresolved issues concerning the constitutive relationships and probably a more fundamental understanding of the underlying mechanisms would provide a direct explanation of the temperature effect.

8. Conclusions

Steam injection may be used to remediate sites contaminated with volatile NAPLs. The main benefit of heating the soil is that the vapor pressure of contaminants increases with temperature. Furthermore, when NAPL is present with water the two phases boil at a temperature below each of the individual boiling points. There are four mechanisms responsible for the removal of NAPL from the subsurface during steam injection:

1) Frontal removal
2) Conduction-induced boiling
3) NAPL flow
4) Transport in gas and water phase

Steam injected in the saturated zone is strongly influenced by buoyancy, which causes the steam zone to rise to the unsaturated zone. Only in simple cases is it possible to predict steam zone development in the saturated zone without doing a full-scale numerical simulation. Steam zone development in the unsaturated zone is somewhat simpler to predict as it mainly depends on the geology. Downward migration of contaminant is a potential problem when remediating with steam. The capillary pressure decreases with temperature thus facilitating downward migration of DNAPL in the saturated zone but more importantly the accumulation of NAPL on the steam front can make the NAPL mobile. The latter is especially a problem in the unsaturated zone where the downward migrating NAPL only has to displace air. Mixing the injected steam with air may overcome this problem.

9. References

Atkins, P. W., 1994. Physical Chemistry. Oxford University Press, Oxford, Melbourne, Tokyo. 1994.

Bear, J., 1988. Dynamics of fluids in porous media. Dover Publications, New York

Brooks, R. H. and Corey, A. T., 1966. Properties of porous media affecting fluid flow. J. Irrigation Drainage Division, ASCE 92 (IR2), 61-88.

Burdine, N. T., 1953. Relative permeability calculations from pore-size distribution data. Petroleum Transactions of the American Institute of Mining Engineering, 198: 71-77.

Danish EPA, 1999. Natur og Miljøpolitisk Redegørelse 1999. Miljø- og Energiministeriet. In Danish.

Davis, E. L., 1994. Effect of temperature and pore size on the hydraulic properties and flow of a hydrocarbon oil in the subsurface. Journal of Contaminant Hydrology, 16: 55-86.

Dullien, F. A. L., 1992. Porous media. Fluid transport and pore structure. Academic Press, London.

Dury, O., Fischer, U. and Schulin, R., 1999. A comparison of relative nonwetting-phase permeability models. Water Resources Research, 35: 1481-1493.

Falta, R. W., Pruess, K., Finsterle, S. and Battistelli, A., 1995. T2VOC User's Guide. Lawrence Berkeley Laboratory Report, LBL-36400 University of California, Berkeley.

Falta, R. W., Pruess, K., Javandel, I., and Witherspoon, P. A., 1992. Numerical modeling of steam injection for the removal of nonaqueous phase liquids from the subsurface 2. Code validation and application. Water Resources Research. 28: 451-465.

Grant, S. A., 2003. Extension of a temperature effects model for capillary pressure saturation relations. Water Resources Research. 39 doi:10.1029/2000WR000193.

Grant, S. A., 1996. Calculation of temperature effects on wetting coefficients of porous solids and their capillary pressure functions. Water Resources Research. 32: 261-270.

Gudbjerg, J., Sonnenborg, T. O., and Jensen, K. H., 2003a Remediation of NAPL below the water table by steam induced heat conduction. Submitted to Journal of Contaminant Hydrology.

Gudbjerg, J., Trötschler, O., Färber, A., Sonnenborg, T. O. and Jensen, K. H., 2003b. On spurious water flow during numerical simulation of steam injection into water saturated soil. Submitted to Journal of Contaminant Hydrology.

Gudbjerg, J., Heron, T., Sonnenborg, T. O., and Jensen, K. H., 2003c. Three-dimensional numerical modeling of steam override observed at a full-scale remediation of an unconfined aquifer. Submitted to Ground Water Monitoring and Remediation.

Heron, G., Christensen, T. H. and Enfield C. G., 1998. Henry's law constant for trichloroethylene between 10 and 95 °C. Environmental Science and Technology, 32: 1433-1437.

Hofstee, C., Dane, J. H., and Hill, W. E. 1997. Three-fluid retention in porous media involving water, PCE and air. Journal of Contaminant Hydrology, 25: 235-247.

Lenhard, R. J. and Parker, J. C., 1987a. A model for hysteretic constitutive relations governing multiphase flow 2. Permeability-saturation relations. Water Resources Research, 23: 2197-2206.

Lenhard, R. J. and Parker, J. C., 1987b. Measurement and prediction of saturation-pressure relationships in three phase porous media systems. Journal of Contaminant Hydrology, 1: 407-424.

Liu, H. H. and Dane, J. H., 1993. Reconciliation between measured and theoretical temperature effects on soil water retention curves. Soil Science Society of America Journal. 57: 1202-1207.

Luckner, L., Van Genuchten, M. Th. and Nielsen, D. R., 1989. A consistent set of parametric models for two-phase flow of immiscible fluids in the subsurface. Water Resources Research. 25: 2187-2193.

MacKinnon, L. K. and Thompson, N. R., 2002. Laboratory-scale in situ chemical oxidation of a perchloroethylene pool using permanganate. Journal of Contaminant Hydrology, 56: 49-74.

Mercer, J. W. and Cohen, R. M., 1990. A review of immiscible fluids in the subsurface: Properties, models, characterization and remediation. Journal of Contaminant Hydrology. 6:107-163.

Mortensen, A. P., Glass, R. J., Hollenbeck, K. and Jensen, K. H., 2001. Visualization of microscale phase displacement processes in retention and outflow experiments: Nonuniqueness of unsaturated flow properties. Water Resources Research, 37: 1627-1640.

Mualem, Y., 1976. A new model for predicting the hydraulic conductivity of unsaturated porous media. Water Resources Research, 12: 513-522.

Newmark R. and various authors, 1994. Dynamic underground stripping project. Lawrence Livermore National Laboratory, UCRL-ID-116964-V-1-4.

Oostrom, M. and Lenhard, R. J., 1998. Comparison of relative permeability-saturation-pressure parametric models for infiltration and redistribution of a light nonaqueous-phase liquid in sandy porous media. Advances in Water Resources. 21: 145-157.

Oostrom, M., Hofstee, C., Walker, R. C. and Dane, J. H., 1999. Movement and remediation in a saturated, heterogeneous porous medium 2. Pump-and-treat and surfactant flushing. Journal of Contaminant Hydrology, 37: 179-197.

Parker, J. C., Lenhard, R. J. and Kuppusamy, T., 1987. A parametric model for constitutive properties governing multiphase flow in porous media. Water Resources Research, 23: 618-624.

Parker, J. C. and Lenhard, R. J., 1987. A model for hysteretic constitutive relations governing multiphase flow 1. Saturation-pressure relations. Water Resources Research, 23: 2187-2196.

Philips, J. R. and de Vries, D. A., 1957. Moisture movement in porous media under temperature gradients. Eos Trans. AGU, 38(2): 222-232

Pruess, K., 1987. TOUGH User's Guide. Lawrence Berkeley Laboratory Report, LBL-20700 University of California, Berkeley.

Pruess, K., 1991. TOUGH2 - A general purpose numerical simulator for multiphase fluid and heat flow. Lawrence Berkeley Laboratory Report, LBL-29400 University of California, Berkeley.

Sale, T. C. and McWhorter, D. B., 2001. Steady state mass transfer from single-component dense nonaqueous phase liquids in uniform flow fields. Water Resources Research. 37: 393-404.

Schmidt, R., 2001. Wasserdampf- und Heissluftinjektion zur thermischen Sanierung kontaminierter Standorte. Heft 106. Institut für Wasserbau, Universität Stuttgart. In German.

Schmidt, R., Gudbjerg, J., Sonnenborg, T. O. and Jensen, K. H., 2002. Removal of NAPLs from the unsaturated zone using steam: prevention of downward migration by injecting mixtures of steam and air. Journal of Contaminant Hydrology, 55: 233-260.

Sleep, B. E. and McClure, P. D., 2001a. Removal of volatile and semivolatile organic contamination from soil by air and steam flushing. Journal of Contaminant Hydrology, 50: 21-40.

Sleep, B. E. and McClure, P. D., 2001b. The effect of temperature on adsorption of organic compounds to soils. Canadian Geotechnical Journal, 38: 46-52.

She, H. Y. and Sleep, B. E., 1998. The effect of temperature on capillary pressure-saturation relationships for air-water and perchloroethylene-water systems. Water Resources Research, 34: 2587-2597.

Udell, K. S., 1994. Thermally enhanced removal of liquid hydrocarbon contaminants from soils and ground water. In Newmark et al 1994.

van Genuchten, M. T., 1980. A closed-form equation for predicting the hydraulic conductivity of unsaturated soils. Soil Science Society of America Journal, 44: 892-898.

van der Ham, A. G. J. and Brouwers, H. J. H., 1998. Modeling and experimental investigation of transient, nonequilibrium mass transfer during steam stripping of a nonaqueous phase liquid in unsaturated porous media. Water Resources Research, 34: 47-54.

White, M. D., and Oostrom, M., 1996. Subsurface Transport Over Multiple Phases. Theory Guide. Pacific Northwest National Laboratory. Richland, Washington.

Wildenschild, D., Høgh Jensen, K., Hollenbeck, K.J., Illangasekare, T.H., Znidarcic, D., Sonnenborg, T. and Butts, M.B., 1997. Two-stage procedure for determining unsaturated hydraulic characteristics using a syringe pump and outflow observations. Soil Science Society of America Journal, 61: 347-359.

Wilkins, M. D., Abriola, L. M. and Pennell, K. D., 1995. An experimental investigation of rate-limited nonaqueous phase liquid volatilization in unsaturated porous media: steady state mass transfer. Water Resources Research, 31:2159-2172

Removal of NAPLs from the unsaturated zone using steam: prevention of downward migration by injecting mixtures of steam and air

Schmidt, R. [a], Gudbjerg, J. [b], Sonnenborg, T. O. [b], Jensen, K. H. [b]

[a] Institut für Wasserbau, Universität Stuttgart, Germany

[b] Environment & Resources, Technical University of Denmark

Published in Journal of Contaminant Hydrology 55: 233-260

Abstract

Steam injection for remediation of porous media contaminated by non-aqueous phase liquids has been shown to be a potentially efficient technology. There is, however, concern that the technique may lead to downward migration of separate phase contaminant. In this work a modification of the steam injection technology is presented where a mixture of steam and air was injected. In two-dimensional experiments with unsaturated porous medium contaminated with non-aqueous phase liquids it was demonstrated how injection of pure steam lead to severe downward migration. Similar experiments where steam and air were injected simultaneously resulted in practically no downward migration and still rapid cleanup was achieved. The processes responsible for the prevention of downward migration when injecting steam-air mixtures were analyzed using a non-isothermal multiphase flow and transport model. Hereby, three mechanisms were identified and it was demonstrated how the effectiveness of these mechanisms depended on the air to steam mixing ratio.

Keywords: steam injection, unsaturated zone, remediation, air, sand box models, modeling

1. Introduction

Steam injection is a rather new and very promising technology for remediating subsurface hydrocarbon contamination. Conventional technologies like pump-and-treat and soil vapor extraction have shown to be inadequate in many cases, in particular for highly heterogeneous conditions (Rathfelder et al., 1991; Ho and Udell, 1992; CGWCA, 1994). Very often these techniques have failed to reach the desired cleanup level (Danish EPA, 1999) and therefore new technologies are needed to remediate the large number of contaminated sites.

Several one-dimensional laboratory experiments have shown that steam can efficiently remove volatile or semi-volatile contaminants in any concentration from both saturated and unsaturated porous media (Hunt et al., 1988b; Hadim et al., 1993; Betz et al., 1997; Udell and McCarter, 1998). Two-dimensional studies have shown that also heterogeneous porous media can be remediated by steam injection (Itamura, 1996; She and Sleep, 1999). Full-scale operations have supported these results suggesting that the technique ensures rapid and satisfactory cleanup of even very complicated contaminations (Newmark et al., 1994; Newmark et al., 1998). However, there has been concern that the application of steam injection may lead to downward migration of separate phase contaminant (USEPA, 1995; Sleep and Ma, 1997). This problem is one of the most severe drawbacks of the technology. Especially downward migration of DNAPL (Dense Non Aqueous Phase Liquid) is of great concern since a DNAPL may be able to penetrate the groundwater table. However, also downward migration of LNAPL (Light Non Aqueous Phase Liquid) will pose a problem at sites where the LNAPL resides in the unsaturated zone and has not yet reached the groundwater table. There are two main potential pathways of downward migration, namely downward migration of DNAPL pooled on top of a low permeable layer and downward migration of DNAPL or LNAPL accumulated ahead of the heat front.

When a DNAPL is spilled into the subsurface it migrates downwards until it reaches residual saturation or until it is arrested by a low permeable, water saturated layer. To enter the low permeable layer a pool of DNAPL has to build up until the entry pressure is exceeded. The entry pressure is a function of the interfacial tension and entry is facilitated with decreasing interfacial tension (Kueper and Frind, 1991). In consequence of this it could be expected that the heating of a pooled DNAPL may lead to downward migration since the interfacial tension decreases with increasing temperature (Reid et al., 1987). Sleep and Ma (1997) found 6% decrease in interfacial tension of PCE when the temperature increased from 20 °C to 80 °C and they concluded that downward migration of PCE trapped on low permeable lenses was not a major concern. However, She and Sleep (1998) measured the temperature dependence of capillary pressure-saturation relationships for water and PCE in silica sand and found 50 % decrease in entry pressure in the same temperature interval. This indicates that the entry pressure decreases more than would be expected from the change in interfacial tension alone. Nevertheless, the mechanism is expected to be responsible for downward migration only under very special circumstances when the pressure of the DNAPL is very close to the entry pressure. Additionally, since the width of the heat front is generally very small the pool will begin to evaporate very shortly after heating is initiated.

Downward migration ahead of the heat front occurs because of the way the contaminant is removed during steam injection. When steam is injected into the subsurface it heats up the porous medium and creates a steam zone around the injection point. With time, as more steam is injected, the steam zone expands and the front, separating the steam zone from the surroundings at ambient temperature, moves away from the injection point. Contaminant present in the steam zone volatilizes and condenses again at the heat front where a pool of separate phase contaminant accumulates (Hunt et al., 1988b). As the steam zone advances through the contaminated area more and more contaminant accumulates and the saturation in the pool may exceed the residual saturation. When this occurs the contaminant becomes mobile and can migrate vertically due to gravitational forces. This is mainly a problem in the unsaturated zone where the displaced phase is air.

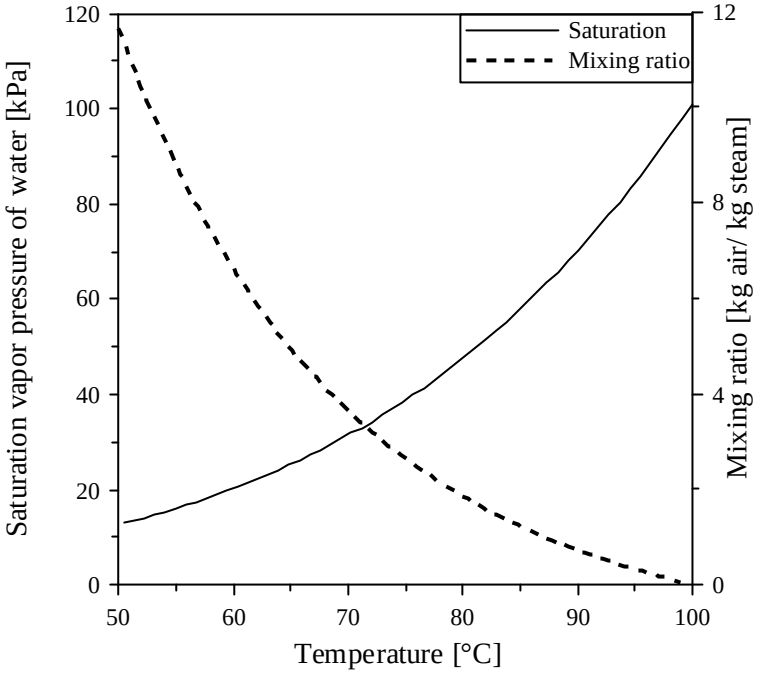

Fig. 1. Vapor pressure of water versus temperature (from ASME (1993)) and temperature of steam-air mixture at atmospheric pressure versus mixing ratio.

The problem has received little attention since in many cases the saturated zone is already contaminated when steam injection is applied in the unsaturated zone. To avoid downward migration of separate phase contaminant it has been proposed to heat up the area below the contamination (USEPA, 1995). Gerdes et al. (1998) showed how an underlying steam zone could arrest downward migration of separate phase contaminant. In two-dimensional experiments PCE was injected in the top of a steam zone where it evaporated. Separate phase PCE penetrated the steam zone when the PCE injection rate was too high compared with the height of the steam zone and the steam injection rate. Three-dimensional modeling was able to simulate the experimental results and could in a given situation be used to find the necessary height of the underlying steam zone when the amount of contaminant migrating downwards was known. However, creating a continuous steam zone from the injection well to the extraction well below the contaminated zone may be difficult to achieve since the steam zone will expand in an isotropic way. Additionally, the exact location and distribution of the non-aqueous phase contamination has to be known when using this strategy. Also the soil volume to be heated and thereby the energy consumption will be larger than necessary.

In the present study the downward migration of NAPL ahead of the heat front is examined experimentally and numerically. Two-dimensional experiments were performed where steam was injected in unsaturated porous media contaminated with a hydrocarbon. Additionally, similar experiments were conducted where a mixture of steam and air was injected. The experiments were analyzed using the numerical code T2VOC (Falta et al., 1995).

Using mixtures of steam and air instead of pure steam allows for a more controlled heating of the subsurface due to variable injection temperatures, which are determined by the mixing ratio of the two components. This may help to prevent

downward migration of separate phase contaminant, which will be demonstrated in this study. Fig. 1 shows the well-known relationship between the saturated vapor pressure of water and temperature. As the temperature rises air can contain more water vapor until the boiling point of water is reached. At this point the vapor pressure of water corresponds to the surrounding pressure and pure water vapor or steam can exist as a single component gas phase. In these experiments a mixture of steam and air was created by mixing atmospheric air at ambient temperature with steam. Subsequently steam will condense and heat up the air to a temperature where all the water vapor can be contained in the gas phase. Since the enthalpy of vaporization of water is very high compared to the heat capacity of air, only a small fraction of the steam will condense and there will be no significant change in the mixing ratio between steam and air. Throughout this paper the mixing ratio will be used to characterize the steam-air mixture instead of the ratio in partial pressures. Fig. 1 also shows the relationship between air to steam mixing ratio and the resulting temperature, which is an inversion of the first curve and a scaling with the ratio between the molecular weights of steam and air. The curve shows how the temperature decreases when more air is mixed with steam but it should be noted that the mixture still has a higher energy content than for instance hot water or dry air due to the high enthalpy of vaporization of water.

Islam and Kaluarachchi (1995) investigated the removal of less-volatile contaminants by the injection of hot air in the temperature interval from 20 °C to 90 °C and relative humidity interval from 10% to 35%. In a numerical study they showed how the removal rate increased compared to normal soil venting. The removal was faster with increasing relative humidity indicating that using a steam-air mixture (relative humidity 100%) may further enhance the effectiveness. Downward migration or flow of separate phase contaminant was not considered by Islam and Kaluarachchi (1995).

2. Experimental materials and methods

Steam and steam-air mixture injection experiments were conducted in a two-dimensional sand box with the interior dimensions 110 x 74 x 8.5 cm (Fig. 2). The sand box was constructed of stainless steel and a front glass panel allowed visual access to the sand. Teflon® and Viton® seals and tubings were used to minimize loss of contaminant. Water inlet and an outlet were located at the bottom left and right hand side of the sand box, respectively. Steam was generated using a 2 kW steam generator and injected into the sand box through three injection ports. The tubing from the steam generator to the sand box was electrically heated, which ensured that the injected steam had a quality of approximately 100%. Effluent gas left the sand box through the extraction port and was passed through a condenser. The condensate was led into a two-stage liquid separator where the contaminant was separated from the water. Non-condensable gases flowed through an activated carbon filter.

During the experiments, injection and extraction pressures were measured using a U-tube water manometer connected to the inflow and outflow ports of the sand box. The sand box was equipped with 100 Pt-100 temperature sensors (Thermokon Sensortechnik GmbH, Mittenaar, Germany) to monitor the heating process (Fig. 2) and additionally the temperatures of the injected and extracted gases were measured.

To minimize heat loss the sand box was insulated during the experiments. The insulation of the front could be rapidly removed for visual inspection and for taking photographs.

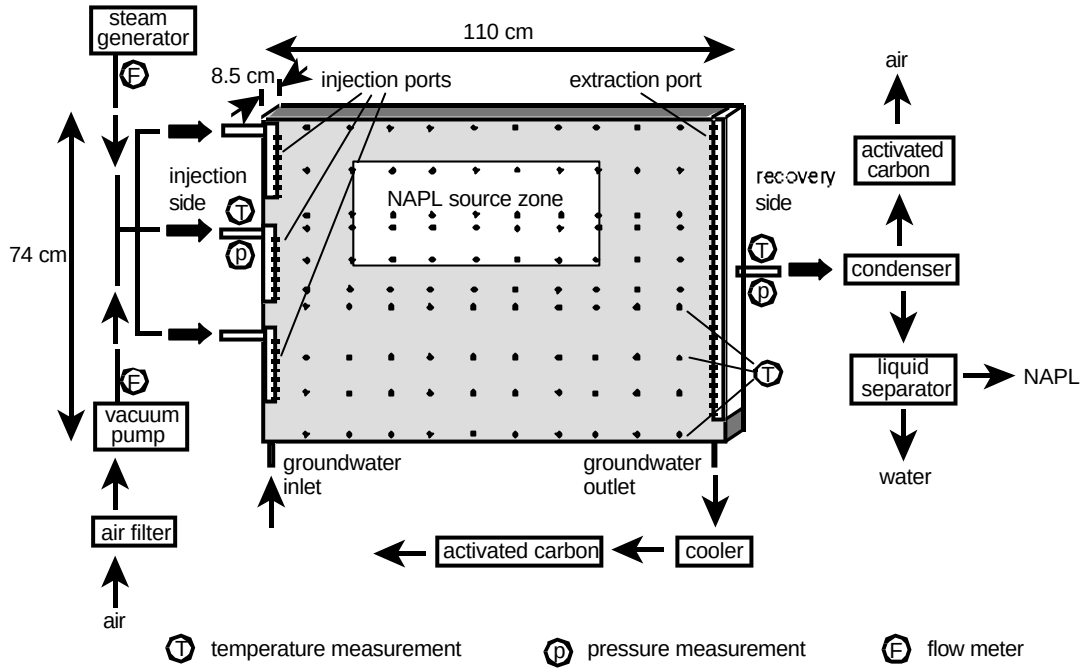

Fig. 2. Schematic of experimental setup

2.1 Porous medium and fluid properties

The porous medium consisted of equal amounts (by weight) of quartz sand #5F and #7 (Gebrüder Dorfner GmbH & Co., Hirschau, Germany). A sieve analysis showed that the mixed sand had grain sizes ranging from 0.5 to 2.0 mm with d_{50} = 1.2 mm. The relationships of the relative permeability and the capillary pressure to the phase saturation were determined using a flow cell and a pressure cell, respectively. In both cases the porosity of the oven dried sand packing was 0.40. To obtain full saturation the dry sample was flushed with CO_2 and saturated from below with degassed water.

The air-water capillary pressure-saturation relationship was measured using the syringe pump method (Wildenschild et al., 1997). Fig. 3 shows the measured primary drainage, main imbibition and secondary drainage paths. The van Genuchten (1980) capillary pressure-saturation model was fitted to the secondary drainage data following the procedure of Liu and Dane (1995).

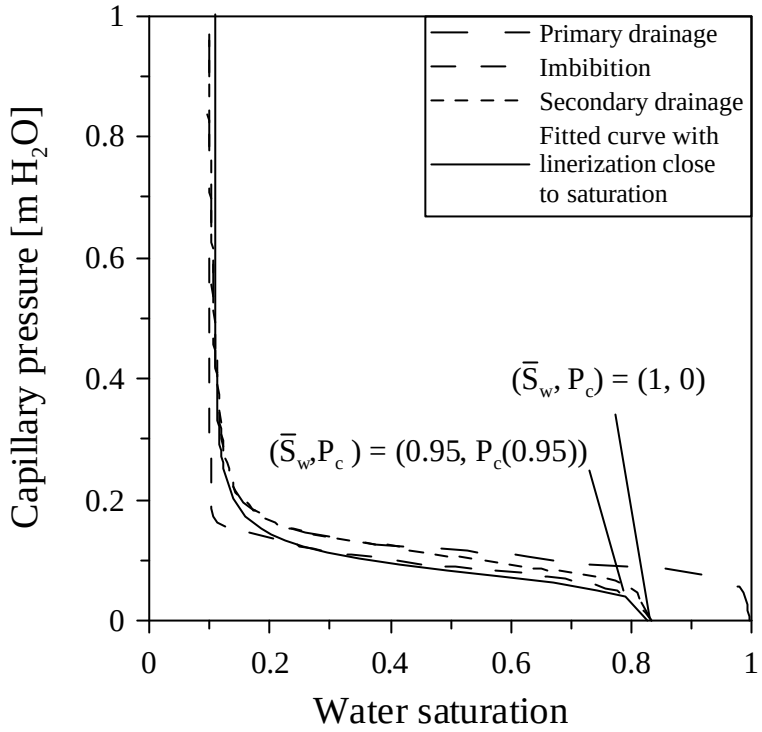

Fig. 3. Experimentally determined capillary pressure-saturation relationship and the fitted curve used in the simulations. Note: The curve is fitted following the procedure of Liu and Dane (1995) and cannot be compared directly to the experimental data.

The absolute permeability was measured to be $5 \cdot 10^{-10}$ m^2. To determine the relative permeability-saturation relationship a displacement experiment was carried out in a flow cell. A mineral oil was used to displace water from the initially water saturated soil sample. By inverse analysis of the measured phase pressures and effluent volumes using the model ITOUGH2 (Finsterle, 1997) the parameters λ and S_{wr} of the following two-phase relative permeability-saturation model were estimated:

$$k_{rw} = (\bar{S}_w)^{(3+2/\lambda)} \quad , \quad k_{rn} = (\bar{S}_n)^2 \left[1 - (\bar{S}_w)^{(1+2/\lambda)}\right]$$

$$\bar{S}_w = \frac{S_w - S_{wr}}{1 - S_{wr}} \quad , \quad \bar{S}_n = \frac{S_n - S_{nr}}{1 - S_{nr}} \qquad \textbf{(1)}$$

where k_r is the relative permeability, S is the saturation, S_{xr} is the residual saturation of phase x and subscript w and n refer to the water- and NAPL-phase, respectively. This model corresponds to the Brooks-Corey-Burdine model (White and Oostrom, 1996) except that a residual NAPL content S_{nr} is included. In the displacement experiment only two-phase primary drainage occured and there was no residual NAPL and consequently $S_{nr} = 0$ was used in the inverse analysis. However in the performed steam and steam-air injection experiments NAPL was entrapped in the unsaturated zone. In the literature there are several explanations on how the NAPL relative permeability can become zero at non-zero saturations in a three-phase system. Hofstee et al. (1997) stated that non-spreading NAPLs at low saturations can break up into microlenses on the water-air interface and thus become discontinuous. Parker and Lenhard (1987) developed hysteretic constitutive relations where NAPL can get entrapped in the water phase during imbibition. Also several authors have shown that it may not always be valid to assume that the porous medium is strongly water-wet (e.g. Powers and Tamblin (1995)) and therefore NAPL could replace residual water.

In order to find a NAPL saturation in a three-phase system below which no NAPL-migration would take place within the time frame of an experiment a series of 1D-experiments was performed where different amounts of dyed mesitylene were mixed with sand at residual water saturation and left to drain in a glass column. The packing procedure was the same as used later in the 2D-experiments and with this procedure it is not possible to distinguish between any of the aforementioned entrapment mechanisms. The saturation where no migration could be visually observed within a period of 48 hours was used as residual NAPL saturation. The determined hydraulic parameters are presented in Table 1.

Table 1. Hydraulic parameters.

Parameter	Value		Measurement method
Capillary pressure function			
n	4.2		Pressure cell
α (m^{-1})	13.2		Pressure cell
S_{wr}	0.11		Pressure cell
S_{gr}	0.17		Pressure cell
	Mesitylene	DCB	
b^{a}_{gn}	1.6	2.1	Calculated (30 °C)
b^{a}_{nw}	2.6	2.0	Calculated (30 °C)
Relative permeability			
λ	4.5		Displacement experiment
S_{wr}	0.06		Displacement experiment
S_{nr}	0.082		Drainage experiment
S_{gr}	0.17		Pressure cell

[a] calculated from: $b_{gn} = \frac{s_w}{s_n}$, $b_{nw} = \frac{1}{1 - \frac{1}{b_{gn}}}$ *and* $s_n = s_w - s_{nw}$

where σ_n is the surface tension (interfacial tension with air) and σ_{nw} is the interfacial tension between water and NAPL. The values have been calculated from measured interfacial tension at 30 °C with dye.

The NAPLs used in the experiments were mesitylene (1,3,5-trimethylbenzene) dyed with 0.9 g·L^{-1} Oil Red O (Sigma Chemical Co., St. Louis, USA) and DCB (1,2-dichlorobenzene) dyed with 1.6 g·L^{-1} Oil Blue N (Sigma Chemical Co., St. Louis, USA). Measurements (Winkler, 2000) showed that the addition of dye did not change the viscosity or density of the NAPL. The interfacial tension between water and NAPL was, however, affected. For mesitylene the interfacial tension decreased as a result of the dye by approximately 23% at 30 °C and 16 % at 90 °C whereas for DCB the interfacial tension increased by approximately 15% at 30 °C and 13% at 90 °C. Relevant chemical and physical properties of the two NAPLs are listed in Table 2. Of importance to these experiments two differences between the compounds should be noted: Mesitylene is more volatile than DCB and mesitylene is an LNAPL whereas DCB is a DNAPL.

Table 2. Physical-chemical properties of NAPLs and water.

	Mesitylene	DCB	Water
Chemical formula	$C_6H_3(CH_3)_3$	$C_6H_4Cl_2$	H_2O
Density at 20 °C [g cm^{-3}]	0.865 [a]	1.306 [a]	0.997 [b]
Vapor pressure at 20 °C [kPa]	0.25 [a]	0.18 [a]	2.3 [b]
Vapor pressure at 100 °C [kPa]	13 [a]	8.5 [a]	101.3 [b]
Boiling point at 101.3 kPa [°C]	164.8 [a]	178.9 [a]	100.0 [b]
Viscosity at 20 °C [N s m^{-2}]	$7.34 \cdot 10^{-4}$ [a]	$1.42 \cdot 10^{-3}$ [a]	$8.91 \cdot 10^{-4}$ [b]
Interfacial tension between water and NAPL at 30 °C [mN m^{-1}]	35.4 (27.8[e]) [c]	31.2 (36.5[e]) [c]	71.20 [d]
Interfacial tension between water and NAPL at 90 °C [mN m^{-1}]	31.3 (26.3[e]) [c]	26.1 (30.0[e]) [c]	60.82 [d]

[a](Reid et al., 1987), [b](Atkins, 1994), [c](Winkler, 2000), [d]Surface tension from ASME (1993), [e] NAPL + dye.

2.2. Experimental procedure

Firstly the sand box was packed with air-dried sand up to a level of 41 cm. The sand was then saturated from below by raising the water table. Subsequently, the water table was lowered to 10 cm above the bottom of the sand box, and the sand was allowed to drain for several hours. After drainage the sand had settled approximately one centimeter. Contaminated sand was prepared by mixing residually water-saturated sand with NAPL to give a NAPL saturation of 0.082 corresponding to the experimentally determined residual saturation for mesitylene. In order to make the experiments comparable the same initial saturations were chosen for the two contaminants by mixing 18 kg of moist sand with 360 g mesitylene and 546 g DCB, respectively. Before mixing, sand and contaminant were cooled to 5°C to minimize mass loss due to evaporation. The well mixed contaminated sand was packed in the sand box to occupy an area of 60 x 25 cm in lateral and vertical dimensions, respectively (Fig. 2) and the remaining space was filled with residually water-saturated sand. Although the contaminated sand was cooled some mass loss due to evaporation may have occurred during mixing and emplacement of the contaminant source.

Before each experimental run the system was allowed to equilibrate for one day with a fixed water table 10 cm above the bottom of the sand box at the left hand side and 8 cm at the right hand side. This ensured initial stationary conditions in the sand box. Ambient temperatures were approximately 20 °C.

Saturated steam was injected into the sand box at an almost constant rate of 1.5 kg h^{-1} during the experiments. The steam flow was monitored with a flow meter and manually adjusted using a flow valve. Due to the high permeability of the sand the injection pressure was only a few centimeters of water column above atmospheric pressure and this corresponded to the measured injection temperature. In the steam-air mixture experiments the air was induced by means of a vacuum pump and mixed with steam before injection. The air flow rate was controlled by monitoring the injection temperature and the steam injection rate was the same as in the pure steam experiments. In the beginning of the steam-air mixture injection experiments the mixing ratio was high (12 kg air to 1 kg steam) and then it was gradually lowered until finally pure steam was injected. With the high mixing ratio the injection pressure was in the order of 15 cm of water column above atmospheric pressure and then decreased with the mixing ratio.

In order to maintain a groundwater flow the fixed head boundary at the inlet side had to be adjusted according to the injection pressures. Only the outflow of groundwater at the extraction side was measured.

3. Experimental results

The results of four experiments are reported. Two experiments with pure steam injection were carried out using mesitylene and DCB, respectively, as contaminants. In order to isolate the effect of injecting air together with steam, two additional experiments were carried out where a steam-air mixture was injected in otherwise similar experimental systems. The operation practice used and the mass recoveries in the four experiments are listed in Table 3.

Table 3. Contaminant, injection mode and mass recovery in the different experiments.

Experiment no.		1	2	3	4
Contaminant		Mesitylene	DCB	Mesitylene	DCB
Operation		Steam	Steam	Steam-air	Steam-air
Recovery (%) as separate phase		89	67	0	0
Recovery (%) in the gas phase	Carbon	0	0	64	25
	Condensate	0	21	29	66

3.1. Steam injection

In the two pure steam injection experiments a steam zone was created above the water table (Fig. 4 a-c). The heat front was almost vertical and it moved with a nearly constant velocity of 35 cmh^{-1} through the sand box. Fig. 5 shows photographs of the contaminant behaviour at two different times during experiment 1. As the contaminated area was heated, the vaporized mesitylene was transported to the heat front where it condensed and accumulated. Mesitylene was visually observed to migrate downwards (t = 50 minutes) and pooled on top of the water table (t = 1 hour and 20 minutes). Mobilized DCB (photographs of experiment 2 not shown) migrated into the saturated zone. 89 % of the emplaced mesitylene was recovered as separate phase liquid from the top of the water table and the remaining part not accounted for was due to losses during this recovery and measurement uncertainties. 67 % of the DCB was recovered as separate phase liquid and 21 % was recovered in the gas phase after steam breakthrough. It should be noted that the total recovery is almost the same for the two compounds even though mesitylene is more volatile suggesting that the mass loss due to evaporation during emplacement is negligible. If this loss had been significant the total recovery rate of mesitylene would have been smaller.

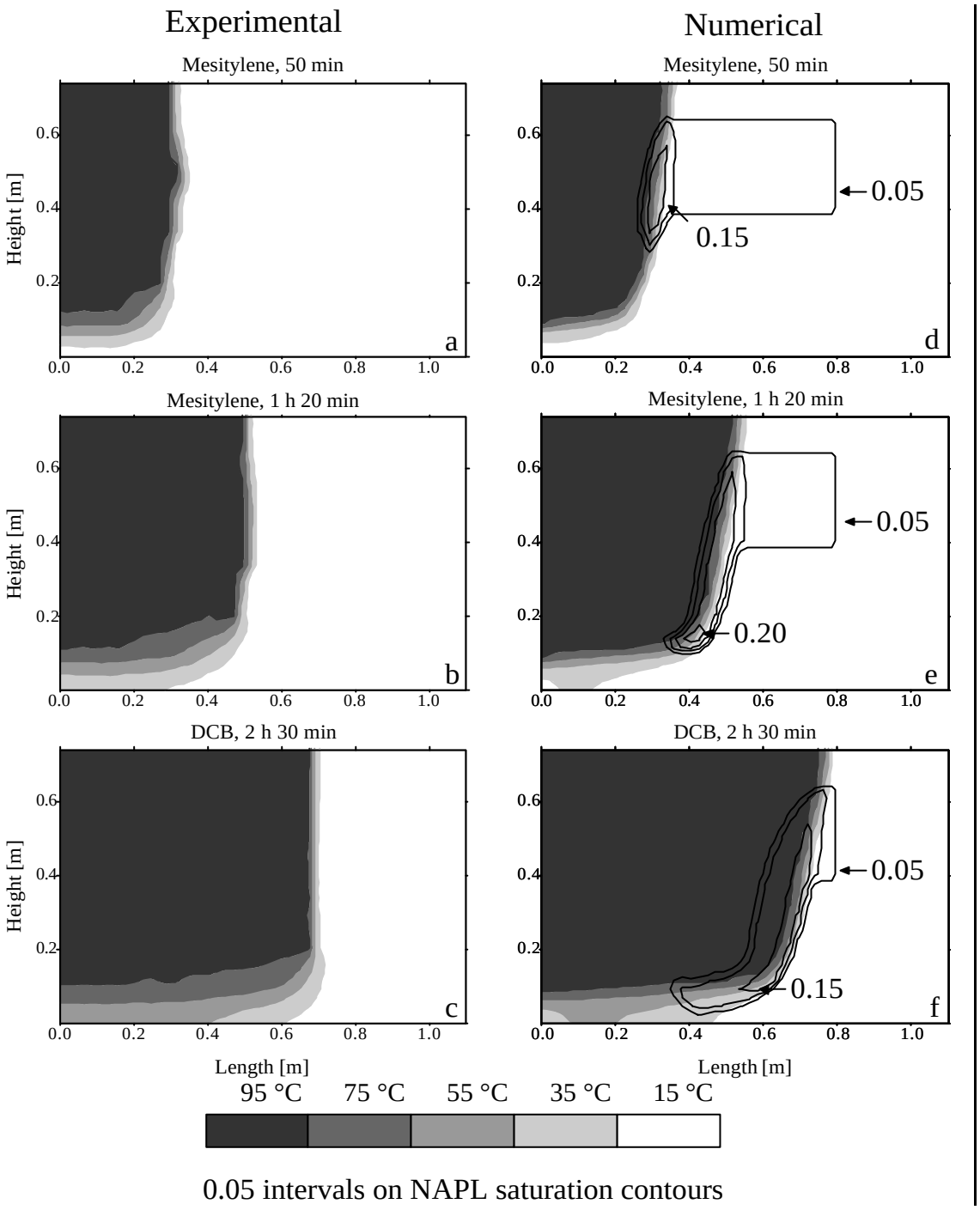

Fig. 4. Experimental and numerical heat zones for pure steam injection at different times. In the plotting procedure of the experimental heat zones it has been assumed that the shape and velocity of the heat front does not change over time and thereby the fine discretization in time can be used to achieve a finer discretization in space.

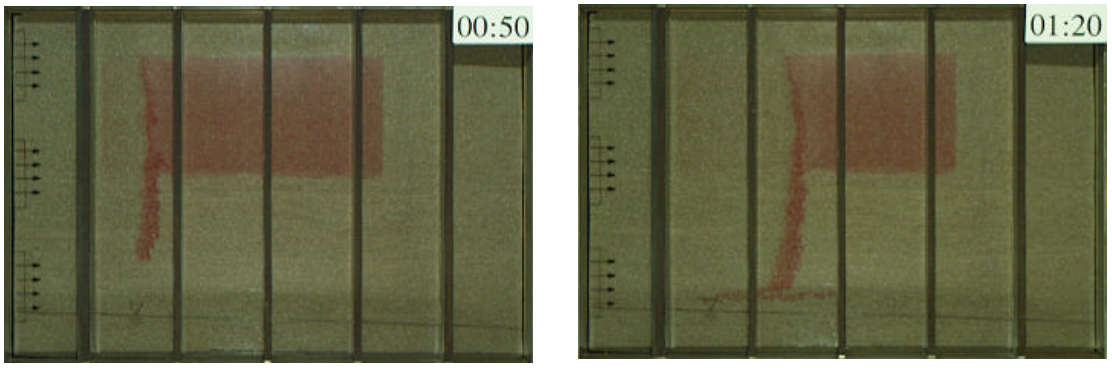

Fig. 5. Mobilization of mesitylene after injecting steam for 50 minutes (left) and 1 hour and 20 minutes (right).

3.2. Steam-air mixture injection

In the steam-air mixture experiments the heated zone developed and propagated quite differently from the pure steam experiments (Fig. 6 a-c). The front of the heated zone was not vertical and it propagated faster in the middle of the sand box. In these experiments all the contaminant was removed in the gas phase and there was no transport of separate phase contaminant to the saturated zone. DCB was removed from the left side of the source without any mobilization in the vertical direction (Fig. 7). In the experiment with mesitylene (photographs not shown) some minor accumulation ahead of the heat front and a few centimeters of downward migration could be observed. In the beginning of the experiments the contaminant was recovered on the activated carbon and after breakthrough of the heated zone the contaminant was also recovered as condensate resulting in a higher removal rate (Fig. 8). 29 % of the mesitylene was removed as condensate and 64 % was removed on the activated carbon whereas 66 % of the DCB was removed as condensate and 25 % on the activated carbon. Also shown on Fig. 8 is the air to steam mixing ratio from experiment 3, which is almost the same as in experiment 4.
After the completion of each experiment soil samples were analyzed and in all cases contaminant concentrations were well below 0.5 mg$\cdot$kg^{-1}.

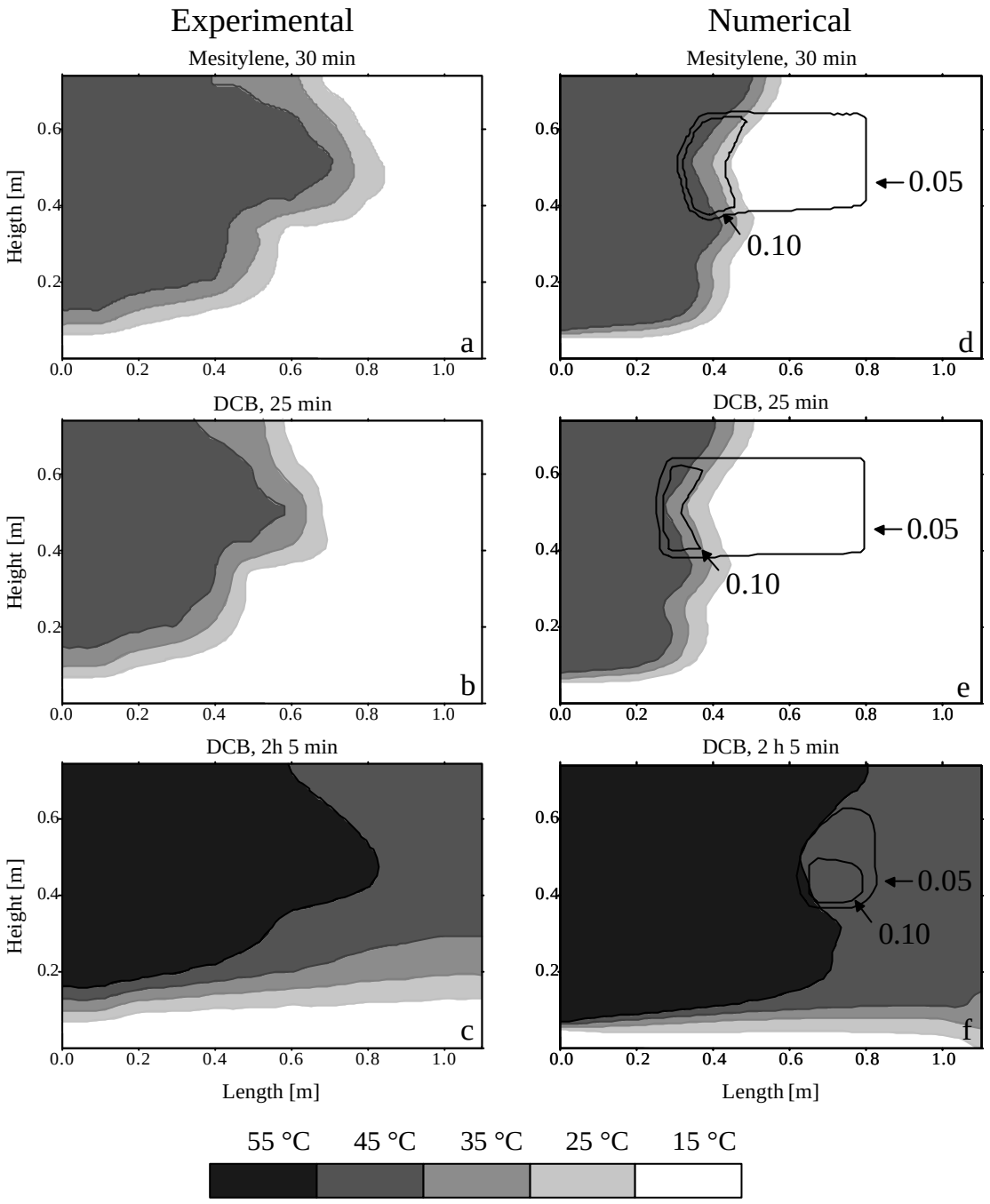

Fig. 6. Experimental and numerical heat zones for steam-air mixture injection at different times.

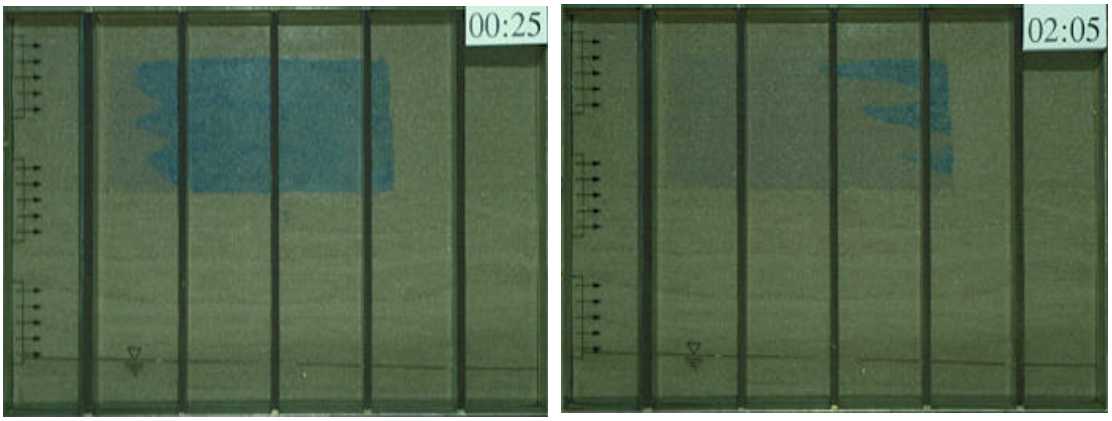

Fig. 7. Removal of DCB by injecting steam-air mixtures (time: 25 minutes (left) and 2 hours and 5 minutes (right) after beginning of injection).

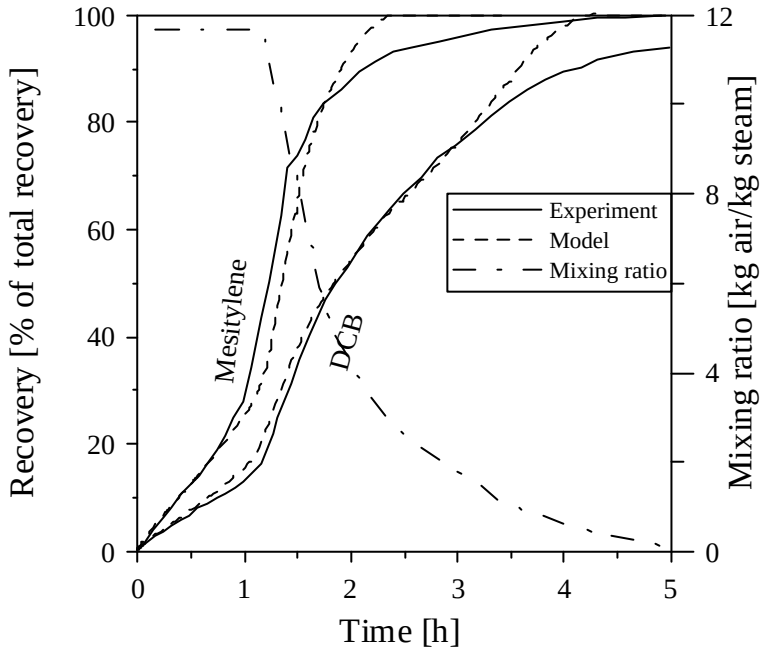

Fig. 8. Experimentally and numerically determined recovery (in % of total recovery) of contaminant in the gas phase from experiment 3 and 4, and the air to steam mixing ratio as a function of time from experiment 3.

4. Numerical simulation

The four experiments were modeled using the numerical code T2VOC (Falta et al., 1995), which is a member of the TOUGH family of codes developed to simulate multidimensional, non-isothermal, multiphase flow and transport in porous media (Pruess, 1987; Pruess, 1991). The code considers simultaneous flow of up to three phases (water, air and NAPL) according to a multiphase extension of Darcy's law. Hydrodynamic dispersion is neglected and only gas phase diffusion is included. Heat transfer occurs due to convection and conduction. Three components (water, air

and contaminant) are partitioned among the phases according to the temperature dependent equilibrium equations except that water in the NAPL phase is neglected. To close the system of equations three mass balances (one for each component) and one energy balance are formulated. The set of equations are solved by integral finite difference techniques.

The sand box was considered as a two-dimensional system and was discretized into cells with dimensions 2 x 2 cm. Because of the dimensions of the contaminated area it was necessary to reduce the vertical dimension to 1 cm for two rows of cells thus, a total of 2090 cells were used to resolve the sand box.

The initial conditions were defined by a sloping water table fixed at a level of 10 cm at the left hand side of the sand box and 8 cm at the right hand side. For the unsaturated zone above the water table stationary conditions were assumed in accordance with the experimental procedure. The cells in the contaminated area were assigned a NAPL saturation of 0.082 corresponding to the amount of NAPL added to the sand box. It was not attempted to correct for a possible mass loss during emplacement of the contaminant source.

The measured steam injection rate was used as a flux boundary condition at the injection side of the sand box. For the steam-air mixture experiments the air injection rate was calculated from the measured injection temperature and the relation between mixing ratio and temperature shown in Fig. 1. The initial injection temperature was 50 °C corresponding to an air to steam mixing ratio of approximately 12 kg of air to 1 kg of steam. Steam and steam-air mixtures were injected into a cell outside the model area, which was connected to the cells at the location of the injection ports in the sand box.

At the right hand side of the sand box, a mixed boundary condition was specified that allowed outflow of a phase when the phase pressure exceeded atmospheric pressure and otherwise the boundary was a no-flux boundary.

The inflow of water to the saturated zone was adjusted by trial and error until simulated temperatures close to the water inlet corresponded to measured temperatures. The measurements of water flowing out from the saturated zone were used to specify a flux boundary condition at the extraction side of the sand box.

During the experiments the sand box was insulated to minimize the heat loss but the frame and glass of the sand box were heated to the same temperature as the porous medium. To account for this heat loss the heat capacity of the sand box was added to the heat capacity of the soil grains. The sand box consisted of 90 kg stainless steel with a heat capacity of 0.5 $kJ \cdot kg^{-1} \cdot K^{-1}$ and 16.8 kg of glass with a heat capacity of 0.83 $kJ \cdot kg^{-1} \cdot K^{-1}$. Adding these two components to the heat capacity of the soil grains gives an effective heat capacity for the soil grains of 1.38 $kJ \cdot kg^{-1} \cdot K^{-1}$ instead of 0.84 $kJ \cdot kg^{-1} \cdot K^{-1}$(quartz sand). Brouwers (1996) used the same procedure when modeling the propagation of a steam zone in a column experiment.

The air-water capillary pressure-saturation relationship defined by the van Genuchten parameters a, n, S_{wr} and S_{gr} determined from the secondary drainage data was used as reference. Adapting the scaling theory proposed by Lenhard and Parker (1987) capillary pressure-saturation relationships for other two-phase combinations (mesitylene-water, mesitylene-air) were derived using the scaling parameters $ß_{gn}$ and $ß_{nw}$ (Table 1) calculated from the measured interfacial tension between water and dyed NAPL. Several authors (Liu and Dane, 1993; Davis, 1994; She and Sleep, 1998) have pointed out that the capillary pressure decreases when the temperature increases and that this temperature effect is larger than would be expected from the changes in interfacial tension alone. It has not been attempted to correct for this in the

simulations since no data were available. To avoid convergence problems in the numerical simulations, the capillary pressure-saturation relationship close to saturation was approximated with a straight line from ($\bar{S}_w$, P_c) = (1, 0) to ($\bar{S}_w$, P_c) = (0.95, $P_c(0.95)$) as shown on Fig. 3.

The three-phase relative permeability-saturation relationships were formulated as an extension of equation (1):

$$k_{rw} = (\bar{S}_w)^{(3+2/l)} \;,\; k_{rg} = (\bar{S}_g)^2 \left[1 - (\bar{S}_t)^{(1+2/l)}\right] \;,\; k_{rn} = (\bar{S}_n)^2 \left[(\bar{S}_t)^{(1+2/l)} - (\bar{S}_w)^{(1+2/l)}\right]$$

$$\bar{S}_w = \frac{S_w - S_{wr}}{1 - S_{wr}} \quad , \quad \bar{S}_n = \frac{S_n - S_{nr}}{1 - S_{nr}} \quad , \quad \bar{S}_g = \frac{S_g - S_{gr}}{1 - S_{gr}} \;,\; \bar{S}_t = \frac{S_w + S_n - S_{wr}}{1 - S_{wr}} \qquad (2)$$

where k_r is the relative permeability, S is the saturation, S_{xr} is the residual saturation of phase x and subscript w, g, n, t refer to the water-, gas-, NAPL-, and total liquid-phase, respectively.

The parameters λ and S_{wr} were determined from the inverse analysis of the displacement experiment; S_{gr} was determined from the water-gas secondary drainage data and S_{nr} from the drainage experiments. To avoid convergence problems for low gas saturations the relative permeability of the gas phase was assigned a finite value (10^{-9}) for $S_g = S_{gr}$ and a linearization was introduced for $10^{-9} < k_{rg} < 10^{-4}$.

We have not used a hysteretic model for the constitutive relationships since we do not know exactly how the NAPL was entrapped. Also, the entrapment mechanisms taking place during the simultaneous condensation of NAPL and water at the heat front are not known.

T2VOC automatically maximizes the time step according to the specified convergence and accuracy criteria. For the pure steam injection experiments the time step was approximately 5 seconds whereas it was approximately 50 seconds for the steam-air mixture injection experiments. This difference in time step reflects the larger gradients in temperature and saturation involved in steam injection compared to steam-air mixture injection.

4.1. Steam injection

The propagation of the heated zone in the model and in the experiment corresponds well for both the mesitylene and the DCB experiments (Fig. 4) suggesting that the model simulates the ratio between injected energy and the energy required to heat the porous medium and the sand box satisfactorily. However, the simulated heat front is less vertical than the experimental one. In the model the heat front propagates slower close to the water table due to the capillary rise of water, which lowers the gas phase permeability and increases the overall heat capacity. This could indicate that the simulated water saturation for a given capillary pressure (height over water table) is too high which may be explained by the temperature effect on the capillary pressure-saturation relationship not taken into account. Another factor that could influence the slope of the heat front is that the energy loss to the sand box itself might not be evenly distributed. In the model the energy used for heating of the sand box is incorporated by increasing the heat capacity of the sand grains. However, in the top of the sand box not only the sides but also the lid was heated and consequently more heat was lost from the porous medium in the upper part. A steeper front in the top would presumably be obtained if the heat capacity was adjusted near the lid. However, the depth over which this adjustment should take place would be a

factor of uncertainty and it was therefore not attempted. The slight discrepancy between the slopes of the heat fronts is not suspected to influence the further analysis.

In accordance with the observations the model simulated downward migration of contaminant just ahead of the heat front (Fig. 4 d-f and Fig. 5). 24 % of the DCB was recovered in the gas phase, which corresponded well to the 21% recovered as condensate in the experiment. No mesitylene was recovered in the gas phase and this difference between the two compounds arises because DCB is less volatile. When steam gets in contact with the NAPL it is assumed that the gas phase immediately gets saturated according to the local equilibrium assumption and therefore NAPL is only removed in the upstream part of the contaminated area. The front where evaporation takes place is termed the evaporation front (Falta et al., 1992) and upstream this front no NAPL is present. The evaporation front propagates with a velocity that is determined by the NAPL vapor pressure, the gas flow and the amount of NAPL initially present (see appendix). Due to the low volatility of DCB this velocity was lower than the velocity of the heat front. Consequently there was a zone between the evaporation front and the heat front where DCB was present. After steam breakthrough at the extraction port the mass present in this zone was recovered in the gas phase.

To evaluate the sensitivity of the parameter S_{nr} a simulation of the experiment with mesitylene was performed with $S_{nr,new} = 2\ S_{nr}$. This affected the flow behaviour of the NAPL by increasing the maximum saturation at the heat front but the contaminant still migrated to the water table. Based on this it can be concluded that even if the true S_{nr} is larger than measured by the drainage experiments the simulations still capture the downward migration.

4.2. Steam-air mixture injection

For the steam-air mixture injection experiments relatively large discrepancies between the simulated and the experimental heat zones are observed (Fig. 6). In all the experiments an abrupt change in the appearance of the heated zone approximately 40 cm above the bottom of the sand box can be observed. This shows a faster heating of the contaminated zone compared to the rest of the sand box whereas the model simulates a slower heating of the contaminated zone. In the model the slower heating is caused by a small accumulation of contaminant ahead of the heat front resulting in reduced gas phase permeability. Because of the flow of non-condensable air, the propagation of the heated zone is also dependent on the permeability ahead of the front when injecting steam-air mixtures. It is, of course, possible that the relative permeability-saturation model used in the simulations reduces the gas phase permeability too much but that cannot explain why the contaminated zone is heated faster than the rest of the sand box in the experiments. Another explanation that has been considered is that the fork-like shape of the connection pipe between the boiler and the injection ports resulted in a higher injection pressure in the port in the middle of the sand box. However, a sensitivity analysis showed that different injection pressures in the injection ports could not alone explain the discrepancy between the model and the experiment. The pressure difference had to be specified unrealistically large to influence the shape of the heated zone, and the observed shape could not be maintained throughout the simulation by adjusting this pressure loss. Instead the discrepancy may be explained by small differences in permeability introduced during the packing of the sand box. The lower 40 cm were packed with dry sand whereas the rest was packed with residually saturated sand and this boundary corresponds closely

to the observed change in velocity of the heat front. Introducing a larger permeability in the contaminated area would increase the propagation of the heat front in this region and thus improve the overall agreement between model and experiments. Even though the packing in the experiments with pure steam was performed in the same way the results did not exhibit any effect from a possible non-uniform packing. This is because a pure steam heat front is less subject to small scale fingering since the heat loss by conduction prevents small channels to develop and that makes the front very stable (Baker, 1973). When injecting steam-air mixtures, fingering is not prevented by conduction heat loss and consequently the steam-air mixture heated zone is much more influenced by heterogeneities than a pure steam heated zone. Variations in permeability on an even smaller scale can be seen on the pictures in Fig. 7 where the evaporation front is far from being a straight vertical line. There seem to be layers of higher permeability where the velocity of the evaporation front is larger, which is due to a larger flow. These layers may have been introduced during the packing when the emplaced sand was compacted.

The simulations showed some minor downward migration (Fig. 6d and 6e), which was most obvious in the experiment with mesitylene and that corresponded to the observed results.

Despite the differences between the simulated and the experimental temperature distribution, the recovery of contaminant in the gas phase corresponds quite well (Fig. 8). Mesitylene has the highest vapor pressure and is therefore recovered faster than DCB. This was also reflected by the fact that more mesitylene was recovered on activated carbon compared to DCB where the greatest part was recovered as condensate after temperature breakthrough (Table 3). At late times the recovery rate in the experiment drops due to a tailing effect not simulated by the model. This tailing effect may be explained by non-equilibrium between the small drops of contaminant and the gas phase due to rate-limited mass transfer (Wilkins et al., 1995; van der Ham and Brouwers, 1998). A crucial assumption in the model is that local equilibrium always prevails and consequently the observed behaviour cannot be captured by the model.

Even though heat loss in the top of the sand box, heterogeneous packing and non-equilibrium between phases at low contaminant saturation are not considered in the simulations they nevertheless provide an acceptable overall representation of the experimental results, thus allowing for a closer analysis of the mechanisms involved.

5. Discussion

The experiments clearly document that downward migration ahead of the heat front may be a serious side effect when pure steam is injected for remediation of the unsaturated zone. Even though the performed experiments may be considered a worst-case scenario since the contaminant saturation in the sand box was close to residual throughout the contaminated area, it gives rise to serious concerns that the total amount of mesitylene and most of the DCB migrated to the saturated zone. When the evaporation front is not lacking behind the heat front, which will be the case for highly volatile contaminants, the total mass of contaminant between the injection well and the extraction well will be accumulated at the front. Since the width of the front is generally very small this results in a dramatic increase in the NAPL saturation. If we consider a two-dimensional field scale problem where the distance between injection and extraction is 5 m and the total mass of NAPL is accumulated within a 10 cm wide

front the NAPL saturation would be 50 times the mean initial NAPL saturation when the front reaches the extraction. Therefore the mean initial NAPL saturation has to be below 1/50 of the residual saturation in order to avoid downward migration. This indicates that it is not only at heavily contaminated sites that downward migration will be a problem of serious concerns.

When the injected steam was mixed with air the downward migration of separate phase contaminant to the groundwater zone was prevented for the investigated cases and the total amount of contaminant was recovered in the gas phase.

5.1 Mechanisms preventing downward migration

The numerical simulations allow for a closer examination of the differences between the two injection modes and for an evaluation of the mechanisms that may prevent downward migration. For both steam injection and steam-air mixture injection, the contaminant is volatilized in the heated zone and transported in the gas phase to the front of the heated zone where it condenses as the temperature decreases. However, when co-injecting air some of the contaminant is transported with non-condensable air beyond the heat front.

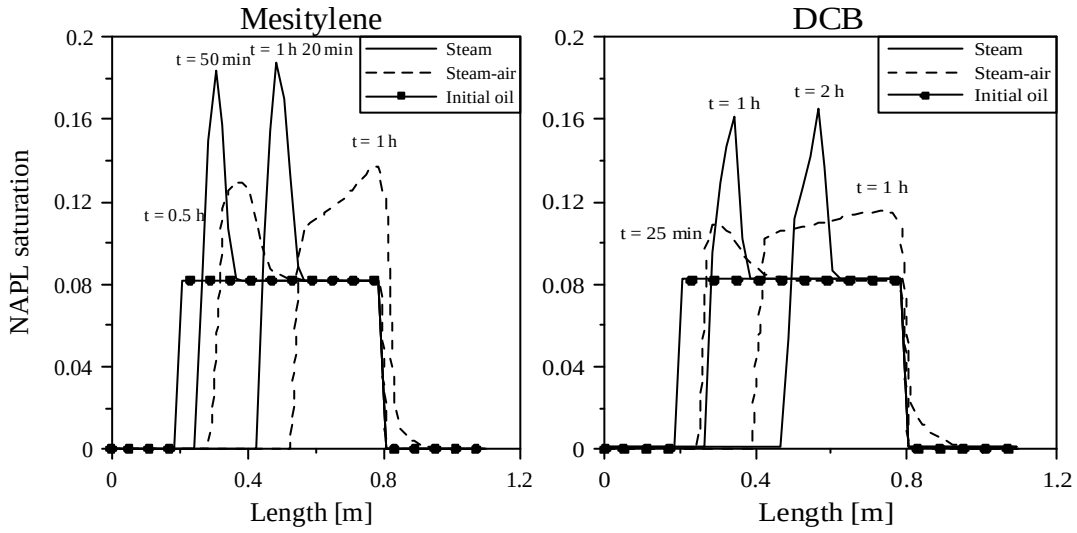

Fig. 9. Horizontal NAPL saturation profiles at various times from the modeling of experiment 1 and 3 (left) and 2 and 4 (right).

The model predicts that 19 % of the mesitylene and 11 % of the DCB has already been removed when heating of the downstream end of the contaminated area is initiated. As expected more mesitylene is removed since it is more volatile.

Fig. 9 compares the simulated accumulation of NAPL in the steam experiments and the steam-air mixture experiments at different times for the two contaminants. Pure steam injection results in high peaks in NAPL saturation both for mesitylene and DCB whereas the peaks are lower and wider when injecting steam-air mixtures. The peaks appear because NAPL condenses at the heat front, but when injecting steam-air mixtures the heat front is wider and consequently the peaks are wider too. Additionally, the velocity of the evaporation front is lower than the velocity

of the heat front in both the mesitylene and the DCB experiment when injecting steam-air. This can be seen because the peaks get wider as the front moves through the contaminated area and the effect is most dominant for DCB with the lowest vapor pressure.

All in all, three mechanisms preventing downward migration can be identified from these experiments: (1) removal of contaminant with the non-condensable air, (2) more spatially distributed accumulation of contaminant due to less steep temperature gradients and (3) lower velocity of evaporation front compared to the velocity of heat front.

In full-scale cleanup operations there might be an additional mechanism not directly shown by these experiments that further limits downward migration. When NAPL is present in small-scale heterogeneities the removal may be slow and limited by diffusion when injecting steam-air mixtures. This means that only a part of the total mass will accumulate and this can be compared to the effect of the reduced velocity of the evaporation front. When injecting pure steam, boiling will occur and the removal will be limited by heat conduction and advective flow out of the heterogeneities, which are faster mass transfer processes than diffusion (De Voe and Udell, 1998).

5.2 Mixing ratio

The mixing ratio of air to steam used in the experiments is unrealistically high to use at field scale cleanup operations. Normally, the maximum pressure that can be applied to the injection well limits the mass injection rate and consequently when the mixing ratio increases more air is injected in lieu of steam. This means that the time needed to heat a porous medium increases with the mixing ratio. When the heating time increases so does the necessary energy input and the total cost of the remediation. However, the effectiveness of the mechanisms preventing downward migration is also a function of the mixing ratio, which will be illustrated by looking at the mechanisms one by one.

The first mechanism was the removal of contaminant with the non-condensable air before heating of the contaminated area. The removal is dependent on the vapor pressure of the contaminant at initial temperature and the airflow through the porous medium before heating. The airflow can be calculated by considering a simple energy balance (see appendix). In Fig. 10 the airflow in terms of number of pore volumes flushed before heating is shown as a function of the mixing ratio. Even though the porous medium will reach a lower temperature when the mixing ratio increases the heating is slower and more pore volumes have to be flushed. As more pore volumes are flushed the velocity of the heat front will necessarily decrease with increasing mixing ratio.

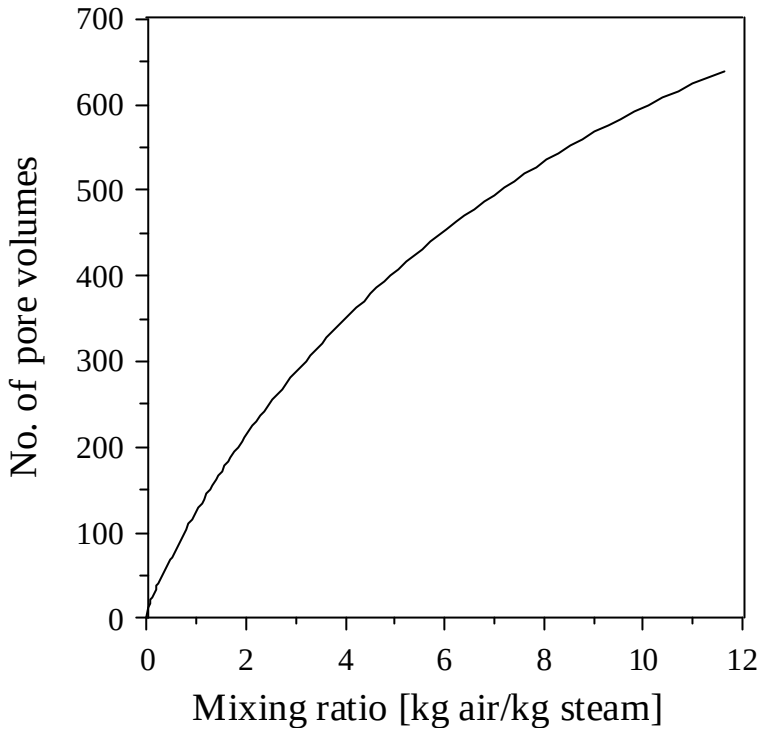

Fig. 10. Number of pore volumes of air being flushed before the soil reaches injection temperature as a function of mixing ratio. The values that have been used in the calculation are: $\phi = 0.4$, $S_w = 0.2$, $c_r = 0.84$ kJ kg^{-1} K^{-1}, $\rho_r = 2650$ kg m^{-3}, $c_w = 4.2$ kJ kg^{-1} K^{-1}, $\rho_w = 1000$ kg m^{-3}, $\rho_a = 1.2$ kg m^{-3} and $T_i = 20$ °C.

The second mechanism was the increased width of the heat front, which can be explained by differences in the condensation processes. When steam is injected into a porous medium it condenses if the temperature is below steam temperature. This means that the condensation takes place exactly at the heat front. The only mechanisms that can extend the heat front in space are heat conduction and any forward flow of condensate. When injecting steam-air mixtures, condensation will take place when the temperature is below the equilibrium temperature of the mixture defined by the mixing ratio. The implication of this may be illustrated by considering the movement of a steam-air mixture through a sequence of infinitesimal volumes of porous medium. In the first volume steam will condense until thermal equilibrium between the steam-air mixture and the porous medium exist. The steam-air mixture, now colder and with a new mixing ratio, will move to the next volume where condensation again will take place. This gives a spatially extended condensation zone where the temperature changes from the injection temperature to the temperature of the surroundings. Consequently, the heat front gets wider when injecting steam-air mixtures and the width increases with the initial mixing ratio. Moreover, since the velocity of the heat front decreases, smoothing of the front by heat conduction is more significant. To illustrate the dependence of the front width on the mixing ratio a series of T2VOC simulations have been performed for different mixing ratios. The model setup (sand box, sand type, discretization, initial conditions etc.) is the same as previously used, except that the contaminant has been removed and a constant injection pressure equivalent to 3 cm of water column defines the injection boundary condition. The characteristic width of the front has been calculated at 40 cm from the injection side as the distance between the point where the temperature is 2 °C below the injection temperature and the point where it is 2 °C above the temperature of the

surroundings. In Fig. 11 the results are shown as the front width normalized to the width for pure steam as a function of the mixing ratio. The figure also shows the relative front velocity calculated as the front velocity when injecting a steam-air mixture normalized by the front velocity when injecting pure steam. The simulation results show that the width increases while the velocity decreases when more air is injected.

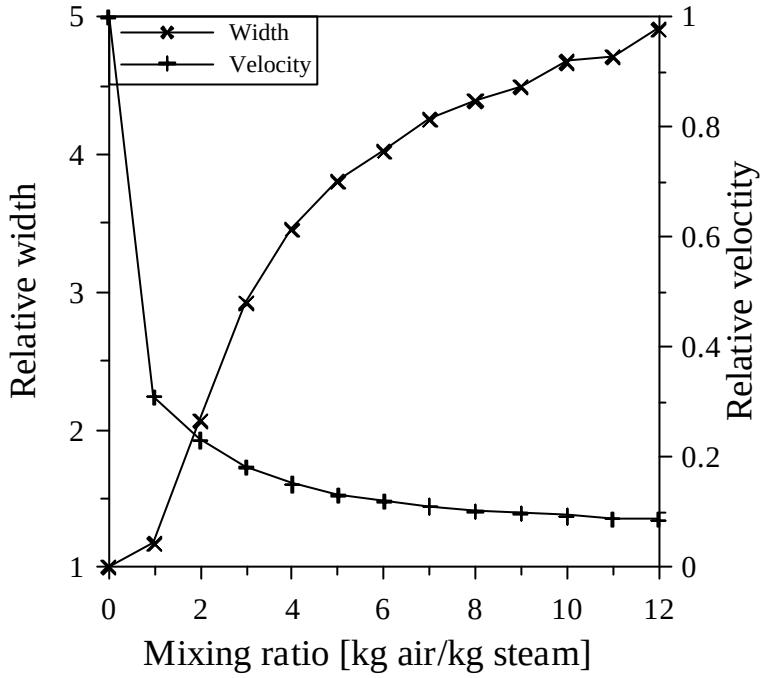

Fig. 11. Simulated relative width and velocity of the heat front as a function of mixing ratio. Width and velocity for injection of pure steam are both set to 1.

The third mechanism responsible for reducing downward migration was the reduced velocity of the evaporation front compared to the velocity of the heat front. The two velocities can be calculated from fairly simple energy balance equations presented in the appendix. In order to reduce the accumulation of NAPL the ratio between the velocity of the evaporation front and the heat front has to be below 1. The functional dependency of this ratio on the mixing ratio has been calculated for both mesitylene and DCB (Fig. 12). To facilitate comparison with the experiments the ratio has been calculated for two heat capacities: a standard heat capacity of soil and the effective heat capacity that includes boundary effects from the sand box. Since mesitylene is more volatile a larger mixing ratio is required to sufficiently reduce the evaporation velocity. The figure shows that the ratio for DCB is above one at pure steam injection (mixing ratio = 0) with the high heat capacity; yet in the experiment some DCB was recovered after steam breakthrough indicating that the heat front propagated faster than the evaporation front. This discrepancy arises because the equation does not take the NAPL accumulation ahead of the front into account where more NAPL than the initial saturation has to evaporate. However, the figure illustrates that the mechanism is only effective under special conditions, which will be very difficult to evaluate, and that the effectiveness increases with the mixing ratio.

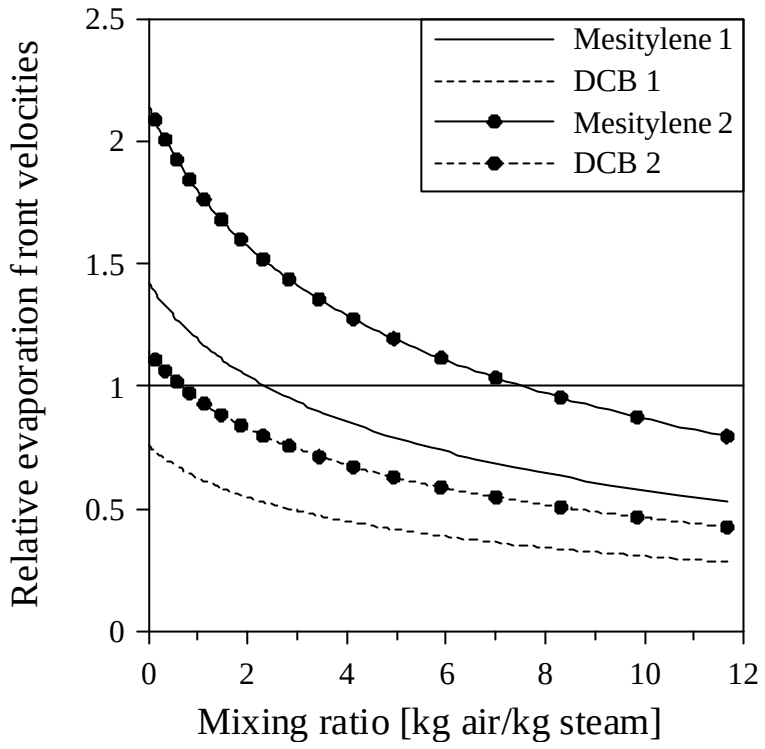

Fig.12. Ratio of front (evaporation and heat) velocities for two situations with different heat capacities: 1 heat capacity of soil (c_r = 0.84 kJ kg^{-1} K^{-1}), 2 heat capacity corresponding to effective heat capacity used in the modeling of the experiments (c_r = 1.38 kJ kg^{-1} K^{-1}).

These derivations illustrate qualitatively how the mechanisms preventing downward migration depend on the mixing ratio. In a field scale clean up of the unsaturated zone where downward migration cannot be allowed it would be of great interest to find the minimal mixing ratio preventing downward migration since cleanup time and costs increase with mixing ratio. In general downward migration out of the heated zone is determined by the following factors: 1) initial NAPL saturation and distribution, 2) residual NAPL saturation, 3) velocity of heat front, 4) velocity of evaporation front, 5) velocity of downwards migrating NAPL, and 6) distance between injection and extraction well.

To accurately determine the optimal mixing ratio factors 1) to 5) should in fact all be known at the pore scale with the initial and residual NAPL saturation being the most critical parameters. As such information is unrealistic to obtain at field scale it will be very difficult to estimate the optimal mixing ratio.

6. Conclusions

Steam and steam-air mixture injection experiments were performed in a two-dimensional sand box to remediate unsaturated porous media contaminated by two different NAPLs.

The numerical code T2VOC was able to provide a satisfying simulation of the experimental results based on independently measured parameters suggesting that such models are helpful for designing and interpreting steam injection.

The pure steam injection experiments demonstrated downward migration of accumulated NAPL ahead of the heat front in the unsaturated zone suggesting the

phenomenon will be a major concern with regard to field scale operations. The steam-air mixture injection experiments showed that downward migration can be avoided when mixing steam and air as a consequence of three mechanisms:
1) the non-condensable air will remove some of the contaminant and consequently less NAPL can accumulate.
2) the temperature gradient at the heat front is less steep implying that the area where the contaminant condenses is larger.
3) the velocity of the evaporation front is lower than the velocity of the heat front and consequently it is not the total mass of NAPL that accumulates at the front.

These mechanisms are all dependent on the mixing ratio of air and steam. Unfortunately, it will be very difficult to estimate the optimal mixing ratio to be used in a given field problem because a number of factors would have to be known at the pore scale.

List of symbols

a	air to steam mixing ratio
c_x	heat capacity of x [$kJ \cdot kg^{-1} \cdot K^{-1}$]
d_{50}	mean grain size diameter [mm]
E	energy [kJ]
H	enthalpy of evaporation of water [$kJ \cdot kg^{-1}$]
k_{rx}	relative permeability of phase x
M_n	molecular weight of NAPL [$g \cdot mol^{-1}$]
$\dot{m}_t$	mass injection rate per cross-sectional area [$kg \cdot s^{-1} \cdot m^{-2}$]
m_x	mass of x [kg]
n	van Genuchten capillary pressure-saturation model parameter
P_c	capillary pressure [m^{-1}]
P_{vap}	vapour pressure of NAPL [Pa]
PV	number of pore volumes
S_x	saturation of phase x
S_{xr}	residual saturation of phase x
$\bar{S}_x$	effective saturation of phase x
T	temperature [K / °C]
V	volume [m^3]
v_{evap}	velocity of evaporation front [$m \cdot s^{-1}$]
v_{heat}	velocity of heat front [$m \cdot s^{-1}$]

Subscripts

a	air
g	gas
i	initial
n	NAPL
r	soil grain
s	steam
s-a	steam-air
w	water

Greek letters

α	van Genuchten capillary pressure-saturation model parameter [m^{-1}]

β_{gn} gas-NAPL scaling factor
β_{nw} NAPL-water scaling factor
ϕ porosity
λ relative permeability-saturation model parameter
ρ_x density of x [kg·m^{-3}]

Appendix. Derivation of equations

A.1. Number of pore volumes of air flushed before heating

The energy, E, needed to heat a volume, V, of soil to a temperature, T, can be calculated from (Hunt et al., 1988a):

$$E = V(T - T_i)(c_r \rho_r (1 - f) + \rho_w c_w S_w f) = V(T - T_i)\overline{\rho c} \quad \text{(A1)}$$

where T_i is the initial temperature, c_r and ρ_r is the heat capacity and density of the soil grains, c_w and ρ_w is the heat capacity and density of water, ϕ is the porosity, S_w is the water saturation in the heated zone and $\overline{\rho c}$ is an overall heat capacity. The heating of air or NAPL is neglected.
The energy released when injecting steam into a porous medium with the temperature, T_i, can be calculated from (Hunt et al., 1988a):

$$E = m_s (H + (T - T_i) c_w) \quad \text{(A2)}$$

where m_s is the mass of steam, H is the enthalpy of vaporization of water and T is the steam temperature. When a steam-air mixture is injected the mixture temperature T(a), which is a function of the mixing ratio, $a = \frac{m_a}{m_s}$ where m_a is the mass of air and m_s is the mass of steam, should be inserted instead.
The mass of steam required to heat a volume of porous medium to a temperature T(a) can be calculated by setting equation A1 equal to A2:

$$m_s = \frac{m_a}{a} = \frac{V(T(a) - T_i)\overline{\rho c}}{H + (T(a) - T_i)c_w} \quad \text{(A3)}$$

By dividing with the density of air, ρ_a, and rearranging the equation can be transformed to:

$$\frac{V_a}{V} = \frac{a(T(a) - T_i)\overline{\rho c}}{\rho_a (H + (T(a) - T_i)c_w)} \quad \text{(A4)}$$

where V_a is the volume of air flowing through a volume of soil before it reaches the temperature T(a).
By dividing this expression with the air filled porosity it can be calculated how many times the pore volume of air is changed:

$$PV = \frac{a\left(T(a)-T_i\right)\overline{rc}}{f\,(1-S_w)\,r_a\left(H+(T(a)-T_i)\,c_w\right)} \qquad \text{(A5)}$$

where PV is the number of pore volumes
This equation is plotted as a function of mixing ratio in Fig. 10.

A.2. Velocity of fronts

When combining equation A2 with A1 the heated volume of soil can be calculated:

$$V = \frac{m_t}{a+1}\,\frac{H+(T(a)-T_i)c_w}{(T(a)-T_i)\cdot\overline{rc}} \qquad \text{(A6)}$$

where $m_t = m_a + m_s = m_s(a+1)$
By defining $\dot{m}_t$ as the total mass injection rate divided by the cross-sectional area the equation can be used to find the velocity of the heat front:

$$v_{heat} = \frac{\dot{m}_t}{a+1}\,\frac{H+\left(T(a)-T_i\right)c_w}{\left(T(a)-T_i\right)\overline{rc}} \qquad \text{(A7)}$$

The velocity of the NAPL evaporation front v_{evap} is a function of the vapor pressure of the NAPL, the flow and the NAPL saturation (Falta et al., 1992). When local equilibrium is assumed it can be calculated from:

$$v_{evap} = \frac{\dot{m}_t}{r_{s\text{-}a}(a)}\,\frac{P_{vap}(a)\,M_n}{R\,T(a)\,f\,S_n\,r_n} \qquad \text{(A8)}$$

where $\rho_{s\text{-}a}$ is the density of the steam-air mixture which is a function of the mixing ratio, P_{vap}, M_n, S_n and ρ_n is the vapor pressure, molecular weight, saturation and density of the NAPL respectively and R is the universal gas constant.

The ratio of A8 to A7 is plotted as a function of mixing ratio in Fig. 12. When calculating the vapor pressure of the NAPL in A8 the reduced temperature in the evaporation zone due to the three-phase conditions has been used. This temperature reduction occurs when the saturated steam air mixture comes into contact with the NAPL and a portion of the steam component condenses. The energy released during condensation vaporizes the contaminant. This leads to a mixture of three components in the gas phase. The sum of the partial pressures of the steam component and the chemical component in the gas mixture is equal to the partial pressure of steam in the injected steam air mixture before entering the contaminant source. These processes result in a temperature reduction in the evaporation zone, which is illustrated in Fig. A1 for injection temperatures between 50°C and 100°C for mesitylene and DCB.

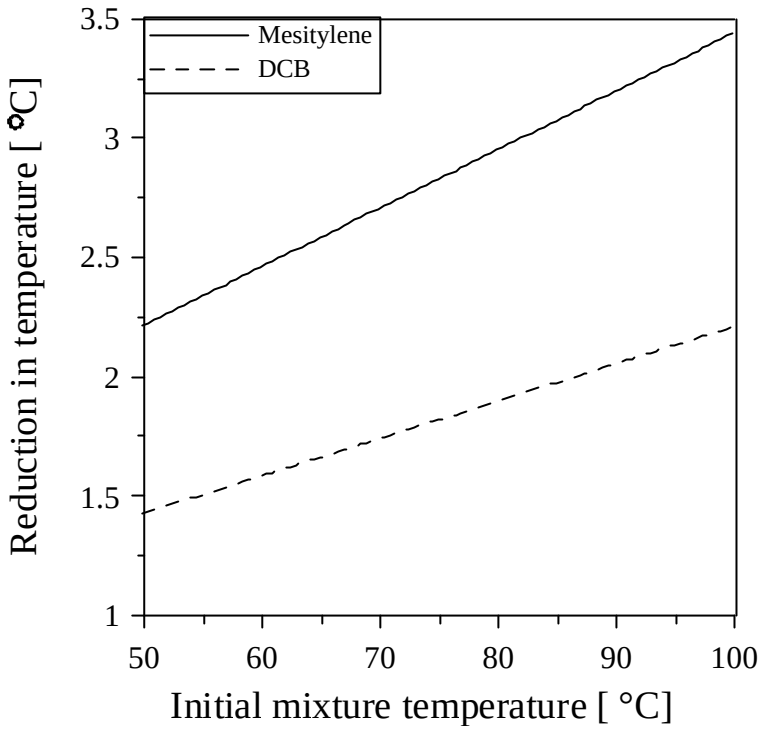

Fig. A1. Reduction in temperature during evaporation of mesitylene and DCB as a function of the initial temperature.

References

ASME, 1993. ASME Steam Tables. Thermodynamic and Transport Properties of Steam. 6. ed. The American Society of Mechanical Engineers, New York.

Atkins, P. W., 1994. Physical Chemistry. Oxford University Press, Oxford, Melbourne, Tokyo. 1994.

Baker, P.E., 1973. Effect of pressure and rate on steam zone development in steamflooding, Society of Petroleum Engineers Journal, 13: 274-284.

Betz, C., Färber, A. and Schmidt, R., 1997. Lab and technical scale experiments for NAPL removal by steam injection into porous media. In: Groundwater: An Endangered Resource. Proc. of Theme C, 27th IAHR Congress. San Franciso, USA, pp. 101-106. American Society of Civil Engineers.

Brouwers, H. J. H., 1996. An experimental study of constant-pressure steam injection and transient condensing flow in an air-saturated porous medium. Journal of Heat Transfer, 118: 449-454.

Committee on Ground Water Cleanup Alternatives, 1994. Alternatives for Ground Water Cleanup. National Academy Press, Washington, D. C. 1994.

Danish EPA, 1999. Vakuumventileringssager fra Oliebranchens Miljøpulje. Miljø- og Energiministeriet, Miljøstyrelsen. In Danish.

Davis, E. L., 1994. Effect of temperature and pore size on the hydraulic properties and flow of a hydrocarbon oil in the subsurface. Journal of Contaminant Hydrology, 16:55-86.

De Voe, C. and Udell, K. S.,1998. Themodynamic and Hydrodynamic Behavior of Water and DNAPLS During Heating. Proceedings of First International Conference on Remediation of Chlorinated and Recalcitrant Compounds. Monterey, USA, pp. 61-66. Batelle Press. Columbus, Ohio.

Falta, R. W., Pruess, K., Javandel, I. and Witherspoon, P. A., 1992. Numerical modeling of steam injection for the removal of nonaqueous phase liquids from the subsurface, 2. Code validation and application. Water Resources Research, 28: 451-465.

Falta, R. W., Pruess, K., Finsterle, S. and Battistelli, A., 1995. T2VOC User's Guide. Lawrence Berkeley Laboratory Report, LBL-36400 University of California, Berkeley.

Finsterle, S., 1997. ITOUGH2 User's Guide Version 3.1. Lawrence Berkeley Laboratory Report, LBL-40041,UC-400 University of California, Berkeley.

Gerdes, K. S., Kaslusky, S. and Udell, K. S., 1998. Containment of downward migration of DNAPLS during steam enhanced extraction. Proceedings of First International Conference on Remediation of Chlorinated and Recalcitrant Compounds. Monterey, USA, pp. 31-36. Batelle Press. Columbus, Ohio.

Hadim, A., Shah, F. H. and Korfiatis, G. P., 1993. Laboratory studies of steam stripping of LNAPL-contaminated soils. Journal of Soil Contamination, 2: 27-58.

Ho, C. K. and Udell, K. S., 1992. An experimental investigation of air venting of volatile liquid hydrocarbon mixtures from homogeneous and heterogeneous porous media. Journal of Contaminant Hydrology, 11: 291-316.

Hofstee, C., Dane, J. H., and Hill, W. E. 1997. Three-fluid retention in porous media involving water, PCE and air. Journal of Contaminant Hydrology, 25: 235-247.

Hunt, J. R., Sitar, N. and Udell, K. S., 1988a. Nonaqueous phase liquid transport and cleanup, 1. Analysis of mechanisms. Water Resources Research, 24: 1247-1258.

Hunt, J. R., Sitar, N. and Udell, K. S., 1988b. Nonaqueous phase liquid transport and cleanup, 2. Experimental studies. Water Resources Research, 24: 1259-1269.

Islam, K. M. Mesbah-Ul and Kaluarachchi, J. J., 1995. Thermal venting to recover less-volatile hydrocarbons from the unsaturated zone, 2. Model applications. Journal of Contaminant Hydrology, 17: 313-331.

Itamura, M. T., 1996. Removal of chlorinated hydrocarbons from homogeneous and heterogeneous porous media using steam. UMI Dissertation Services, Ann Arbor MI.

Kueper, B. H. and Frind, E. O., 1991. Two-phase flow in heterogeneous porous media 2. Model application. Water Resources Research, 27: 1059-1070.

Lenhard, R. J. and Parker, J. C., 1987. Measurement and prediction of saturation-pressure relationships in three phase porous media systems. Journal of Contaminant Hydrology, 1: 407-424.

Liu, H. H. and Dane, J. H., 1993. Reconciliation between measured and theoretical temperature effects on soil water retention curves. Soil Science Society of America Journal. 57: 1202-1207.

Liu, H. H. and Dane, J. H., 1995. An improved computational procedure for retention relations of immiscible fluids using pressure cells. Soil Science Society of America Journal. 59: 1520-1524.

Newmark R. and various authors, 1994. Dynamic underground stripping project. Lawrence Livermore National Laboratory, UCRL-ID-116964-V-1-4.

Newmark, R. L.., Aines, R. D., Knauss, K. G., Leif, R. N., Chiarappa, M., Hudson, B., Carraigan, C., Tompson, A., Richards, J., Eaker, C., Wiedner, R., and Sciarotta, T., 1998. In situ destruction of contaminants via hydrous pyrolysis/oxidation: Visalia field test. Lawrence Livermore National Laboratory, UCRL-ID-132671.

Parker, J. C. and Lenhard, R. J., 1987. A model for hysteretic constitutive relations governing multiphase flow 1. Saturation-pressure relations. Water Resources Research, 23: 2187-2196.

Powers, S. E., and Tamblin, M. E., 1995. Wettability of porous media after exposure to synthetic gasolines. Journal of Contaminant Hydrology, 19: 105-125.

Pruess, K., 1987. TOUGH User's Guide. Lawrence Berkeley Laboratory Report, LBL-20700 University of California, Berkeley.

Pruess, K., 1991. TOUGH2 - A general purpose numerical simulator for multiphase fluid and heat flow.. Lawrence Berkeley Laboratory Report, LBL-29400 University of California, Berkeley.

Rathfelder, K., Yeh, W. W-G., Mackay, D., 1991. Mathematical simulation of soil vapor extraction systems: model development and numerical examples. Journal of Contaminant Hydrology, 8: 263-297.

Reid, R. C., Prausnitz, J. M. and Poling, B. E., 1987. The properties of gases and liquids. McGraw-Hill, New York.

She, H. Y. and Sleep, B. E., 1998. The effect of temperature on capillary pressure-saturation relationships for air-water and perchloroethylene-water systems. Water Resources Research, 34: 2587-2597.

She, H. Y. and Sleep, B. E., 1999. Removal of perchloroethylene from a layered soil system by steam flushing. Ground Water Monitoring and Remediation, 19: 70-77.

Sleep, B. E.and Ma, Y., 1997. Thermal variation of organic fluid properties and impact on thermal remediation feasibility. Journal of Soil Contamination, 6: 281-306.

Udell, K. S. and McCarter, R. L., 1998. Steam enhanced extraction of wood treatment chemicals from soils. Proceedings of First International Conference on Remediation of Chlorinated and Recalcitrant Compounds. Monterey, USA, pp. 121-126. Batelle Press. Columbus, Ohio.

U.S. Environmental Protection Agency, 1995. In Situ Steam Enhanced Recovery Process, Hughes Env. Systems, Inc., Innovative Technology Evaluation Report, EPA/540/R-94/510.

van der Ham, A. G. J. and Brouwers, H. J. H., 1998. Modeling and experimental investigation of transient, nonequilibrium mass transfer during steam stripping of a nonaqueous phase liquid in unsaturated porous media. Water Resources Research, 34: 47-54.

van Genuchten, M. T., 1980. A closed-form equation for predicting the hydraulic conductivity of unsaturated soils. Soil Science Society of America Journal, 44: 892-898.

White, M. D., and Oostrom, M., 1996. Subsurface Transport Over Multiple Phases. Theory Guide. Pacific Northwest National Laboratory. Richland, Washington.

Wildenschild, D., Høgh Jensen, K., Hollenbeck, K.J., Illangasekare, T.H., Znidarcic, D., Sonnenborg, T. and Butts, M.B., 1997. Two-stage procedure for determining unsaturated hydraulic characteristics using a syringe pump and outflow observations. Soil Science Society of America Journal, 61: 347-359.

Wilkins, M. D., Abriola, L. M., and Pennell, K. D., 1995. An experimental investigation of rate-limited nonaqueous phase liquid volatilization in unsaturated porous media: Steady state mass transfer. Water Resources Research, 31: 2159-2172.

Winkler, A., 2000. Unpublished laboratory data, Institut für Wasserbau, Universität Stuttgart, Germany.

Remediation of NAPL below the water table by steam induced heat conduction

Gudbjerg, J. [a], Sonnenborg, T. O. [a], Jensen, K. H. [b]

[a] Environment & Resources DTU, Technical University of Denmark
[b] Geological Institute, University of Copenhagen

Submitted to Journal of Contaminant Hydrology

Abstract

Previous experimental studies have shown that NAPL will be removed when it is contacted by steam. However, in full-scale operations steam may not contact the NAPL directly and this is the situation addressed in this study. A two-dimensional intermediate scale sand box experiment was performed where an organic contaminant was emplaced below the water table at the interface between a coarse and a fine sand layer. Steam was injected above the water table and after an initial heating period the contaminant was recovered at the outlet. The experiment was successfully modeled using the numerical code T2VOC and the dominant removal mechanism was identified to be heat conduction induced boiling of the separate phase contaminant. Subsequent numerical modeling showed that this mechanism was insensitive to the porous medium properties and that it could be evaluated by considering only one-dimensional heat conduction.

Keywords: Steam injection, Remediation, Sand box models, Modeling, Boiling

1. Introduction

Steam injection is a promising technology for remediating subsurface hydrocarbon contamination. Full-scale clean-up operations have suggested that the technique ensures rapid and satisfactory clean-up of even very complicated contaminations (Newmark et al., 1994; Newmark et al., 1998). Several one-dimensional laboratory experiments have shown that volatile NAPL will rapidly vaporize when it contacts with steam (Hunt et al., 1988; Hadim et al., 1993; Betz et al., 1997). Two-dimensional laboratory studies have shown that heterogeneous porous media can also be remediated by steam injection (Itamura, 1996; She and Sleep, 1999). In these experiments the steam zone eventually occupied the entire sand pack and the emplaced NAPL was completely removed. Thus, the investigations suggest that the soil volume contacted by steam will be cleaned. However, if NAPL is present in a low permeable heterogeneity or in a saturated zone, steam may not contact directly. This will significantly reduce the removal rate, but remediation may still be

orders of magnitude faster than with other technologies. The focus of this study is to quantify the removal when steam does not contact the contaminant directly. Specifically, we address the situation where a steady-state steam zone overlies a saturated zone contaminated with NAPL. This is a very common situation in a full-scale application of steam injection. When injecting steam below the water table a steam zone will tend to move upwards due to buoyancy and may override a part of the contamination, e.g. when a DNAPL is pooled on top of a low permeable layer. Likewise, Schmidt et al. (2002) showed how injection of pure steam in an unsaturated zone containing NAPL could lead to downward migration resulting in a lens of LNAPL residing between the steam zone and the water table. In these cases there will be no steam flow through the contaminated soil and the only heating mechanism will be conduction from the overlying steam zone. At a certain temperature, below the normal boiling point of water, the two immiscible liquids will boil because the sum of their individual vapor pressures will equal the surrounding pressure (Atkins, 1994). The produced gas will, due to buoyancy, be transported from the saturated zone into the steam zone where it can be extracted. In clean-up operations limited by conduction a performance assessment should not be based on the steam zone development, which would provide a too optimistic estimate of the clean-up time.

The objective of this study is to examine the removal mechanisms when steam is not in direct contact with NAPL. A two-dimensional intermediate scale sand box experiment was conducted where separate phase TCE (TriChloroEthylene) was emplaced below the water table at the interface between a coarse and a fine sand layer. Steam was injected above the water table and the remediation process was monitored by measurements of temperature inside the box and recovery of contaminant at the outlet. The experimental data were interpreted with the numerical code T2VOC that subsequently was used for analyzing the involved processes in details.

2. Materials and methods

2.1 Experimental setup

Fig. 1 illustrates the experimental setup. The sand box had the interior dimensions 122 x 8.5 x 58 cm and was constructed of stainless steel with a front glass cover allowing for inspection of the sand packing. During the experiment the sand box was insulated to minimize heat loss. The sand box was equipped with 98 Pt-100 temperature sensors connected to a data acquisition system that continuously logged the temperature. At the location of the bottom row of temperature sensors, pressure transducers were hydraulically connected to the sand packing allowing for continuous measurements of pressure. A well divided into four sections allowed injection of steam at different levels at the left side; however, in this experiment only the uppermost section was used. An extraction well screened over the entire depth was located at the right side. The bottom of the extraction well was connected to a moveable water reservoir outside the sand box, which ensured a fixed hydraulic head. Water flowing out of the sand box was measured continuously on an electronic balance. At the top of the extraction well, gas flowed out and was cooled to ambient temperature in a condenser. The condensed liquid was collected in a phase separator and non-condensable gas was led through an activated carbon filter. Water was removed from the top of the phase separator via an overflow tube and weighed. The

inlet of the overflow tube was located 2 cm below the water table to avoid removing small droplets of TCE that were able to float on the water surface. From the bottom of the phase separator a tube was connected to a bottle where the condensed TCE was collected. This tube was filled with TCE during the entire experiment and by opening a valve condensed TCE could flow from the phase separator into the bottle, which was subsequently weighed. Thus, the system was closed to prevent evaporative losses. It was only possible to measure separate phase TCE with this system and no measurements of dissolved TCE were performed.

Steam was generated in a steam generator and led into the sand box via electrically heated tubing that ensured a steam quality of approximately 100%. The steam injection rate was measured with a flow meter. Steam pressure and temperature were measured just before the inlet.

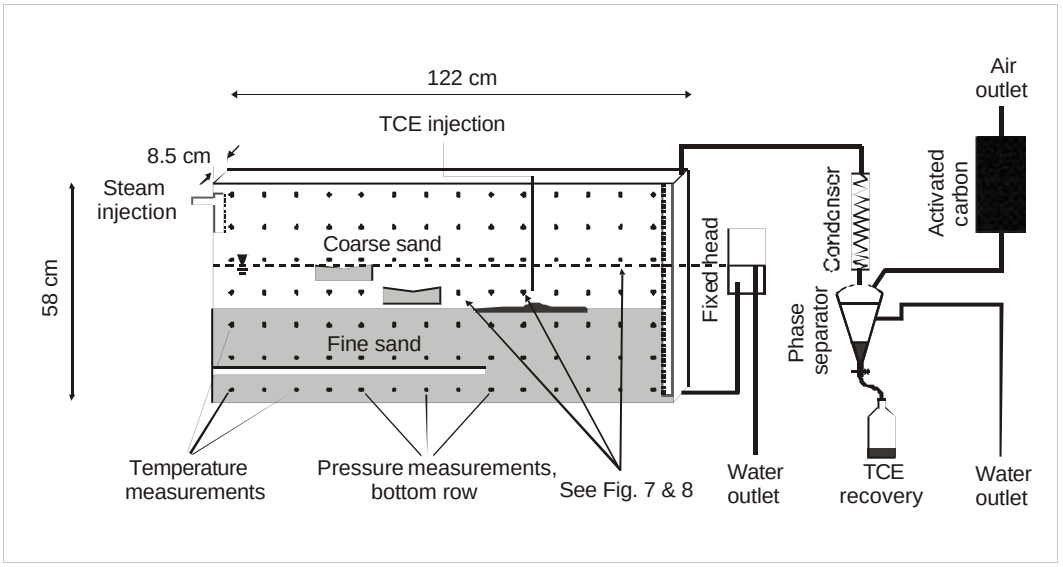

Fig 1. Schematic of experimental setup.

2.2 Porous media

Two types of uniform quartz sand (grain density: 2650 kg m^{-3} (Incropera and DeWitt 1996)) were used in the experiment: coarse sand with an absolute permeability of $1.8 \cdot 10^{-9}$ m^2 and fine sand with an absolute permeability of $9 \cdot 10^{-12}$ m^2 ("#5F" and "GEBA", respectively, Gebrüder Dorfner GmbH & Co., Hirschau, Germany). For the two sand types the primary drainage air-water capillary pressure-saturation relationship was measured using the syringe pump method (Wildenschild et al., 1997). To obtain full saturation, the dry sample was initially flushed with CO_2 and subsequently saturated from below with degassed water. The porosity of the sample was 0.40. The Brooks and Corey (1966) capillary pressure-saturation model was fitted to the data following the procedure of Liu and Dane (1995) that corrects for a vertically non-uniform water distribution within the sample.

2.3 Experimental procedure

The sand was packed in layers of 3 cm below the water table to avoid entrapment of air. During packing the level of the water table was gradually increased so it was always at least 2 cm above the top of the sand packing. To ensure a constant fall distance the sand was poured through a tube (80 cm long). No visible layering

was present within the two sand types. The lower 25 cm of the sand box was packed with the fine sand and the upper part was packed with coarse sand. At a distance of 70 cm from the left, a 1 cm deep and 30 cm long depression was made in the fine sand to accommodate the NAPL to be emplaced. Furthermore, two lenses of fine sand were built into the coarse layer and a lens of coarse sand was built into the fine layer. These lenses were built in for a subsequent experiment and they had no influence on this experiment. The porosities of the fine and coarse layers were 0.39 and 0.41, respectively. During packing the temperature sensors were withdrawn from the box and they were subsequently pushed into the middle of the sand packing. The top of the sand pack was sealed with a 5 cm thick layer of a mixture of bentonite and sand. This ensured that no preferential flow path developed between the sand packing and the lid.

After packing, the water table was lowered to 33 cm above the bottom of the box. A thin stainless steel tube had been installed during packing from the top of the sand box to 5 cm above the bottom of the depression in the fine sand. Through this tube 69 g of TCE was injected. To avoid injection of air below the water table the tube was initially water filled by extracting a small amount of water. After TCE was injected the tube was flushed with water to ensure that no TCE remained in the tube. When the experiment had been terminated, it was visually ensured that the TCE distributed throughout the depression by repeating the injection procedure with dyed TCE.

The sand box was equilibrated for 24 hours before steam injection was initiated. Steam was injected in the top section of the injection well (46 to 56 cm above the bottom of the sand box) at a constant rate of 1.2 kg $hour^{-1}$ for the first 1½ hour and then adjusted to 1.0 kg $hour^{-1}$ for the rest of the experiment. When separate phase TCE appeared in the phase separator it was carefully let out and weighed every 10 minutes. After approximately 10 and 12 hours of steam injection the water table was lowered to 28 and 26 cm above the bottom of the sand box, respectively. When TCE no longer condensed in the phase separator the water table was lowered to a few centimeters above the bottom of the box and the entire sand packing was heated to steam temperature but no more TCE was recovered.

2.4 Numerical setup

The experiment was modeled using the numerical code T2VOC (Falta et al., 1995), which is a member of the TOUGH family of codes developed to simulate multidimensional, non-isothermal, multiphase flow and transport in porous media (Pruess, 1987; Pruess, 1991). The code considers simultaneous flow of up to three phases (water, gas and NAPL) according to a multiphase extension of Darcy's law. Hydrodynamic dispersion is neglected and only gas phase diffusion is included. Heat transfer occurs due to convection and conduction. Three components (water, air and contaminant) are partitioned among the phases according to the temperature dependent equilibrium equations except that water in the NAPL phase is neglected. To close the system of equations three mass balances (one for each component) and one energy balance are formulated. The set of equations are solved by integral finite difference techniques. The original code was slightly modified to account for the distinct entry pressure when using the Brooks and Corey formulation for the capillary pressure-saturation relationship.

The sand packing was discretized into a two-dimensional (2-D) grid containing 7076 gridblocks with the dimensions 1 x 8.5 x 1 cm. The measured steam

injection rate was applied as a flux boundary condition at the injection side of the sand box. Steam was injected into a gridblock outside the model area, which was connected to the gridblocks at the location of the injection port in the sand box. A column of high permeable gridblocks with zero capillary pressure simulated the extraction well where outflow of water was allowed at the bottom against a constant hydraulic head and at the top outflow of gas against atmospheric pressure was allowed. The layer of bentonite was simulated by a single row of gridblocks with zero permeability. A 1-D simulation of 24-hour drainage from full saturation to a water table located 33 cm above the bottom provided the initial conditions. Furthermore, the gridblocks in the depression were assigned a TCE saturation of 0.45, which summed to the same mass as injected in the experiment.

No transient heat loss was accounted for; however, the heat capacity of the sand box materials were added to the heat capacity of the soil grains to account for the heating of the sand box. The sand box consisted of 64 kg stainless steel with a heat capacity of 0.5 kJ kg^{-1} K^{-1} and 15.8 kg of glass with a heat capacity of 0.78 kJ kg^{-1} K^{-1}. Adding these two components to the heat capacity of the soil grains gave an effective heat capacity of 1.2 kJ kg^{-1} K^{-1} instead of 0.75 kJ kg^{-1} K^{-1} (quartz sand, Incropera and DeWitt (1996)).

The heat conductivity coefficients of the wet and dry sand were calculated from the following empirical equations (Sundberg, 1988):

$$\begin{aligned} Kh_{wet} &= Kh_w^{\phi} \cdot Kh_{quartz}^{1-\phi} \\ Kh_{dry} &= 0.034\phi^{-2.1} \end{aligned} \qquad \textbf{(1)}$$

where Kh_w = 0.57 W m^{-1} K^{-1}, Kh_{quartz} = 7.7 W m^{-1} K^{-1} and ϕ is the porosity (Table 1).

The heat conductivity coefficient as a function of saturation was calculated by the following equation (Falta et al., 1995):

$$Kh(S_w) = Kh_{dry} + (Kh_{wet} - Kh_{dry}) \cdot \sqrt{S_w} \qquad \textbf{(2)}$$

In gridblocks containing NAPL, the heat conductivity of NAPL was added to the overall heat conductivity coefficient. Bentonite was assigned a heat capacity of 0.75 kJ kg^{-1} K^{-1} and a heat conductivity coefficient of 2 W m^{-1} K^{-1}, regardless of saturation. The experimentally determined air-water capillary pressure-saturation relationship was described by the Brooks and Corey model. Adapting the scaling theory proposed by Lenhard and Parker (1987) capillary pressure-saturation relationships for other two-phase combinations (TCE-water, TCE-air) were derived using the scaling parameters ß$_{gn}$ and ß$_{nw}$ calculated from the interfacial tension between water and TCE (Table 1). Several authors (Liu and Dane, 1993; Davis, 1994; She and Sleep, 1998) have pointed out that the capillary pressure decreases when the temperature increases and that this temperature effect is larger than would be expected from the changes in interfacial tension alone. It has not been attempted to correct for this in the simulations since no data were available. The following formulations of the three-phase relative permeability-saturation relationships based on Brooks and Corey-Burdine were used (White and Oostrom, 1996):

$$\begin{aligned} &k_{rw} = \overline{S}_w^{\frac{2+3\lambda}{\lambda}}, \quad k_{rn} = \overline{S}_n^2\left(\overline{S}_l^{\frac{2+\lambda}{\lambda}} - \overline{S}_w^{\frac{2+\lambda}{\lambda}}\right), \quad k_{rg} = \overline{S}_g^2\left(1 - \overline{S}_l^{\frac{2+\lambda}{\lambda}}\right) \\ &\overline{S}_w = \frac{S_w - S_{wr}}{1 - S_{wr}}, \quad \overline{S}_n = \frac{S_n}{1 - S_{wr}}, \quad \overline{S}_l = \frac{S_w + S_n - S_{wr}}{1 - S_{wr}}, \quad \overline{S}_g = \frac{S_g}{1 - S_{wr}} \end{aligned} \qquad \textbf{(3)}$$

where S is saturation and index w, n, l, g and r refer to water, NAPL, total liquid, gas and residual, respectively.

Physical-chemical properties of TCE were taken from Reid et al. (1987).

Table 1. Soil parameters.

Parameter	Coarse sand	Fine sand
Permeability	$1.8 \cdot 10^{-9}$ m^2	$9 \cdot 10^{-12}$ m^2
Porosity	0.39	0.41
Brooks and Corey pore distribution index, λ	5.4	4.55
Brooks and Corey entry pressure, P_e	4.1 cm	62 cm
Residual water content, S_r	0.05	0.12
Scaling parameter, gas-NAPL, β_{gn}	2.14[a]	2.14[a]
Scaling parameter, NAPL-water, β_{nw}	1.88[a]	1.88[a]
Heat conductivity coefficient, wet, Kh_{wet}	2.6 W m^{-1} K^{-1}	2.8 W m^{-1} K^{-1}
Heat conductivity coefficient, dry, Kh_{dry}	0.23 W m^{-1} K^{-1}	0.23 W m^{-1} K^{-1}

[a] calculated from: $\beta_{gn} = \frac{\sigma_w}{\sigma_n}$, $\beta_{nw} = \frac{1}{1 - \frac{1}{\beta_{gn}}}$

where σ is the surface tension (interfacial tension with air) and subscripts w and n refer to water and NAPL, respectively. Surface tension of TCE and water from Stephens (1996).

Full upstream weighting between gridblocks was used for permeability and mobility. The heat conductivity coefficient was arithmetically averaged. Interface density was arithmetically averaged to calculate the gravity term and upstream weighted to calculate flow. However, during the last part of the simulation the weighting factor for density was slightly changed due to numerical convergence problems (see discussion in Appendix A).

The simulation of the steam injection experiment required approximately 27 hours of computer time on a 2 GHz Pentium 4 PC.

3. Results

The injection of steam created a zone with steam temperature in the upper part of the coarse sand layer with convection as the dominant heat transfer process. A vertical steam front, where the temperature rapidly changed from steam temperature to the temperature of the surroundings, moved with a constant velocity through the sand box. Fig. 2 compares the measured and the simulated temperature after 1, 2 and 3 hours of steam injection. The experimental and simulated temperature compare well showing that the model captures the overall heat balance satisfactorily suggesting that it is indeed not necessary to include the transient heat loss. Note that the distance between temperature sensors in the experiment was 8.5 cm resulting in a more coarse resolution on the contour plots of the experiment. After 2.5 hours of steam injection, steam broke through at the extraction side. At this time the steam zone had reached steady-state and further heating of the porous media was only due to conduction and flow of condensate. The lower limit of the steam zone was the boundary between unsaturated and saturated conditions. Because of the high permeability of the coarse sand the injection pressure was low and steam could not displace much water.

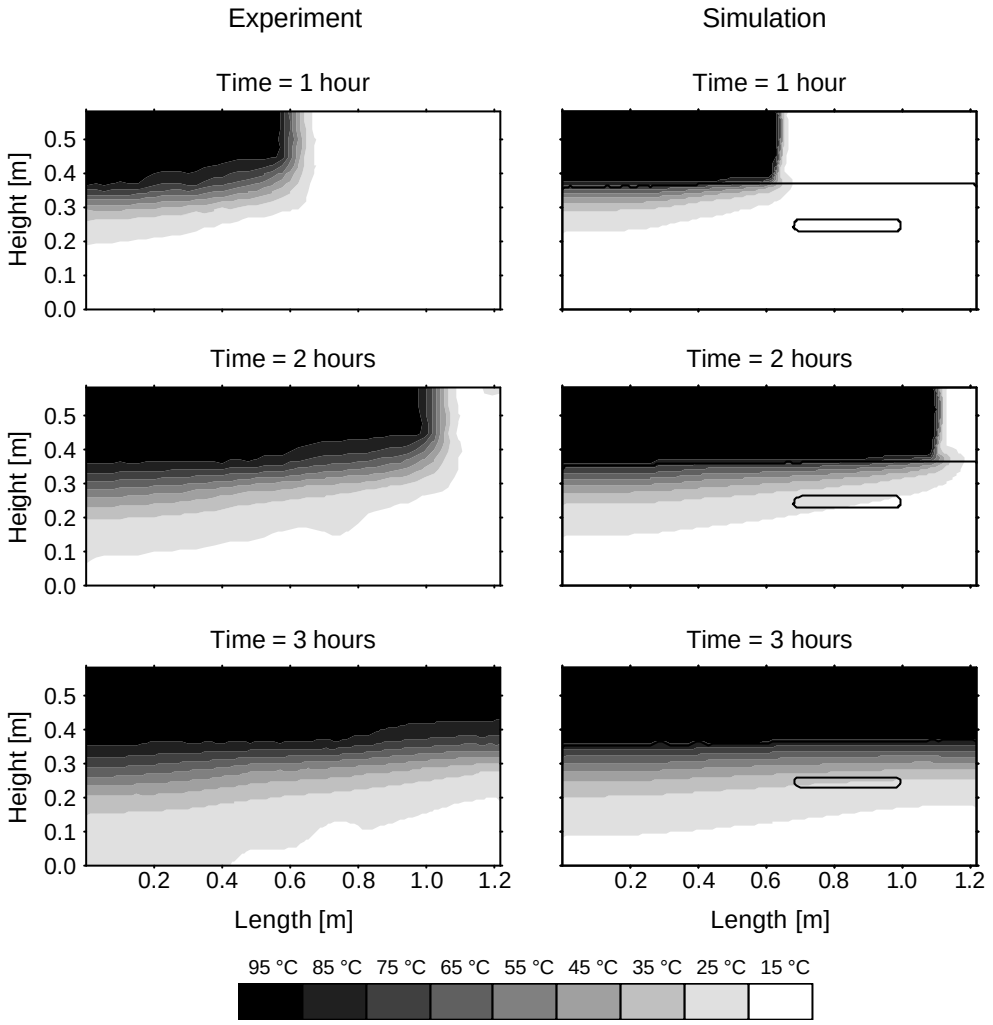

Fig 2. Contour plots of temperature from experiment and simulation. The black line on the simulation plots indicate where the water saturation is larger than 0.98, thus also indicating the emplaced NAPL.

This is seen in Fig. 3 showing the measured and simulated injection pressure. The fluctuations in the measurements were caused by the steam delivery system and reflect the unstable nature of steam where heat loss leads to condensation and pressure loss. The model slightly underestimated the injection pressure, which may be caused by either an underestimation of the steam injection rate or an overestimation of the permeability to the gas phase in the coarse sand. The "global" shifts in pressure were caused by the reduction in injection rate (1½ hour), the steam breakthrough (2½ hour) and the lowering of the water table (~10 and 12 hours). Fig. 3 also indicates that the steam zone was at steady-state after steam breakthrough, as the average injection pressure was almost constant. The slight increase in pressure occurred because less steam was condensing as the temperature below the steam zone increased, thus leading to an overall larger flow. The injection pressure corresponded to approximately 2 cm of water column implying that the water table was suppressed 2 cm at the injection side of the sand box. The almost horizontal water table is also revealed on the contour plot of temperature after 3 hours (Fig. 2) where the abrupt change in temperature indicates the water table.

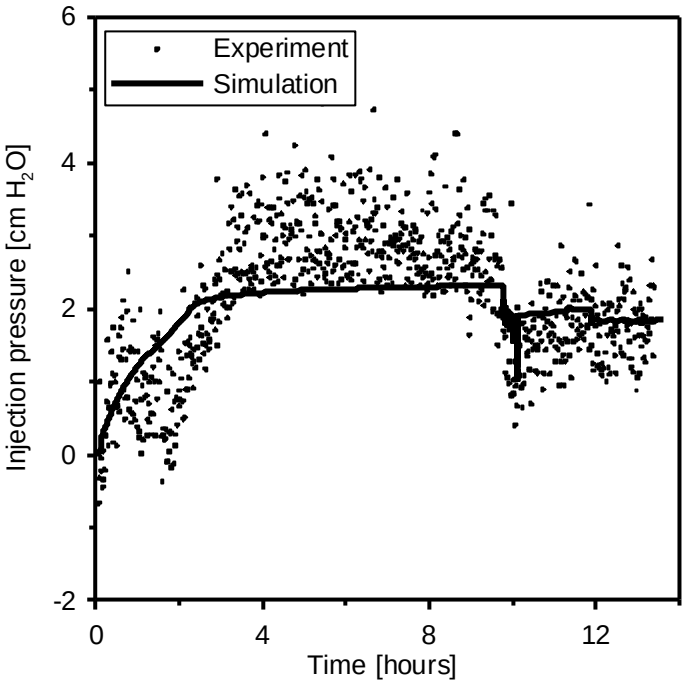

Fig 3. Measured and simulated steam injection pressure.

After approximately 11 hours, separate phase TCE began to appear in the condenser and within the next 3 hours 85 % of the initially emplaced mass was recovered. The mass not accounted for must be due to loss during emplacement, sorption or measurement uncertainties during recovery. It is not expected that any NAPL remained in the sand box since the total volume of the box was heated to steam temperature at the termination of the experiment.

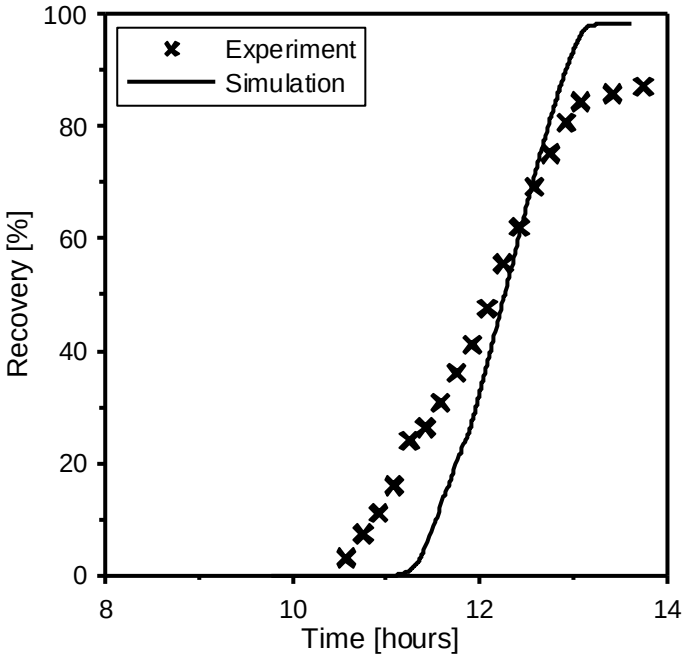

Fig 4. Recovery in experiment and simulation.

In Fig. 4 the observed recovery is compared with the simulated recovery. In constructing the experimental recovery curve it was assumed that water removed from the separator was saturated with TCE during the period where separate phase TCE was observed to condense. This approach appears valid since TCE and water was condensing simultaneously and a film of TCE was always present at the top of the water table in the separator bottle ensuring a large contact area between the two phases. The calculated mass of TCE removed with the water equals 3 % of the total. In the simulation the removal of separate phase TCE is 100 % but some dissolved mass remains in the sand box. There is a slight discrepancy between experiment and simulation both in the beginning of recovery and in the recovery rate. However, when comparing the two graphs it should be kept in mind that the recovery is very sensitive to small deviations in temperature. This will be discussed in Section 4.

She and Sleep (1998) have shown that increasing the temperature reduces the capillary pressure, which facilitates downward migration into a low permeable layer; however, there was no evidence that this occurred during the experiment. This was also not to be expected since the TCE entry pressure of the saturated fine sand was in the order of 33 cm (calculated from the measured air entry pressure).

Based on temperature, injection pressure and recovery of contaminant it seems appropriate to conclude that the model captures the dominant processes and consequently it can be used to perform a detailed analysis of the mechanisms. In the simulation all the parameters were measured independently and it cannot be expected to obtain a better match with the experimental data when no calibration is performed.

4. Discussion

Fig. 5a shows a contour plot of the simulated gas saturation after 12 hours, which is in the period of the TCE-recovery. Above the contaminated layer an unsaturated zone has formed from gas created by boiling of separate phase TCE. The gas moves upwards due to buoyancy and in the steam zone it is transported towards the extraction well. This is shown in Fig. 5b where a plume of TCE is present in the gas phase from the contaminated area to the extraction well.

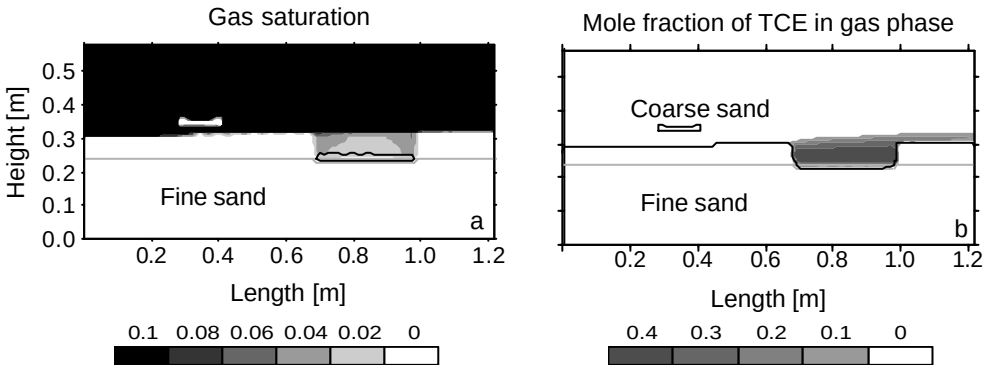

Figure 5. Simulated gas saturation (a) and the mole fraction of TCE in the gas phase (b) after 12 hours. The gray line indicates the boundary between the fine and the coarse sand. On (a) the black line indicates the NAPL saturation and on (b) it indicates where the total liquid saturation is larger than 0.98. The small water-saturated area in the otherwise unsaturated part of the box is one of the built-in heterogeneities.

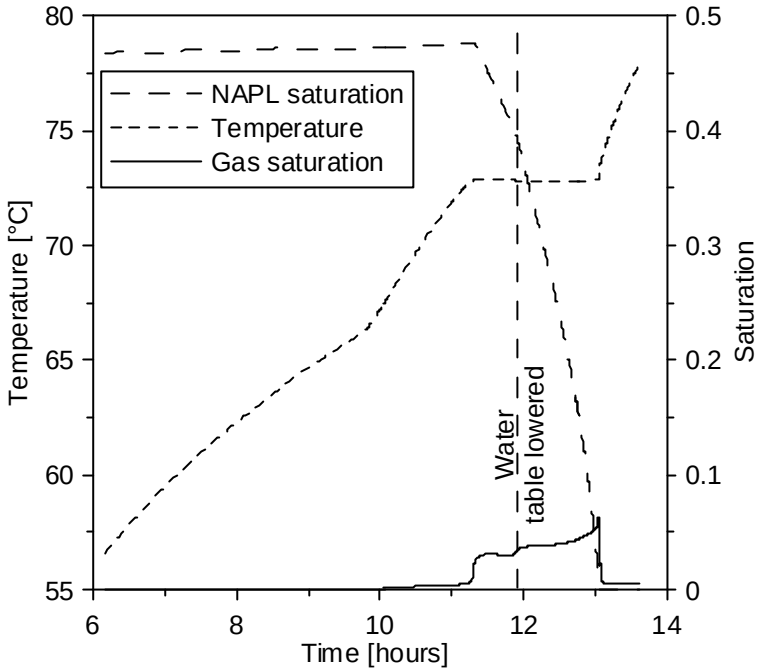

Fig. 6. Simulated temperature and saturation of NAPL and gas in the contaminant pool.

Fig. 6 shows the temporal development in temperature and phase saturations in a single gridblock containing NAPL and provides a more detailed illustration of the boiling phenomenon. The temperature increases until it reaches the common boiling point of TCE and water. Then the contaminant starts to boil resulting in a decrease in NAPL saturation and an increase in gas saturation. Because of dissolved air a gas phase consisting of air, water and TCE vapor has developed just before boiling. Gas created by boiling only consists of TCE and water vapor. Shortly before 12 hours the gas saturation increases slightly, due to the lowering of the water table. This results in increased heat transfer and a more rapid gas formation. Immediately before the NAPL disappears from the gridblock the gas saturation increases because of increased horizontal heat transfer from the upstream gridblocks where the NAPL has already been removed. When the NAPL has disappeared the temperature increases and the gas phase saturation decreases asymptotically towards zero. This asymptotic behavior is caused by the reduction in relative permeability of the gas phase with saturation. The water phase is still close to saturation with contaminant, however as the low gas saturation indicates the contaminant removal is very slow. This is also seen in Fig. 4 where the recovery rate drops significantly at late times and complete recovery is not obtained. Thus, since the water solubility of most contaminants is orders of magnitude higher than the regulation level, it will not be possible to remediate the contaminated soil completely by this boiling mechanism.

Fig. 7 compares the temporal variation of the temperature measured at a point just above the contaminant pool (see Fig. 1 for location) and the simulated temperature in a gridblock centered at that exact point. There is a small discrepancy between the simulation and the experiment indicating that the model underestimates the conductive heat transfer from the steam zone. This may be related to the thermal properties of the porous media; however, it is more likely related to the location of the steam zone boundary.

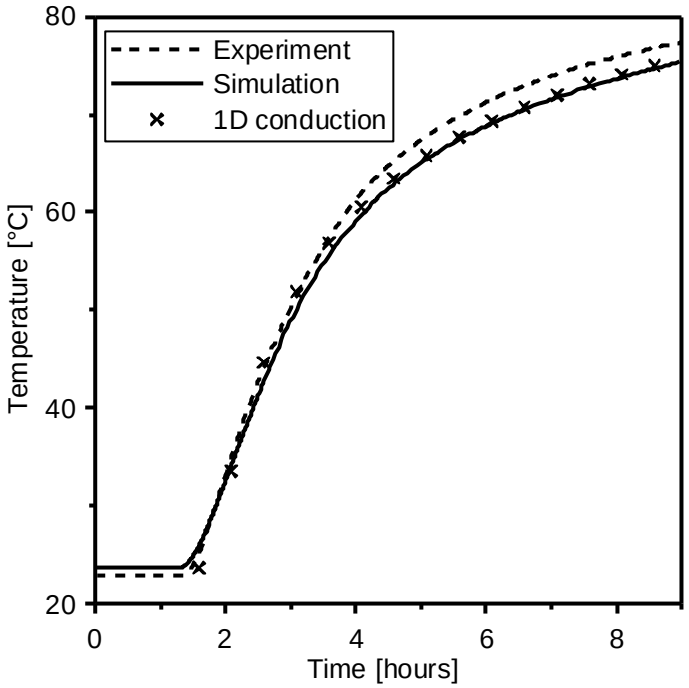

Fig. 7. Temperature 4 cm above contaminant pool.

In the gridblock immediately above, the temperature matches the measurement almost perfectly (not shown on graph). Thus, the discrepancy in temperature corresponds to an uncertainty of only 1 cm in the location of the lower boundary of the steam zone. This uncertainty may be explained by: (a) measurement uncertainty in the height of the water reservoir outside the sand box, (b) underestimation of injection pressure (Fig. 3), and (c) temperature dependence of the capillary pressure curve that is not accounted for in the model. Furthermore, the porosity was 0.40 when determining the capillary pressure-saturation relationship compared to 0.41 in the experiment, which adds to the uncertainty.

The difference in temperature may explain the difference in the onset of recovery observed in Fig. 4, since recovery starts when the temperature in the contaminated area reaches the boiling point. As heating by conduction is a slow process the small uncertainty in location of the steam zone boundary (~1cm) may result in a seemingly large uncertainty in the onset of recovery (~1 hour). Furthermore, the recovery will be influenced by the NAPL-distribution, which may not be perfectly homogeneous in the experiment as assumed in the model.
The slow increase in temperature is a clear indication of heating by conduction. Fig. 7 further demonstrates this by showing the solution to the 1-D heat conduction equation:

$$\frac{\rho C}{Kh}\frac{\partial T}{\partial t} = \frac{\partial^2 T}{\partial z^2} \qquad \textbf{(4)}$$

where ρC is the overall volumetric heat capacity and Kh is the heat conductivity coefficient. The upper boundary is a constant temperature corresponding to the steam zone and the lower boundary is a no-flux boundary corresponding to the bottom of the sand box. A quite complicated analytical solution to the equation with these boundary conditions has been developed (Incropera and DeWitt, 1996); however, we have instead applied a numerical solution due to simplicity. The input parameters and the boundary conditions are taken from the 2-D model and the starting time has been

adjusted to fit the numerical simulation. The perfect match between the numerical model and the 1-D heat conduction equation shows that the process is indeed conduction-dominated and that it can be assumed to be one-dimensional.

In Fig. 8 the temperature curves from Fig. 7 are continued through the boiling period and compared with the temperature upstream the contaminant pool at the same depth (see Fig. 1 for location). The upstream temperature increases continuously throughout the period whereas the increase in temperature above the pool levels off at the onset of boiling and in the simulation it actually decreases. This occurs because the contaminant vapor influences the temperature. To understand this, it is helpful to examine the thermodynamics at the gridblock scale. The gas phase pressure is equal to the sum of partial pressures of the gas phase components: TCE and water in this case. When a component is present as a separate phase liquid the partial pressure is equal to the saturated vapor pressure. The gas created by boiling of water and TCE moves upwards into a gridblock with higher temperature where it needs to come to equilibrium. With respect to water this means that the partial pressure needs to equal the saturated vapor pressure at the new temperature. This is obtained by vaporization of water, which requires energy and therefore lowers the temperature. Contrarily, TCE is not present as a separate phase in the gridblock and the partial pressure does not need to equal the saturated vapor pressure.

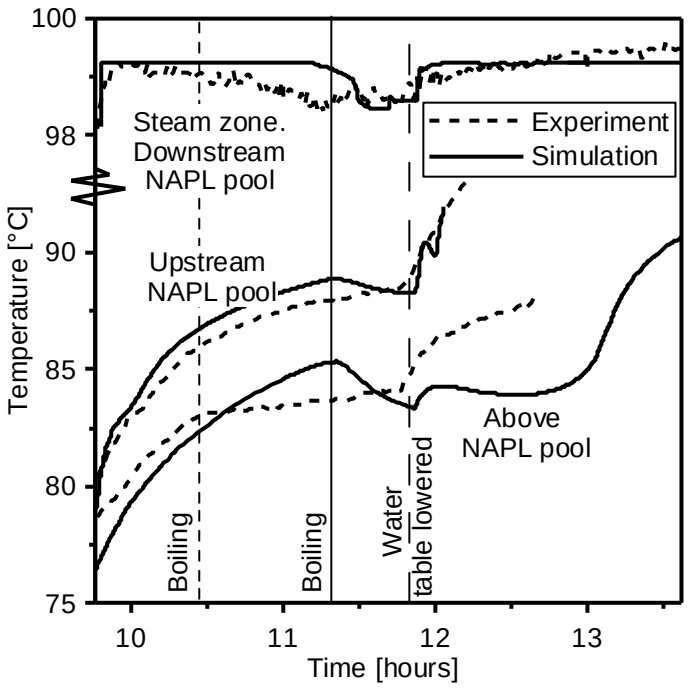

Fig. 8. Temperature 4 cm above contaminant pool during boiling. Also shown are the temperature upstream (not affected by boiling) and the temperature downstream in steam zone (affected by TCE). The vertical lines indicate when boiling initiates in experiment and simulation, respectively, and when the water table is lowered.

In the simulation where the recovery curve was slightly steeper (Fig. 4) than in the experiment the gas transport rate from the contaminated zone was consequently larger and therefore it would be expected that the temperature above the contaminant pool be more influenced. However, the large difference observed in Fig. 8 seems to imply that there is a more fundamental discrepancy. The numerical model assumes

local thermodynamic equilibrium, which may not be valid if the gas phase moves in distinct channels and/or pulses instead of continuous flow. Several air sparging experiments have shown that in coarse sand gas migrates upwards in fingers causing chemical non-equilibrium between gas bubbles and contaminated water (e.g. Mortensen et al., 2000). Thus, in our experiment with gas moving upwards in coarse sand similar non-equilibrium mechanisms may be expected. Hence, a dual-media approach similar to the one proposed by Falta (2000) was applied. The analysis is presented in appendix B, and the results indicate that thermal non-equilibrium caused by mass transfer limitations at the gas-water interface is responsible for the observed behavior.

This conclusion is supported in Fig. 8 by the temperature observations in the steam zone just above the water table downstream the contaminant pool (in the TCE gas plume, Fig. 5). Since development of fingering or gas bubbles will not occur here, thermal equilibrium is expected to prevail. This corresponds well with the measured decrease in temperature during boiling and the good agreement between experiment and simulation.

When modeling air sparging it may be crucial for the results if the kinetic mass transfer is not accounted for. In this case, however, the kinetic heat transfer is of little significance to the modeling objective, which is to predict the recovery and not so much to simulate the temperature in the area of the gas transport accurately.

5. Perspectives

The above findings show how TCE is rapidly removed in an experiment due to a boiling mechanism. The numerical model can be used to generalize this into something more applicable at field scale by varying the significant parameters within the interval to be expected in the field. The parameters significant to the process are identified as (a) porous medium properties, (b) the dimensions, and (c) the type of contaminant. We assume that a 1-D model was sufficient to capture the dominant mechanisms and this will be used to analyze the significance of the various parameters. When the areal variation of the steam zone is small compared to the distance to the contaminant this assumption will be fulfilled.

To investigate the influence of the porous medium properties on the recovery mechanism a series of simulations with a 1-D model extracted from the 2-D model of the experiment has been performed. The upper boundary is a steady-state steam zone, the lower boundary is a no-flux boundary and the contaminant is located at the same distance from the steam zone as in the experiment.

Fig. 9a shows the effect of the intrinsic permeability on the recovery keeping all other properties the same as in the experiment. As the permeability is reduced it is more difficult for the gas to escape, which causes the pressure to increases and with that the boiling temperature. Additionally, the saturation of the gas phase increases, which reduces the heat conduction coefficient according to Equation (2) and thereby the total heat transfer. However, a reduction in permeability by five orders of magnitude only results in a two-fold increase in total recovery time.

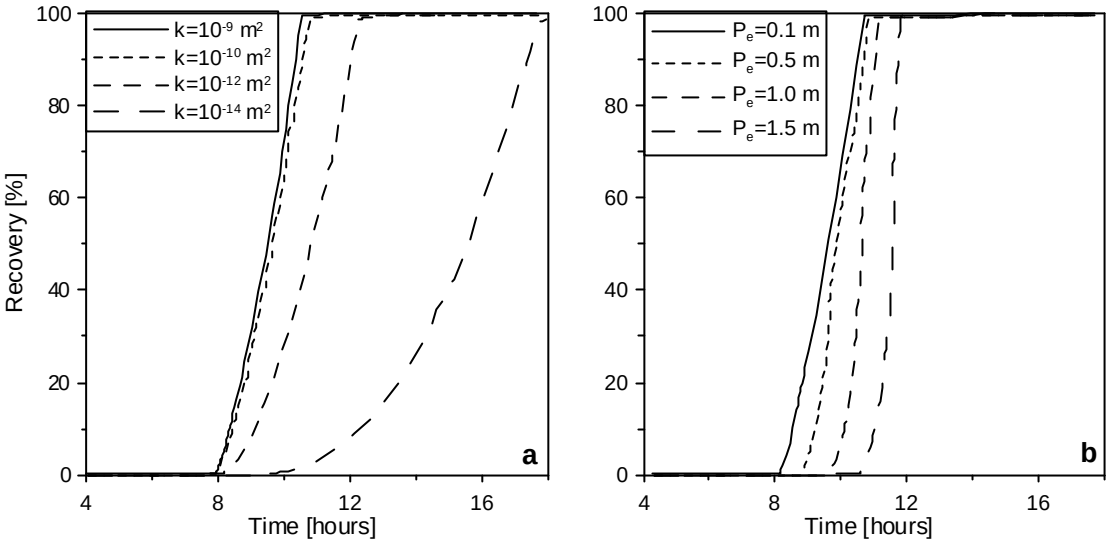

Fig. 9. Recovery with different intrinsic permeabilities (a) and entry pressures (b).

In Fig. 9b the permeability is constant ($k = 10^{-9} m^2$) but the capillary air entry pressure of the porous medium is varied. The relative permeability to the NAPL phase has been set to zero to avoid spreading caused by the larger capillary drive. Boiling occurs when the gas phase pressure exceeds the surrounding pressure plus the capillary entry pressure. Thus, increasing the entry pressure increases the boiling temperature and thereby the onset of recovery. As for the permeability the recovery is rather insensitive to the entry pressure and it can be concluded that porous medium properties only have a minor influence on boiling induced by heat conduction.

These 1-D simulations show that once the porous medium is heated to the common boiling point the recovery occurs rapidly and almost independently of the porous medium properties. The tested porous medium properties are expected to span the parameter space where separate phase contaminant can be found. The gas transport out of the porous medium does not appear to provide a limitation and therefore it will be sufficient to consider the time to heat the porous medium to the boiling point by conduction in order to estimate the clean-up time. This has important computational implications, as it is very simple to perform a 1-D conduction calculation compared to a full-scale non-isothermal multiphase flow simulation. Furthermore, thermal properties show little variation and heterogeneity between different soil types. Thus, to analyze the influence of the dimensions and the type of contaminant it suffices to consider heat transfer.

In the experiment the lower boundary of the sand box was a no-flux boundary and therefore it cannot be compared directly to the more general situation of a contaminant pooled on top of a low permeable layer where the steam zone is present above. In that case the lower boundary will be constant temperature at infinity and the solution to equation (4) can be expressed as (Incropera and DeWitt 1996):

$$\frac{T(z,t) - T_s}{T_i - T_s} = \mathrm{erf}\left(\frac{z}{2\sqrt{\frac{Kh \cdot t}{\rho C}}} \right) \qquad \textbf{(5)}$$

where T_s is the temperature of the steam zone and T_i is the initial temperature.

Fig. 10a shows how the time before boiling starts increases with the distance to the steam zone calculated by (5). The corresponding curves for PCE (PerChloroEthylene) and mesitylene (1,3,5-trimethylbenzene) with lower vapor pressures are also shown. The only difference between contaminants will be the temperature of the common boiling point. This temperature will always be below the boiling point of water so in principle any NAPL can be removed by this boiling mechanism. However, as the figure shows the time to heat the porous medium increases dramatically when the common boiling point approaches the boiling point of water. With these contaminants it will therefore be crucial to ensure that the steam zone gets very close to the contaminant and very little steam override can be accepted. Note, that these calculations assume a stagnant water phase. If there is significant water flow the 1-D assumption no longer holds and this may very well occur in situations with aggressive ground water extraction. The above conclusions would also hold for the situation where the contaminant is present inside a low permeable lens not directly accessible to the steam. In the case with a steam zone on both sides of a low permeable lens the middle of the lens will correspond to a no-flux boundary and equation (4) can again be solved numerically. The result is shown in Fig. 10b and within one week separate phase TCE or PCE will be removed from heterogeneities of up to 1 m in width inside a steam zone due to this boiling mechanism. This demonstrates one of the main advantages of steam injection compared to most other remediation technologies, namely that NAPL will be rapidly removed from small-scale heterogeneities by boiling where other technologies may be limited by diffusion.

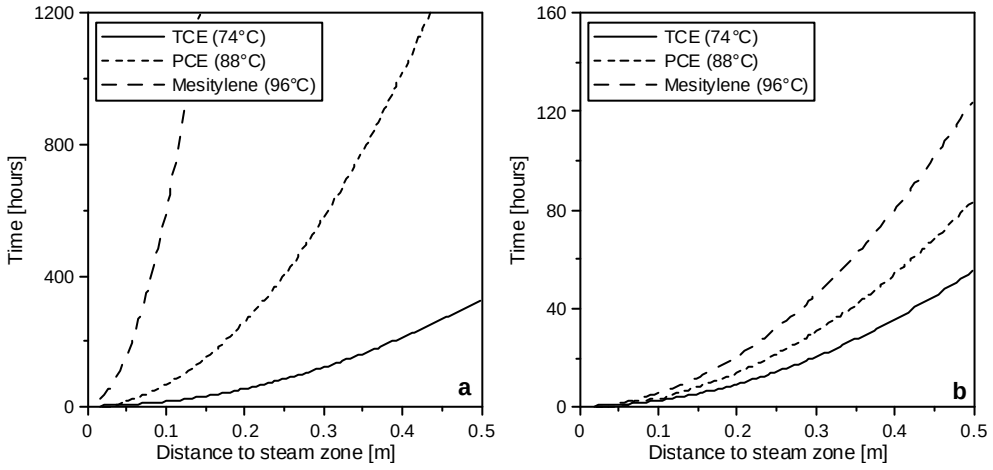

Fig. 10. Required time to reach boiling point for three different contaminants as a function of the distance to the steam zone. In (a) the lower boundary is constant temperature at infinity and in (b) there is a no-flux lower boundary. Common boiling points are indicated in the legends.

The findings in this study illustrate why recovery continues after steam breakthrough in full-scale clean-up operations. When steam has broken through at the extraction wells the steam zone will be very close to steady-state provided that the injection pressure is constant. Since it has been shown that steam rapidly removes contaminant in the steam zone the continuing recovery may be explained by conduction induced boiling removing NAPL from the boundaries of the steam zone. This removal can in many cases be evaluated by 1-D calculations.

Since the boiling mechanism is driven by heat conduction it could be argued that it would be more efficient to use thermal wells, which can be heated to a much higher temperature instead of relying on conduction from the low temperature steam zone. The advantage of using steam is that it is possible to obtain a large areal coverage below the soil surface with a steam zone, which is impossible with thermal wells.

5. Conclusions

Steam injection was performed in a two-dimensional sand box to remediate TCE present as a separate phase below the water table. Steam was injected above the water table and after an initial heating period the separate phase TCE was recovered at the outlet. The experiment was successfully modeled with the numerical code T2VOC using independently measured parameters and no calibration. By means of the numerical model the dominant removal mechanism was identified as boiling induced by heat conduction from the overlying steady-state steam zone. This will be the dominant removal mechanism when steam cannot contact the NAPL directly. Dissolved contaminant will not be removed by boiling and it cannot be expected to achieve complete cleanup rapidly in areas not directly contacted by steam. The simulation indicated that the upward moving gas phase was not at thermal equilibrium with the surroundings, similar to the chemical non-equilibrium often observed in air sparging. A 1-D framework could approximate the removal mechanism and this was used to show that the removal was relatively insensitive to the porous medium properties in the interval to be expected in the field. It was shown how a simple 1-D heat conduction calculation could be used to evaluate clean-up time and this may prove useful in the design and performance assessment of full-scale clean-up operations.

Acknowledgements

The experiment was performed at the VEGAS facility at the University of Stuttgart, Germany. We express our great gratitude for being offered access to the experimental facilities and to the staff members for helpful assistance during the experiments.

List of symbols

A	area
C	heat capacity
Kh_x	heat conductivity coefficient of x
k_{rx}	relative permeability of phase x
n	moles
p	pressure
P_e	Brooks and Corey entry pressure
q	Darcy velocity
R	gas constant
S_x	saturation of phase x

S_{xr} residual saturation of phase x
$\overline{S}_x$ effective saturation of phase x
t time
T temperature
V volume

Subscripts
g gas
i initial
l total liquid
n NAPL
r residual
s steam zone
w water

Greek letters
β_{gn} gas-NAPL scaling factor
β_{nw} NAPL-water scaling factor
ϕ porosity
λ Brooks and Corey pore distribution index
ρ density

Appendix A

Density weighting scheme

During the last part of the simulation after NAPL had disappeared from a gridblock and water imbibed we experienced convergence problems that made it impossible to finish the simulation. It only occurred in some instances after NAPL disappearance in a seemingly random way indicating that the problem was not caused by an error in the equation-of-state module. We discovered that changing the way density was weighted between gridblocks for the water flow could mitigate this problem. Normally the mass flux between gridblocks is calculated using the upstream density; however, by slightly changing the weighting factor to $\rho_{ij} = 0.98\rho_i + 0.02\rho_j$, where i is the upstream gridblock the convergence problems were eliminated. To calculate the gravity contribution the standard arithmetic averaging of density was maintained.

The weighting scheme does not introduce mass balance errors, as the effect on flow is similar to the other components of the Darcy equation. Furthermore, this weighting never influenced the water flow between two gridblocks more than 0.08%, thus the overall effect is considered insignificant especially when compared to the uncertainties on the other parameters. We do not have a fulfilling explanation on why this weighting scheme performs better but can only point to the fact that non-isothermal multiphase problems are highly non-linear and therefore very challenging for the equation solvers. Moridis and Pruess (1998) described a very simple setup where a density difference in the water phase caused by temperature resulted in severe convergence problems using the standard solvers in TOUGH2 and this may be a similar situation.

Appendix B

Dual-media simulation of thermodynamic non-equilibrium

In cases where gas bubbles move through an otherwise water saturated porous medium the gas may not be in thermodynamic equilibrium with the water due to either mass transfer limitations (vaporization of water) at the gas-water interface or heat conduction limitations in the water phase. Based on Falta (2000) a dual-media approach is used to capture the non-equilibrium. In this approach an interaction parameter, defined as a contact area between the two media divided by a diffusional length, is used as a fitting parameter. Fig. A shows a schematic of the dual-media approach where medium 2 contains both the water and the gas phase and non-equilibrium arises due to the conduction limitation in the water phase between the two media. Non-equilibrium directly at the gas-water interface cannot be modeled by this approach.

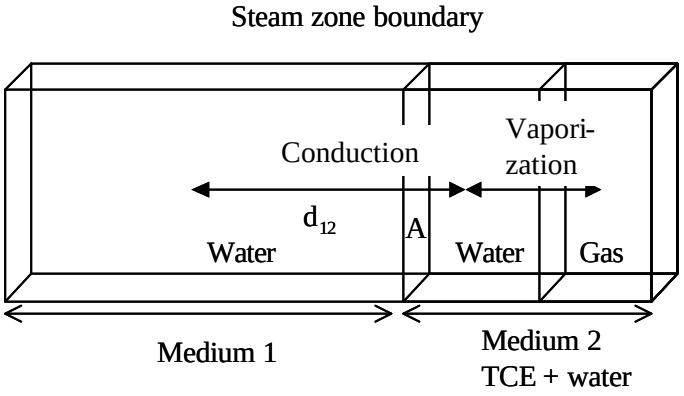

Fig. A. Schematic of dual-media model.

A 1-D dual-media simulation representing a column extracted from the 2-D model, where the steam zone is modeled as a constant temperature boundary, has been performed. The gridblocks have the dimensions 1 x 1 x 1 cm, which are divided into two media where medium 1 accounts for 80 % of the volume. Instead of varying the soil properties in the two media, NAPL was only placed in medium 2 and consequently gas will only be present in medium 2. With an interaction parameter A_{12}/d_2 = 75000 the simulation corresponds to local thermal equilibrium but when reducing the interaction parameter three orders of magnitude the temperature is significantly different in the medium without NAPL present (Fig. B).

The purpose of this simulation was not to find the best fit but only to give a justification of the explanation on the difference between measured and simulated temperature in Fig. 8. Falta (2000) found the best fit using A_{12}/d_2 =75000 in an air sparging experiment with a Darcy velocity of 2.21 cm min^{-1} compared to approximately 0.77 cm min^{-1} in this experiment (see calculation below) and a porous medium with a capillary entry pressure approximately 70% larger. With a lower velocity and a coarser medium it should be expected to find a lower interaction parameter; however, a difference of three orders of magnitude indicates that there are more substantial dissimilarities.

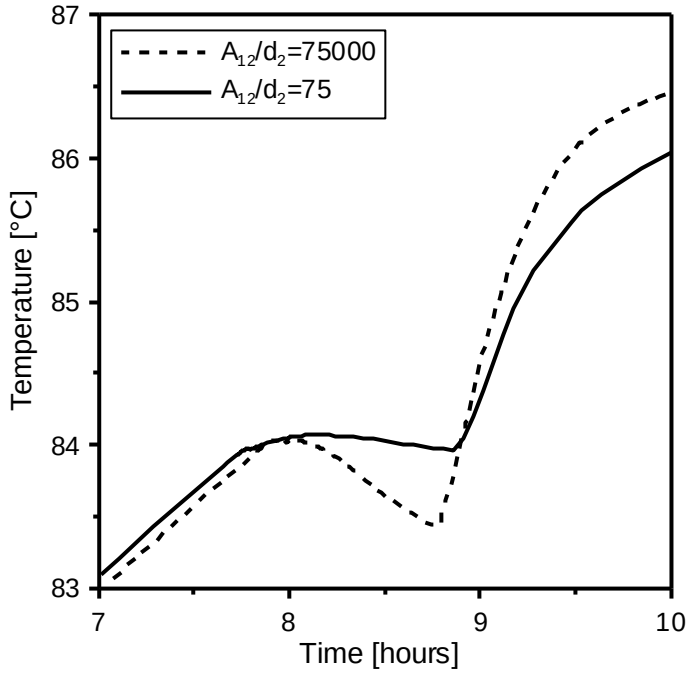

Fig. B. Simulated temperature in medium 1 (without NAPL) using dual-media approach with different interaction parameters.

In the dual-media air sparging approach phase equilibrium is still assumed within each medium and the non-equilibrium arises because the transport between the two media is limited by diffusion. In this experiment it seems more likely that non-equilibrium arises because vaporization of water is the limiting process and not the conduction of heat. Consequently, the interaction parameters for the two processes cannot be compared.

From the considerations above it can be concluded that the difference in simulated and observed temperature during boiling may be explained by thermal non-equilibrium corresponding to chemical non-equilibrium observed in air sparging. However, the dual-media simulation indicates that the dominant resistance was at the gas-water interface and not within the water phase.

The duration of the boiling period, indicated by the length of the temperature plateau, is approximately the same regardless of the interaction parameter. This shows that the recovery will not be influenced by the observed non-equilibrium and contrarily to air sparging it will be acceptable to use a local equilibrium assumption when predicting the recovery.

Calculation of gas phase Darcy velocity

By applying the ideal gas law the emplaced mass of TCE can be converted into a volume of gas:

$$V_{TCE} = \frac{nRT}{p} = \frac{69\,g \cdot 346\,K \cdot 8.314 \cdot 10^{-2}\,L\,bar\,K^{-1}\,mol^{-1}}{131.389\,g\,mol^{-1} \cdot 0.993\,bar} = 15\,L$$

where V_{tce} is the gas phase volume occupied by the TCE molecules, n is moles, R is the gas constant, T is temperature and p is pressure.

The total volume of gas created by boiling can be calculated from:

$$V_g = V_{TCE} + V_w = V_{TCE} + \frac{p_w(246K)}{p_{TCE}(246K)} \cdot V_{TCE} = \left(1 + \frac{35144Pa}{64133Pa}\right) \cdot 15L = 24L$$

where $p_x(T)$ is the saturated vapor pressure at temperature T.

Neglecting the gas created by vaporization above the contaminant pool the gas phase Darcy velocity can be calculated from:

$$q_g = \frac{V_g}{A \cdot t} = \frac{24L}{0.3m \cdot 0.085m \cdot 2h} = 0.77 cm\,min^{-1}$$

since boiling takes place from the depression in the fine sand over a period of 2 hours.

References

Atkins, P. W., 1994. Physical Chemistry. Oxford University Press, Oxford, Melbourne, Tokyo.

Betz, C., Färber, A. and Schmidt, R., 1997. Lab and technical scale experiments for NAPL removal by steam injection into porous media. In: Groundwater: An Endangered Resource. Proc. of Theme C, 27th IAHR Congress. San Francisco, USA, pp. 101-106. American Society of Civil Engineers.

Brooks, R. H., and Corey, A. T., 1966. Properties of porous media affecting fluid flow. J. Irrigation Drainage Division, ASCE 92 (IR2), 61-88.

Davis, E. L., 1994. Effect of temperature and pore size on the hydraulic properties and flow of a hydrocarbon oil in the subsurface. Journal of Contaminant Hydrology, 16:55-86.

Falta, R. W., Pruess, K., Finsterle, S. and Battistelli, A., 1995. T2VOC User's Guide. Lawrence Berkeley Laboratory Report, LBL-36400 University of California, Berkeley.

Falta, R. W., 2000. Numerical modeling of kinetic interphase mass transfer during air sparging using a dual-media approach. Water Resources Research, 36: 3391-3400.

Hadim, A., Shah, F. H. and Korfiatis, G. P., 1993. Laboratory studies of steam stripping of LNAPL-contaminated soils. Journal of Soil Contamination, 2: 27-58.

Hunt, J. R., Sitar, N. and Udell, K. S., 1988. Nonaqueous phase liquid transport and cleanup, 2. Experimental studies. Water Resources Research, 24: 1259-1269.

Itamura, M. T., 1996. Removal of chlorinated hydrocarbons from homogeneous and heterogeneous porous media using steam. UMI Dissertation Services, Ann Arbor MI.

Incropera, F. P. and DeWitt, D. P., 1996. Introduction to heat transfer. 3rd ed. John Wiley and Sons, New York.

Lenhard, R. J. and Parker, J. C., 1987. Measurement and prediction of saturation-pressure relationships in three phase porous media systems. Journal of Contaminant Hydrology, 1: 407-424.

Liu, H. H. and Dane, J. H., 1993. Reconciliation between measured and theoretical temperature effects on soil water retention curves. Soil Science Society of America Journal. 57: 1202-1207.

Liu, H. H. and Dane, J. H., 1995. An improved computational procedure for retention relations of immiscible fluids using pressure cells. Soil Science Society of America Journal. 59: 1520-1524.

Moridis, G. J. and Pruess, K., 1998. T2SOLV: an enhanced package of solvers for the TOUGH2 family of reservoir simulation codes. Geothermics. 27: 415-444.

Mortensen, A. P., Jensen, K. H., Sonnenborg, T. O. and Arvin, E., 2000. Laboratory and numerical investigations of air sparging using MTBE as a tracer. Ground Water Monitoring and Remediation. 20: 87-95.

Newmark R. and various authors, 1994. Dynamic underground stripping project. Lawrence Livermore National Laboratory, UCRL-ID-116964-V-1-4.

Newmark, R. L., Aines, R. D., Knauss, K. G., Leif, R. N., Chiarappa, M., Hudson, B., Carraigan, C., Tompson, A., Richards, J., Eaker, C., Wiedner, R. and Sciarotta, T., 1998. In situ destruction of contaminants via hydrous pyrolysis/oxidation: Visalia field test. Lawrence Livermore National Laboratory, UCRL-ID-132671.

Pruess, K., 1987. TOUGH User's Guide. Lawrence Berkeley Laboratory Report, LBL-20700 University of California, Berkeley.

Pruess, K., 1991. TOUGH2 - A general purpose numerical simulator for multiphase fluid and heat flow. Lawrence Berkeley Laboratory Report, LBL-29400 University of California, Berkeley.

Reid, R. C., Prausnitz, J. M. and Poling, B. E., 1987. The properties of gases and liquids. McGraw-Hill, New York.

Schmidt, R., Gudbjerg, J., Sonnenborg, T. O. and Jensen, K. H., 2002. Removal of NAPLs from the unsaturated zone using steam: prevention of downward migration by injecting mixtures of steam and air. Journal of Contaminant Hydrology, 55: 233-260.

She, H. Y. and Sleep, B. E., 1998. The effect of temperature on capillary pressure-saturation relationships for air-water and perchloroethylene-water systems. Water Resources Research, 34: 2587-2597.

She, H. Y. and Sleep, B. E., 1999. Removal of perchloroethylene from a layered soil system by steam flushing. Ground Water Monitoring and Remediation, 19: 70-77.

Stephens, D. B., 1996. Vadose Zone Hydrology. CRC Press. Lewis Publishers, Boca Raton, Fla.

Sundberg, J., 1988. Thermal properties of soils and rocks. Geologiska Institutionen Publ. A 57. Chalmers Tekniska Högskola & Göteborgs Universitet.

White, M. D., and Oostrom, M., 1996. Subsurface Transport Over Multiple Phases. Theory Guide. Pacific Northwest National Laboratory.

Wildenschild, D., Høgh Jensen, K., Hollenbeck, K.J., Illangasekare, T.H., Znidarcic, D., Sonnenborg, T. and Butts, M.B., 1997. Two-stage procedure for determining unsaturated hydraulic characteristics using a syringe pump and outflow observations. Soil Science Society of America Journal, 61: 347-359.

On spurious water flow during numerical simulation of steam injection into water saturated soil

Gudbjerg, J.[a], Trötschler, O.[b], Färber, A.[b], Sonnenborg, T. O.[a] and Jensen, K. H.[c]

[a] Environment & Resources DTU, Technical University of Denmark
[b] Institut für Wasserbau, Universität Stuttgart
[c] Geological Institute, University of Copenhagen

Submitted to Journal of Contaminant Hydrology

Abstract

Numerical simulation of steam injection into a water saturated porous medium may be hindered by unphysical behavior causing the model to slow down. We show how spurious water flow may arise on the boundary between a steam zone and a saturated zone, giving rise to dramatic pressure drops. This is caused by the discretization of the temperature gradient coupled with the direct relation between pressure and temperature in the steam zone. The problem may be a severe limitation to numerical modeling. A solution is presented where the spurious water flow is blocked and this widely enhances the performance of the model. This new method is applied to a previously reported example exhibiting numerical problems. Furthermore, it is applied to the simulation of 2-D sand box experiments where LNAPL is remediated from a smearing zone by steam injection. These experiments would have been difficult to analyze numerically without the adjustment to prevent spurious flow. The simulation proves to be very sensitive to the type of relative permeability model. The LNAPL is removed by a combination of vaporization and flow. Based on the numerical results it is argued that it is necessary for the steam to contact the NAPL directly to achieve clean-up at field-scale.

1. Introduction

Steam injection is one of the most complex remediation technologies available because it involves non-isothermal flow of up to three phases where rapid phase changes occur due to condensation and vaporization. To use this technology in the most optimal way we need to understand the basic mechanisms and their interaction. Controlled laboratory experiments coupled with numerical modeling have been used to increase our understanding of these processes. Hunt et al. (1988) presented the first 1-D experiments where organic contaminants were removed from water saturated columns. They showed how steam displaced water and how NAPL rapidly volatilized and re-condensed on the steam front. An energy balance could describe the movement

of the steam front that pushed water and NAPL ahead. Falta et al. (1992b) used these experimental data to validate a numerical multiphase model and a simple criterion for complete frontal NAPL displacement was derived. Additionally, it was observed that the simulated pressure would oscillate every time a gridblock was heated to steam temperature. In 2-D sand box experiments Schmidt et al. (2002) showed how steam injection in the unsaturated zone would lead to downward migration of NAPL initially present at residual saturation. Mixing of steam with air prevented the downward migration and by means of numerical modeling, three responsible mechanisms were identified and quantified. Class and Helmig (2002) validated a numerical model against 1-D experiments and showed with 2-D simulations how heterogeneous soil could be remediated by steam and air. Using 2-D sand box experiments and numerical modeling Gudbjerg et al. (2003a) showed how DNAPL pooled on a low permeable layer below the water table could be remediated by steam injection in the overlying unsaturated zone. The removal mechanism was identified as conduction induced boiling of the immiscible liquids and it was further shown how this mechanism would be insensitive to the soil parameters.

In these examples, the coupling of experimental and numerical work has served to validate the models but more importantly to analyze the experimental outcome and obtain insight in the interacting processes. Numerical modeling has also been used at field-scale in predictive studies to support the design of steam remediation schemes (Adenekan and Patzek 1994, Lee 1994, Ochs et al. 2003) and in studies analyzing the lessons learned from full-scale clean-up operations (Kuhlmann 2002, Gudbjerg et al. 2003b). Thus, numerical modeling has played an essential part throughout the development of steam injection as a remediation technology and several numerical multiphase models have been presented (Falta et al. 1992a, Adenekan et al. 1993, Forsyth 1993, Panday et al. 1995, Class et al. 2002). However, to benefit from these models it is essential that the description of the physical processes is correct and if not, that the limitations are well understood. Furthermore, since simulation of non-isothermal multiphase flow is computationally intensive it is important that these models operate in the most efficient way.

In this study an example on unphysical behavior simulated by multiphase models is reported. This is illustrated by numerical examples showing how spurious water flow gives rise to fluctuations in pressure, which cause a simulation to slow down considerably. In many cases it will be impossible to perform the desired simulation with a model that exhibits this behavior and this strongly limits the practical use of the multiphase models. The objectives of the study are (1) to analyze the problem of spurious water flow at the boundary between the saturated zone and the steam zone, (2) to develop a method that minimizes the problem and (3) to test the applicability of the proposed solution method on realistic data sets. A previously reported numerical example (Panday et al. 1995) and two laboratory experiments (Trötschler et al. 2003) are simulated. These laboratory experiments were conducted to analyze steam removal of LNAPL from a smearing zone.

2. Unphysical behavior and spurious water flow

2.1 Numerical model

The simulations are performed using the numerical model T2VOC (Falta et al., 1995), which is a member of the TOUGH family of models developed to simulate

multidimensional, non-isothermal, multiphase flow and transport in porous media (Pruess, 1987; Pruess, 1991). T2VOC is probably the most widely used model for simulating remediation by steam injection. The model considers simultaneous flow of up to three phases (water, gas and NAPL) according to a multiphase extension of Darcy's law. Hydrodynamic dispersion is neglected and only gas phase diffusion is included. Heat transfer occurs due to convection and conduction. Three components (water, air and contaminant) are partitioned among the phases according to the temperature dependent equilibrium equations except that water in the NAPL phase is neglected. To close the system of equations three mass balances (one for each component) and one energy balance are formulated. The set of equations are solved by integral finite difference techniques. The original code was slightly modified to account for the distinct entry pressure when using the Brooks and Corey (1966) formulation for the capillary pressure-saturation relationship.

2.2 1-D setup

A hypothetical example of gravity drainage where a steam zone is applied as upper boundary is considered. The column is 0.5 m high and two different discretizations are used: a fine discretization using 50 gridblocks and a coarse discretization using 10 gridblocks. Initially the temperature is 20 °C and the column is fully water saturated with no dissolved air and a bottom pressure of 106 kPa. At the upper boundary saturated steam at a pressure of 105.4 kPa is applied and the lower boundary is a fixed pressure at 106 kPa. The Brooks and Corey (1966)-Burdine (1953) model is used to describe the capillary pressure/relative permeability-saturation relationships (see Table 1 for soil properties).

Fig. 1 shows the saturation and temperature with depth after two hours when drainage has almost ceased and quasi steady-state has been reached. True steady-state will not be reached before also the temperature is at steady-state.

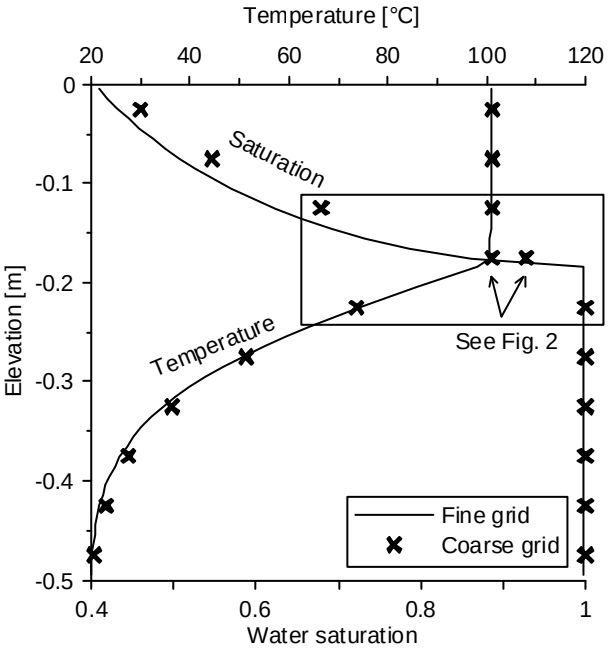

Fig.1. Simulated water saturation and temperature after two hours with two different grids. The crosses reflect the coarse discretization. The box encompasses the three gridblocks considered in Eq. (2-6).

Table 1. Soil properties.

Parameter	Value
Intrinsic permeability	$9 \cdot 10^{-11}$ m^2
Porosity	0.39
Brooks and Corey pore distribution index	1.55
Brooks and Corey air entry pressure	0.2 m
Residual water saturation	0.12
Grain density	2650 kg m^{-3}
Soil grain heat capacity	750 J kg^{-1} K^{-1}
Heat conductivity, wet	2.6 W m^{-1} K^{-1}
Heat conductivity, dry	0.23 W m^{-1} K^{-1}

The pressure at the bottom is now increased with 10 Pa and the simulation is continued. With the fine grid, the saturated boundary moves slightly upwards and a small increase in water saturation is observed in the steam zone. With the coarse grid, however, a much different behavior is observed in the gridblock just above the boundary to the saturated zone as shown in Fig. 2. The saturation increases rapidly to one and after some time it starts to decrease and then reaches the quasi steady-state value. Simultaneously, the pressure decreases substantially and also the temperature decreases.

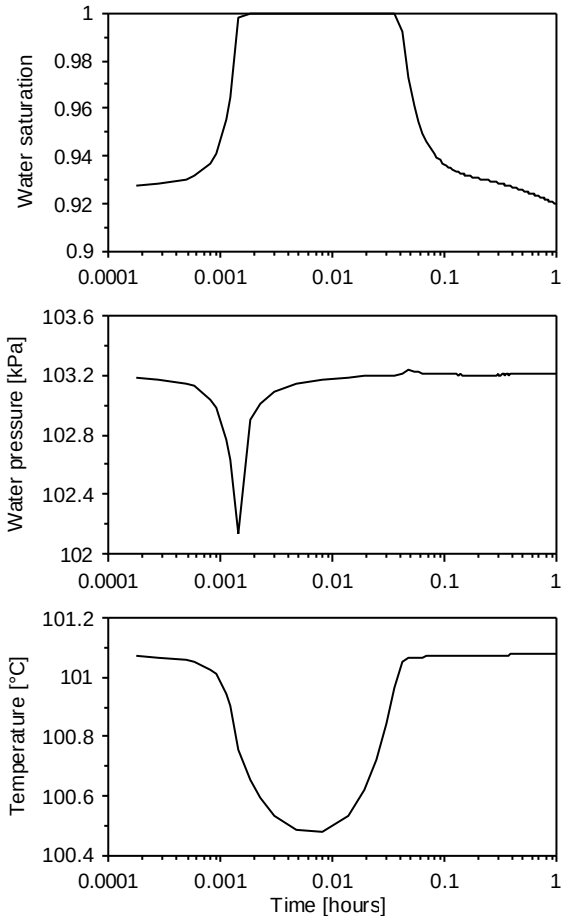

Fig. 2. Temporal development of water saturation, pressure and temperature in a steam zone gridblock located on the boundary to the saturated zone. Note that the x-axis is logarithmic to capture both the very rapid early behavior and the late behavior.

This behavior is clearly unphysical and it arises because of the discretization. Due to the pressure increase at the bottom, water flows upwards into the steam zone from the gridblock below where the temperature is around 70 °C (Fig. 1). This water needs to be heated to steam temperature, which can only take place by condensation of steam. If the volume of steam condensing is larger than the volume of water flowing into the gridblock, the pressure and consequently the temperature will decrease. The ratio of these volumes is a function of the temperature difference between the water and the steam:

$$\frac{V_{c,s}}{V_w} = \frac{r_w c_w \Delta T}{\Delta H_s r_s} = \frac{\Delta T \cdot 4.2 \cdot 10^3 J\ kg^{-1}\ K^{-1} \cdot 958 kg\ m^3}{2.26 \cdot 10^6 J\ kg^{-1} \cdot 0.58 kg\ m^3} = 3K^{-1}\Delta T \quad (1)$$

where $V_{c,s}$ is the volume of condensed steam, V_w is the volume of inflowing water ΔH_s is the enthalpy of evaporation of water, ρ is the density, ΔT is the temperature difference between cold water and steam and c_w is the heat capacity of water. This equation shows that for temperature differences larger than 1/3 K the volume of steam condensing will be larger than the volume of water. The volume of water can therefore be neglected when considering the pressure change.

In the steam zone, temperature and pressure are directly related via the saturated vapor pressure of water. Thus, when cold water flows into the steam zone the temperature and thereby the pressure decreases leading to more inflow of water making the process self-enhancing. Water will keep flowing into the steam gridblock until the pressure is uncoupled from the temperature, which occurs when the gridblock is saturated with water. In this paper this phenomenon is termed type 1 spurious water flow. With the fine grid type 1 spurious water flow does not occur because the water flowing into the steam zone has a higher temperature due to the fine discretization. This is closer to the physical situation where the temperature gradient will be continuous and water flowing into the steam zone will have steam temperature.

The pressure drop will not only result in more water flow from below but also in more steam flow from above, which may balance the inflow of water. This can be evaluated by considering the flow between the three gridblocks on the steam zone boundary to the saturated zone (Marked with a rectangle in Fig. 1). The upper two gridblocks are unsaturated and at steam temperature whereas the lower gridblock is saturated and at lower temperature. Initial conditions are hydrostatic and heat conduction is not considered. It is assumed that the properties remain constant in the upper and lower gridblock. A pressure drop in the middle gridblock will induce inflow of steam from the upper gridblock and inflow of water from the lower gridblock. Water flow from the upper gridblock will not significantly affect the energy balance, as it will have steam temperature and furthermore the relative permeability will limit the flow. The flow contributions can be calculated from the discretized version of the multiphase Darcy equation:

$$q_w = \frac{k k_{rw}}{m_w} \frac{\Delta P}{\Delta z} \quad (2)$$

$$q_s = \frac{k k_{rs}}{m_s} \frac{\Delta P}{\Delta z} \quad (3)$$

where q is Darcy flux, subscripts w and s refer to water and steam, respectively, k is intrinsic permeability, k_r is relative permeability, μ is viscosity, Δz is gridblock size and ΔP refers to the pressure difference from hydrostatic and therefore the gravity term can be excluded. To maintain the temperature and pressure in the gridblock the

inflowing cold water needs to be heated to steam temperature by condensation of the inflowing steam. Thus, an inequality can be set up relating the available enthalpy from the inflowing steam to the enthalpy required to heat the inflowing water:

$$\Delta H_s \rho_s q_s \geq \Delta T c_w \rho_w q_w \qquad (4)$$

where ΔH_s is the enthalpy of evaporation of water, ρ is density, ΔT is the temperature difference between cold water and steam and c is heat capacity. Inserting Eq. (2) and (3) in (4) yields:

$$\begin{aligned} \Delta H_s r_s \frac{k k_{rs}}{m_s}\frac{\Delta P}{\Delta x} &\geq \Delta T c_w r_w \frac{k k_{rw}}{m_w}\frac{\Delta P}{\Delta x} \\ &\Updownarrow \\ \frac{\Delta H_s r_s k_{rs}}{m_s} &\geq \frac{\Delta T c_w r_w}{m_w} \end{aligned} \qquad (5)$$

$k_{rw} = 1$ because upstream weighting is considered and the water saturation is one in the upstream gridblock. Inserting values representative for the current problem we get:

$$\begin{aligned} \frac{k_{rs} \cdot 2.26 \cdot 10^6\, J\, kg^{-1} \cdot 0.58 kg\, m^3}{1.2 \cdot 10^{-5}\, kg\, m^{-1} s^{-1}} &\geq \frac{\Delta T \cdot 4.2 \cdot 10^3\, J\, kg^{-1}\, K^{-1} \cdot 958 kg\, m^3}{2.8 \cdot 10^{-4} kg\, m^{-1} s^{-1}} \\ &\Updownarrow \\ k_{rs} &\geq \Delta T \cdot 0.1\, K^{-1} \end{aligned} \qquad (6)$$

The properties are taken from the T2VOC code and evaluated at 100 °C. They are actually functions of temperature but the variation is insignificant compared to the possible variation in ΔT. When this inequality is not fulfilled the temperature in the gridblock will decrease and the water flow will be self-enhancing. The relative permeability to steam cannot exceed one, thus for temperature differences larger than 10 °C the process will be self-enhancing. Typically the relative permeability to steam will be lower than one and therefore even smaller temperature differences will lead to pressure drops. It is not taken into account that the capillary pressure will decrease when the water saturation increases, however, for sand this has no significance.

Eq. (6) shows that only if the temperature difference between the steam zone and the first water saturated gridblock is below 10 °C, steam flow from above will be able to balance the water flow from below. Thus, to prevent type 1 spurious water flow when water flows into the steam zone the temperature gradient needs to be resolved by a very fine grid. Since the temperature gradient on a steam front may be very steep, this degree of discretization is practically impossible.

So far it has been assumed that water was the only component. The presence of other components such as dissolved air or chemicals will help to stabilize the pressure and may prevent the spurious flow. Any volatile component in the cold water entering the steam zone will vaporize and thereby counteract the pressure drop. In the coarse grid example the fluctuation in water saturation is prevented when the water is saturated with TCE. With air or PCE the type 1 spurious water flow will still occur but the pressure will be uncoupled from the temperature when the saturation becomes approximately 0.97 and not one as in the pure water case. This difference between components arises because of the higher solubility and vapor pressure of TCE.

2.3 2-D setup

The unphysical behavior may appear to be of minor importance, however, in two dimensions it can lead to severe fluctuations as will be demonstrated by another example. Steam is injected into a variably saturated, 2-D medium and again two different grids are used: a fine grid (gridblock dimensions: 1 x 1 cm) and a coarse grid (gridblock dimensions 5 x 5 cm). The model domain is 0.5 m high and 1 m wide and the water table is located 10 cm above the bottom. Saturated steam is injected with a constant rate (58 kg hour^{-1} m^{-2}) in the upper 15 cm at the left. Water may leave the model domain at the lower right corner against a constant pressure. In the upper right corner a constant gas phase pressure is prescribed as boundary. A 1-D simulation of 24-hour drainage from full saturation to a water table located 10 cm above the bottom provides the initial conditions. Soil properties are listed in Table 1.

Fig. 3 shows the simulated steam zone after 1.2 hours and the results are quite similar for the two grids. In both cases the steam zone induces a substantial depression of the boundary between the saturated and the unsaturated zone.

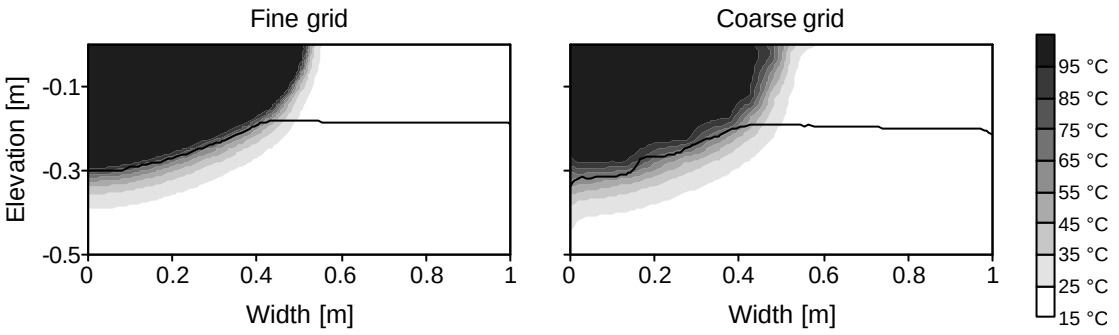

Fig. 3. Simulated steam zone after 1.2 hours. The black line indicates the boundary between unsaturated and saturated conditions.

2.3.1 Variable injection rate, fine grid

After 1.2 hours the injection rate is lowered by 20 % and the simulation is continued using the fine grid. A reduction in injection pressure is expected to result in upwards flow of water from the saturated zone into the steam zone, and it is therefore equivalent to the case where the water table was increased in the 1-D example. Fig. 4 shows the development in water saturation in a gridblock on the steam zone boundary to the saturated zone. The water saturation shows unrealistic, rapid fluctuations before the saturation returns to a more continuous behavior. This is the same mechanism as was observed with the 1-D simulation. In the 2-D simulation it occurs in several gridblocks simultaneously and some gridblocks go through multiple saturation-desaturation cycles before a constant behavior is resumed. Contrary to the 1-D simulation the water saturation does not become one before desaturation begins and this is due to the presence of non-condensable air that uncouples the pressure-temperature relationship. The initial period of fluctuations only affects the overall results in a minor way; however, because of the rapid changes in pressure and saturation the time step becomes extremely low and the simulation time increases dramatically.

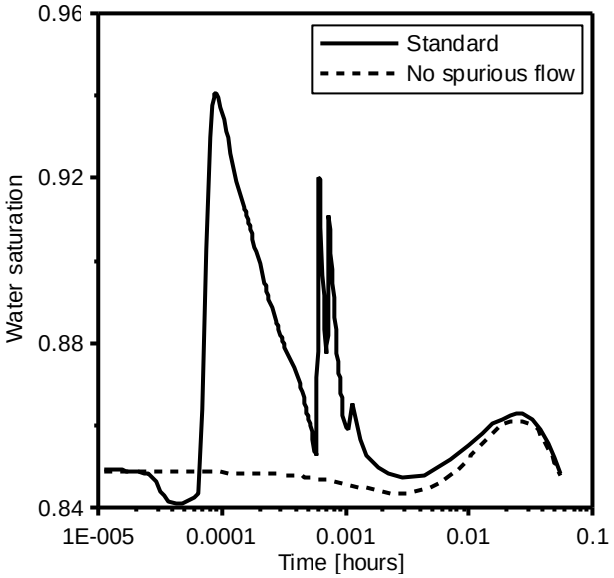

Fig. 4. Fine grid simulation of water saturation in a gridblock on the steam-water boundary after reduction of the injection rate. Note that the x-axis is logarithmic.

2.3.2 Constant injection rate, coarse grid

With the coarse grid, fluctuations arise even though the injection rate is kept constant. Fig. 5 shows how the injection pressure using the coarse grid fluctuates dramatically during two hours with constant steam injection rate. The injection pressure simulated with the fine grid shows no fluctuations. With a constant injection rate there is no physical reason for flow of cold water into the steam zone; however this is still the cause of the fluctuations.

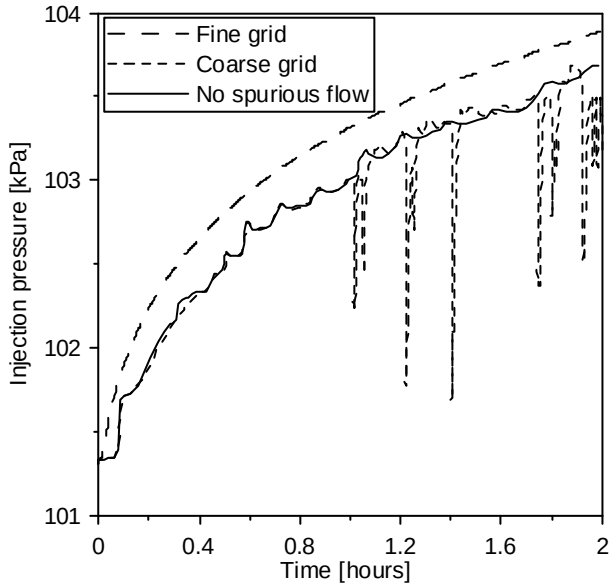

Fig. 5. Simulated injection pressure for constant injection rate with fine and coarse grid.

This is illustrated in Fig. 6 showing the development in the gridblock causing the first two drops in injection pressure (Fig. 5 after approximately 1 hour). The temperature and the pressure decrease simultaneously while the water saturation

increases to almost one. This is the same behavior as was observed previously when water was forced into the steam zone by changing the boundary conditions. Thus, the pressure gradient in the water phase on the steam zone boundary to the saturated zone must have been reversed at some point during the simulation.

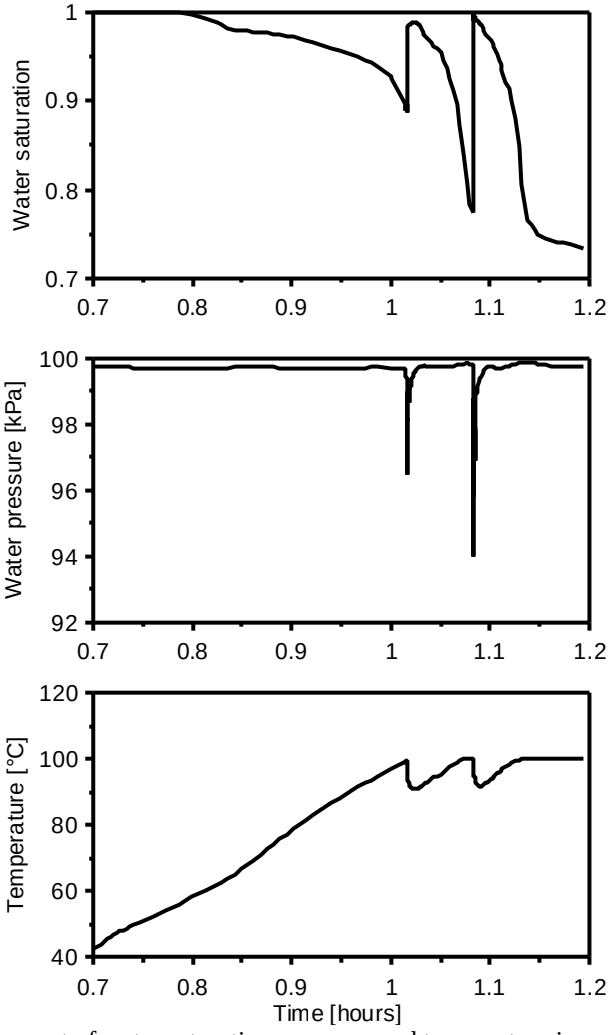

Fig. 6. Temporal development of water saturation, pressure and temperature in a steam zone gridblock on the boundary to the saturated zone.

This unphysical behavior is termed type 2 spurious flow and that may cause type 1 spurious flow. Note that even though the spurious flow occurs in a single gridblock it affects the pressure in the entire model domain as reflected by the injection pressure. Where the other examples on unphysical behavior could be of minor importance to the application of multiphase models, the behavior during constant injection rate provides a severe computational limitation and this is the main motivation for this study.

The change in gradient on the boundary between the steam zone and the saturated zone may be explained by the small pressure fluctuations that are known to occur when steam is injected into a water-saturated medium. Falta et al. (1992b) described how the steam front moves in finite steps from gridblock to gridblock with a pressure peak every time a gridblock is heated to steam temperature. This is seen in the first part of the curve in Fig. 5 where small irregularities in the injection pressure are observed. If these small fluctuations in pressure reverse the gradient on the steam

zone boundary they may cause type 2 spurious flow. Thus, the magnitude of the small fluctuations compared to the magnitude of the water pressure gradient determines whether spurious flow arise during constant rate steam injection. In the simulation with the fine grid the fluctuations are smaller but the gradient in water pressure on the steam zone boundary will be the same and consequently a reversal of the gradient is less likely to occur. Furthermore, the temperature in the water-saturated gridblock on the steam zone boundary will be higher and type 2 spurious flow will not necessarily lead to type 1 spurious flow. The magnitude of the pressure fluctuations depends on the discretization, the boundary conditions and the soil properties and this is also the case for the pressure gradient on the steam zone boundary. Thus, it is very difficult to provide any general conditions under which type 2 spurious flow may arise. When steam is injected close to the water table under unconfined conditions the injection pressure will only increase slowly as the steam zone expands. Consequently the steam zone will get close to steady-state and the gradient in the water pressure will be small. Thus, a very little perturbation is required to reverse the gradient. Contrarily under confined conditions the steam zone will advance more rapidly through the saturated conditions and not get as close to steady-state, thus reversal of the pressure gradient is less likely to occur.

It should be emphasized that the observed unphysical behavior of the model simulation is not merely a result of divergence in the numerical solution of the non-linear equations. Using a more strict convergence criterion actually enhanced the problem. This may be explained by the smoothing of pressure gradients that occur using a less precise solution. The effect was also observed using other capillary pressure-saturation relationships, soil properties and grid configurations. Pruess et al. (1987) reported similar behavior when cold water was injected into a super-heated steam zone in relation to geothermal energy extraction. Every time the water front entered a new gridblock a fluctuation in pressure was observed and this is equivalent to the type 1 spurious flow described here.

2.5 Solution

A simple method of circumventing this problem has been developed by which water flow from the saturated zone into the steam zone is linearly reduced with the temperature difference until complete prevention at $\Delta T = 15$ K. Consequently, water flow that will cause type 1 spurious water flow is not allowed. Note that the method will not only affect type 2 spurious water flow but all flow into the steam zone. The steam zone is detected by evaluating the gas saturation and the air partial pressure. Water flow is restricted from a gridblock where the gas saturation is zero or the air partial pressure is larger than 1 kPa into a gridblock that has a gas saturation larger than zero and an air partial pressure lower than 1 kPa. The threshold values for air partial pressure and temperature difference were found by trial-and-error and no in-depth analysis was performed on their optimality. It is expected that the optimal values will be situation-dependent. The code structure is presented in Table 2.

Table 2. Code structure of solution.

```
If S_g,1 > 0 and P_air,1 < 1 kPa                    {steam zone}
        If S_g,2 = 0 or P_air,2 > 1 kPa             {not steam zone}
                If ΔP < 0 and ΔT > 15 °C            {water flow, large temperature gradient}
                        ΔP = 0                      {flow blocked}
                ElseIf ΔP < 0 and ΔT < 15 °C        {water flow, small temperature gradient}
                        ΔP = ΔP (1 - ΔT/15)         {linear reduction of flow}
                end
        end
end
```

The method does not introduce new convergence problems and does not adversely affect the results. Fig. 4 compares the simulated water saturation using this approach with the traditional approach for the 2-D case with variable injection rate. The new approach completely avoids the fluctuating behavior and the late time saturations are almost identical. It could be argued that in this case it would be incorrect to block the water flow into the steam zone because it is not type 2 spurious water flow. However, water flow into the steam zone is only temporary and the result from the new approach certainly appears more physically correct. For the example with the constant injection rate Fig. 5 shows that except for the large drops the injection pressures are quite similar with the two approaches. In this example the standard approach used 1065 time steps whereas the new approach used only 125 time steps, which is the main advantage.

Intuitively, it seems correct to apply the method to prevent type 2 spurious flow and in cases where the steam front should only move back a distance shorter than the gridblock size. Contrarily, if the general direction of water flow is into the steam zone corresponding to the situation described by Pruess et al. (1987) the method will probably be invalid. However, in that case it is unlikely that the same gridblock will go through multiple saturation-desaturation cycles and the fluctuations may be less severe.

It would, of course, have been more elegant to address the type 1 spurious flow directly as this is the problem causing the numerical simulation to slow down. Type 2 spurious flow is not a problem unless it causes type 1 spurious flow. Unfortunately, no satisfactory method to do this has been identified. It was attempted to set the enthalpy of inflowing water to the enthalpy of the liquid water in the steam gridblock, which corresponds to a downstream weighting of enthalpy. The motivation was that in reality a temperature gradient will be present within the gridblock and it will be the hot water that actually flows into the steam zone. However, this often resulted in much too large temperature drops in the water-saturated cell and it was abandoned.

3. Test examples

3.1 Panday et al. (1995)-example

In a study comparing three different non-isothermal multiphase simulators Panday et al. (1995) presented a 2-D benchmarking example. The model domain was 3.5 m long and 2.25 m high and the rectangular gridblocks had the dimensions 0.25 m x 0.25 m. After a 7-day drainage period from full saturation to a sloping water table (1.6m at x = 0m and 1.5m at x = 3.5m) TCE was injected for 0.1 day at (x,z) = (1m,

1.5m) and subsequently steam was injected at (x,z) = (1m, 0.5m). The three models compared well but after 7.6 days they experienced problems, Panday et al. (1995) pp. 1285: ”The model of Forsyth (1993) exhibited difficulty proceeding beyond 7.6 days. The current model did not have this great difficulty, and the simulation proceeded in a stable though sluggish fashion beyond 7.6 days, as did the model of Falta et al. (1992).” This example has been repeated here and the temperature and oil saturation contours shown in Fig. 7 are comparable to Fig. 7c and Fig. 8c in Panday et al. (1995).

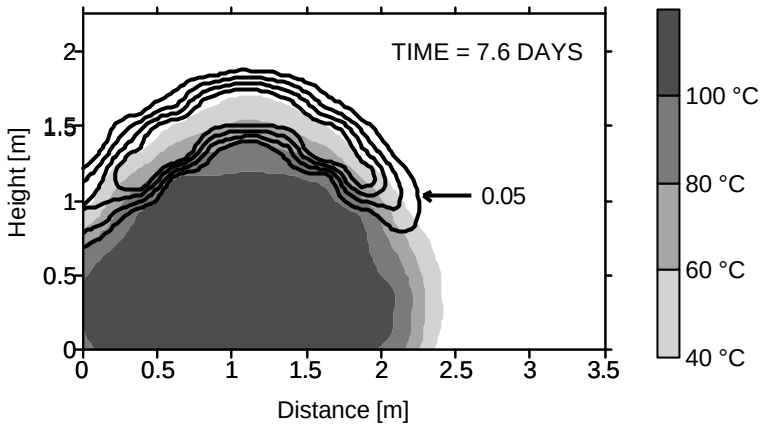

Fig. 7. Temperature and TCE saturation after 7.6 days in the Panday et al. (1995)-example. 0.05 intervals on TCE saturation contours.

There will be minor differences because the model setups may not be completely identical. For instance none of the gridblocks in a finite difference mesh will be centered at the injection points with this discretization, and it is therefore not possible to exactly reproduce the results. Additionally, differences in contouring may introduce apparent discrepancies. Fig. 8b shows the number of time steps as a function of time from the beginning of the steam injection period for the standard approach and the proposed method to avoid spurious flow. For the standard method, periods with very small time steps arise after 7.6 days (182.4 hours) and the model behavior could be termed “stable though sluggish”. When type 2 spurious water flow is prevented the model does not exhibit sluggish behavior, which indicate that this may have been the cause of the problem reported in Panday et al. (1995). The pressure in the steam injection gridblock (Fig. 8a) show large fluctuations, which in the beginning are due to the aforementioned pressure peaks that occur when a gridblock is heated to steam temperature. After 7.6 days there are deviations between the two methods indicating that these pressure drops are caused by spurious flow. TCE and air stabilize the pressure drops; however, the time stepping is still significantly affected. Even though the initial pressure fluctuations are more severe they do not cause the model to slow down. Thus, pressure fluctuations alone cannot always be used to identify spurious flow.

This example not only shows the relevance of the problem but also that it is inherent in steam models and not only a shortcoming of T2VOC.

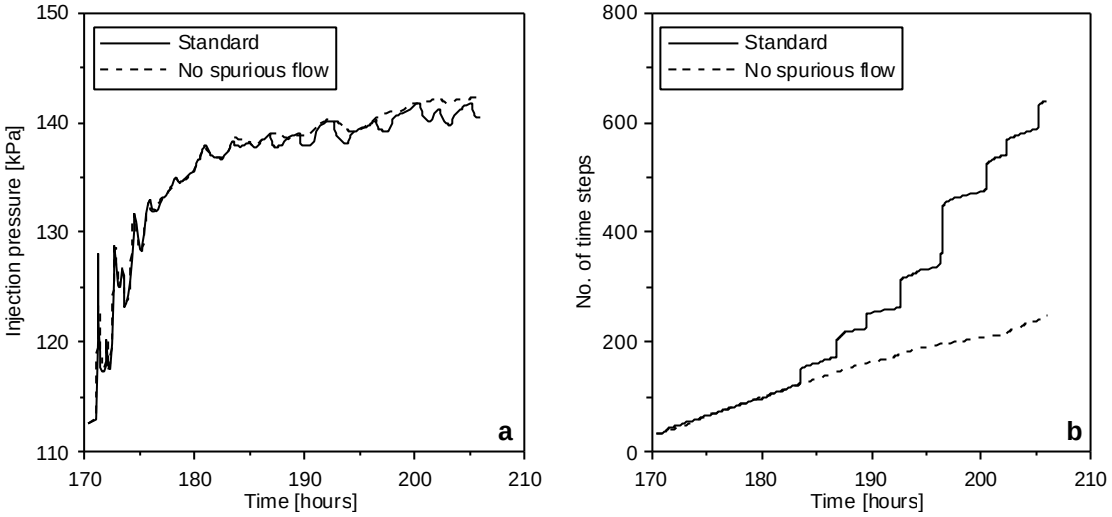

Fig. 8. Steam injection pressure (a) and number of time steps (b) during the steam injection period of the Panday et al. (1995)-example.

3.2 2-D experiments

As a part of a larger project (EU-Project, no.: EVK1CT99-0030) to examine the ability of steam injection to remediate an LNAPL smearing zone at a contaminated site, 2-D sand box experiments were conducted (Trötschler et al., 2003). To get as close to the site conditions as possible, natural sand from the actual site was used in the experiments. This, of course, introduces a certain level of heterogeneity in the porous medium, which adds to the experimental uncertainty. Two of these experiments are simulated to provide a test of the new approach with physically realistic properties.

3.2.1 Experimental and numerical procedure

The experiments are described in detail in Trötschler et al. (2003) and they were performed in the experimental setup (Fig. 9) also used by Gudbjerg et al. (2003a). Here, only the differences between the experimental and numerical procedures in Gudbjerg et al. (2003a) and the procedures in this study are outlined.

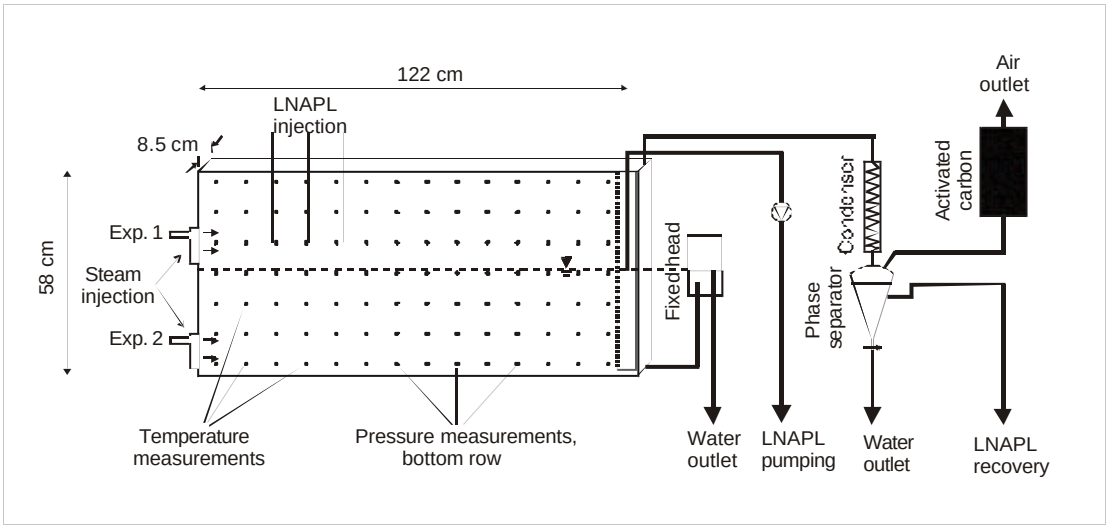

Fig. 9. Schematic of experimental setup.

The sand box was packed with residually water saturated natural sand from a contaminated site. The intrinsic permeability was measured on small-scale samples and during the flushing period on a different sand packing. However, it was not possible to simulate the results with these measurements, which may be explained by the natural heterogeneity or by uncertainties concerning entrapped air both in the measurements and the experiments. Instead the intrinsic permeability was fitted by matching the experimental and simulated steam injection pressure and water pressure close to the inlet for the beginning of experiment 2. Even though the experiments were performed on different sand packs it was not attempted to fit a different permeability in experiment 1. The soil properties are listed in Table 3.

Table 3. Soil properties used to simulate the sand box experiments.

Parameter	Value
Intrinsic permeability	$5 \cdot 10^{-11}$ m^2
Porosity	0.3
Brooks and Corey pore distribution index	1.3
Brooks and Corey air entry pressure	0.11 m
Residual water saturation	0.09
Scaling parameter, gas-NAPL, β_{gn}	2.43
Scaling parameter, NAPL-water, β_{nw}	1.70
Residual non-wetting phase saturation	0.1
Grain density	2650 kg m^{-3}
Soil grain heat capacity	940 J kg^{-1} K^{-1}
Soil grain heat capacity + sand box	1350 J kg^{-1} K^{-1}
Heat conductivity, wet	2.6 W m^{-1} K^{-1}
Heat conductivity, dry	0.23 W m^{-1} K^{-1}

The sand packing was saturated from below with de-aired water (~10% saturated), flushed for 8 hours and subsequently the water table was lowered to 30 cm above the bottom of the box. An LNAPL-mixture (20% toluene, 37% xylene, 10% ethyl. benzene, 32% trimethylbenzene) was injected through three small stainless steel tubes (Fig. 9). To create a smearing zone the water table was lowered to 15 cm above the bottom of the box and then increased to 30 cm again over a period of 6 hours. To model this exactly it would be necessary to use hysteretic constitutive relationships. However, there is already an uncertainty on the capillary pressure due to the heterogeneities in the soil and due to the effect of temperature (She and Sleep 1998) and furthermore the influence of vaporization-condensation processes on hysteresis is not known. It is therefore assessed that it would be over-parameterization to include a fully hysteretic model and instead an experimentally determined imbibition curve is used regardless of saturation path. The Brooks and Corey model is used to describe the imbibition curve together with the scaling theory proposed by Lenhard and Parker (1987) to account for three-phase combinations. Residual non-wetting phase saturations are included in the relative permeability model adjusted from Brooks and Corey-Mualem (White and Oostrom, 1996):

$$k_{rw} = \bar{S}_w^{\frac{4+5l}{2l}}, \quad k_{rn} = \bar{S}_n^{½}\left(\bar{S}_l^{\frac{1+l}{l}} - \bar{S}_w^{\frac{1+l}{l}}\right)^2, \quad k_{rg} = \bar{S}_g^{½}\left(1-\left(1-\bar{S}_g\right)^{\frac{1+l}{l}}\right)^2$$

$$\bar{S}_w = \frac{S_w - S_{wr}}{1-S_{wr}}, \quad \bar{S}_n = \frac{S_n - S_{nr}}{1-S_{nr}}, \quad \bar{S}_l = \frac{S_w + S_n - S_{wr} - S_{nr}}{1-S_{wr}}, \quad \bar{S}_g = \frac{S_g - S_{gr}}{1-S_{gr}} \tag{7}$$

where λ is the Brooks and Corey pore distribution index, S is saturation and index w, n, l, g and r refer to water, NAPL, total liquid, gas and residual, respectively. The effective saturations are only allowed to vary between 0 and 1. The incorporation of

residual gas saturation follows the approach of Luckner et al. (1989) with the saturated hydraulic conductivity as a matching point. The residual NAPL saturation is incorporated in a similar fashion.

As initial conditions the water saturations is set to 0.2 and then the saturation cycles and injection of LNAPL is simulated in accordance with the experimental procedure. The numerical model can only handle a single component NAPL phase and xylene is used to mimic the LNAPL mixture. Physical-chemical properties of xylene are taken from Reid et al. (1987).

The heat loss from the sand box was estimated from a cooling experiment and accounted for by connecting the gridblocks to a constant temperature gridblock, which only allows flux by heat conduction. Furthermore, the heat capacity of the sand box materials are added to the measured heat capacity of the soil grains to account for the heating of the sand box.

When steam broke through at the extraction well the connection from the well to the fixed hydraulic head was closed and instead water and LNAPL was extracted from the top of the water table by pumping at discrete intervals. This is difficult to simulate since the water table in the well is not constant. A compromise is made where the mass of water extracted during pumping periods is applied as a flux boundary condition to the lowest gridblock of the well. Furthermore, a gridblock connected to the entire well continuously extracts LNAPL present in the well. To maintain the stability of the model it was found necessary to assign a relative permeability function to the NAPL phase in the well and the removal will therefore not be instantaneous. Before steam breakthrough the outlet boundary was a constant head.

Steam was injected at a constant rate in the injection port 32-42 cm above the bottom of the box in experiment 1 and in the injection port 0-12 cm above the bottom of the box in experiment 2. Thus, steam was injected into a saturated zone and it could be expected that a simulation of the experiments would exhibit problems with spurious water flow. Additionally, the gridblock dimensions were 2 x 8.5 x 2 cm, which cannot be expected to resolve the temperature gradient fine enough to avoid spurious flow. Consequently the method to avoid this is applied in the simulation.

The experimental procedure is summarized in Table 4.

Table 4. Contaminant mass, injection rate and recovery in the two experiments.

Experiment no.	1	2
Height of injection port [cm]	32-42	0-10
Contaminant mass [kg]	0.207	0.212
Steam injection rate [kg hour^{-1}]	1.52	1.47
Recovery [%]	88.4	97.6

3.2.2 Results

Fig. 10 compares the experimental and simulated temperature zones at two times for the two experiments. Note that because of the distance between the thermocouples in the experiments (8.5 cm) the resolution of the front is coarser and the contoured steam zone will appear smaller than the true steam zone. The simulated steam zones appear a little larger than the experimental ones but in general the model captures the overall energy balance. The analysis of the results will be further detailed in section 3.2.3.

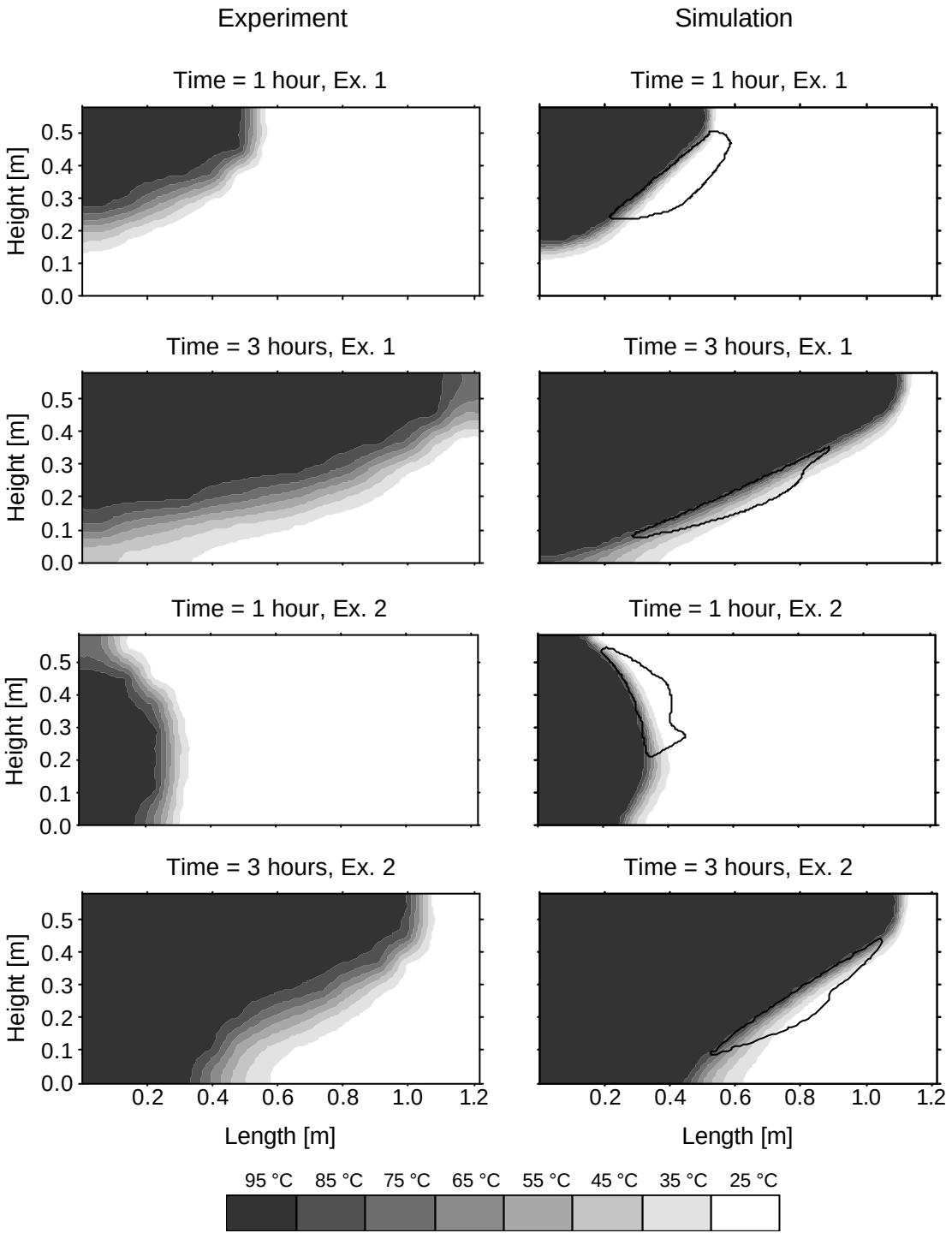

Fig. 10. Contour plots of temperature from experiment and simulation. The black line on the simulation plots indicate where the NAPL saturation is larger than 0.15.

Experiment 2 cannot be simulated without the adjustment to avoid spurious water flow. After 5570 time steps only 30 minutes of steam injection has been simulated whereas the entire experiment (915 minutes) is simulated with the same number of time steps using the new approach. The injection pressures simulated with the two methods are compared in Fig. 11. To see the difference the curves have been

plotted on different y-axes, since they are otherwise overlying. Only small fluctuations due to spurious flow are observed and compared to the overall uncertainty on the pressure they are insignificant. This illustrates that the main reason to address the reported unphysical behavior is not to obtain more correct simulation results but simply to make the simulation more efficient.

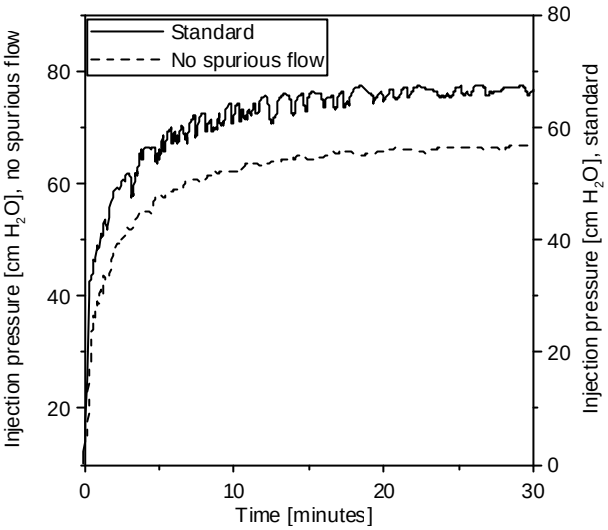

Fig. 11. Simulated steam injection pressure with the standard approach and the method to prevent spurious flow. Note the offset on the y-axes.

For experiment 1 the problem with unphysical flow is less severe. During the first 150 minutes spurious water flow increases the number of time steps from 1761 to 2666. This difference between experiments arises because of entrapped air. The entrapped air close to the extraction well is dissolved during the period when the entire box is flushed with de-aired water. However, when the water table is lowered and subsequently raised, air gets entrapped in the upper 15 cm of the saturated zone. Thus, in experiment 1 steam is injected in a saturated zone containing entrapped air, which is in contrast to experiment 2. It has previously been shown how dissolved air can help to stabilize the pressure fluctuations, however in this case it is more important that the entrapped air reduces the relative permeability to water. With an air saturation of 0.1 the relative permeability to water is 0.5, which means that water flow into the steam zone will be reduced. How this influences the type 1 spurious water flow can be illustrated by Eq. (6). In the derivation the relative permeability of water was assumed to be one; however, inserting a smaller value on the right side of the equation shows that unphysical flow will be less likely to occur since a larger temperature difference can be accepted between gridblocks on the steam-water boundary. Thus, entrapped air will help to stabilize the simulation through the reduction of relative permeability to water.

During the late part of the experiment the pumping in the extraction well introduced fluctuations in the water table and it could be argued that it would be physically incorrect to inhibit flow of cold water into the steam zone. However, the water table rises because steam condenses while the outlet is closed and not because water is pushed up into the steam zone. A simulation of the late part of experiment 2 uses twice as many time steps without the adjustment and there is no discernible difference on the results.

These simulations show that spurious flow can be a problem in realistic situations and that simulation of relevant experiments may not be possible if the problem is not addressed.

3.2.3 Additional observations

In this section some additional discussions and observations regarding these experiments are provided. This is not directly related to the issue about spurious flow but it illustrates some of the information and understanding that would have been difficult to obtain without the new approach.

Fig. 12 shows the steam injection pressure and the water pressure measured close to the extraction well. In experiment 1 the water outlet was closed twice, which caused the pressure peaks observed after 167 and 215 minutes. The late pressure drops in both experiments are due to the pumping from the well. Since it was part of the fitting procedure the steam injection pressure is simulated well in the beginning of experiment 2; however, for experiment 1 the injection pressure appears a little higher in the model until steam breakthrough (208 min).

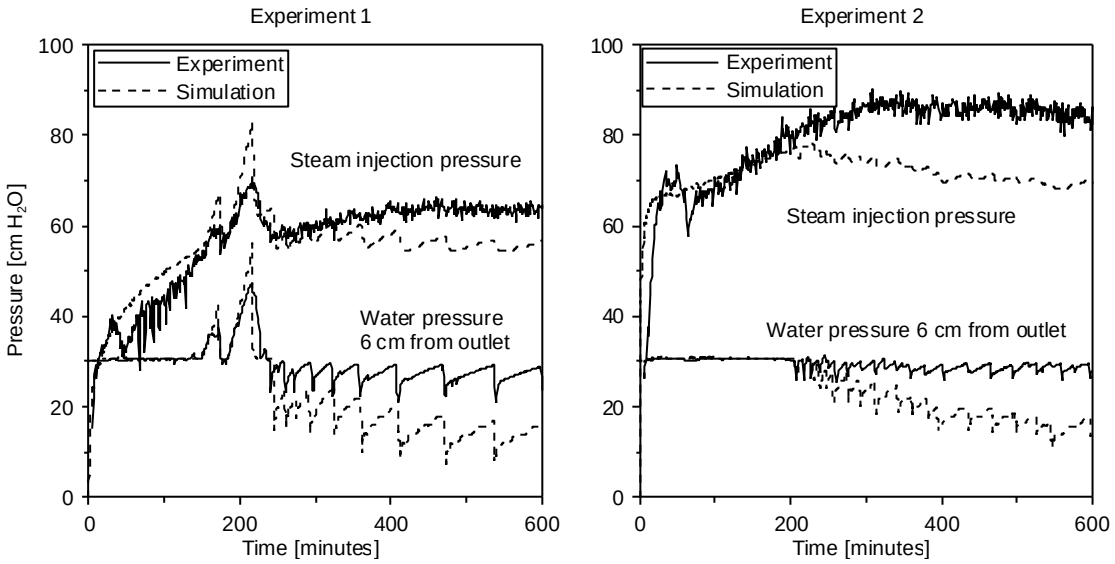

Fig. 12. Experimental and simulated steam injection pressure and water pressure at the bottom of the box close to the extraction well.

This may explain the discrepancies observed on the temperature plots in Fig. 10 where the simulation of experiment 1 underestimates the significance of steam override giving rise to a less horizontal steam front. With a higher injection pressure less steam override will occur and the front will be more vertical. When the pumping in the well starts the simulated pressures decrease too much compared to the experiments. This is a result of deviations in the water balance. In the first experiment 6.7 kg of water was recovered at the outlet after 150 minutes compared to 7.3 in the simulation and for the second experiment 7 kg was recovered compared to 8.4 kg in the simulation. Consequently, the sand box in the simulation contains less water and the extraction of a given mass will necessarily cause larger pressure drops. Entrapped air and the capillary pressure will affect the mass of extracted water; however, discrepancies in these parameters would not translate into discrepancies in pressure when the boundary conditions are changed from a constant pressure to a prescribed flux. A more likely cause of the discrepancy is that the steam zone is more developed

in the simulation so more water has been pushed out. This does also seem likely from the temperature plots, where the simulated steam zones appear slightly larger than in the experiments. Thus, these differences in pressure may be caused by a discrepancy in the energy balance, which illustrates the complexity of these coupled processes.

In the simulation the Mualem (1976) relative permeability model was found superior to the Burdine (1953) model in matching both the steam injection pressure and the water pressure close to the inlet (not shown). Performing the simulation with the Burdine model results in an injection pressure that is 21.5 cm higher on average because the relative permeability for the gas phase is generally lower with this model. In the literature there is no general consensus on which of these functions is more correct for a complex three-phase system like this one. Thus, even with independently measured parameters and no calibration it would not be possible to simulate these experiments in a unique manner. It should be emphasized that even though the Mualem model appears to give the best match in this particular simulation this should not be regarded as a general conclusion since there is a large uncertainty on other parameters.

In Fig. 13 the experimental and simulated NAPL recovery is compared. NAPL is recovered directly from the pumping in the well and through condensation of the recovered gas phase. The simulated recovery curves do not match the results from the experiments. Some NAPL is left in the sand box, the recovery is too slow and most of the NAPL is recovered in the gas phase. The assumption of a single component NAPL introduces a discrepancy between model and experiment and furthermore the extraction from the well is not simulated completely in accordance with the experimental procedure. However, none of these issues can explain the fundamental differences observed. An additional simulation of experiment 2 has been performed where the residual NAPL saturation has been set to zero at the beginning of the steam injection period. This recovery curve matches the experimental results much closer (Fig. 13) indicating that hysteresis is not accounted for correctly. There is no doubt that NAPL will get trapped in the saturated zone during the fluctuations of the ground water table; however, when the NAPL is vaporized by the steam zone and re-condensed these simulations suggest that entrapment does not occur.

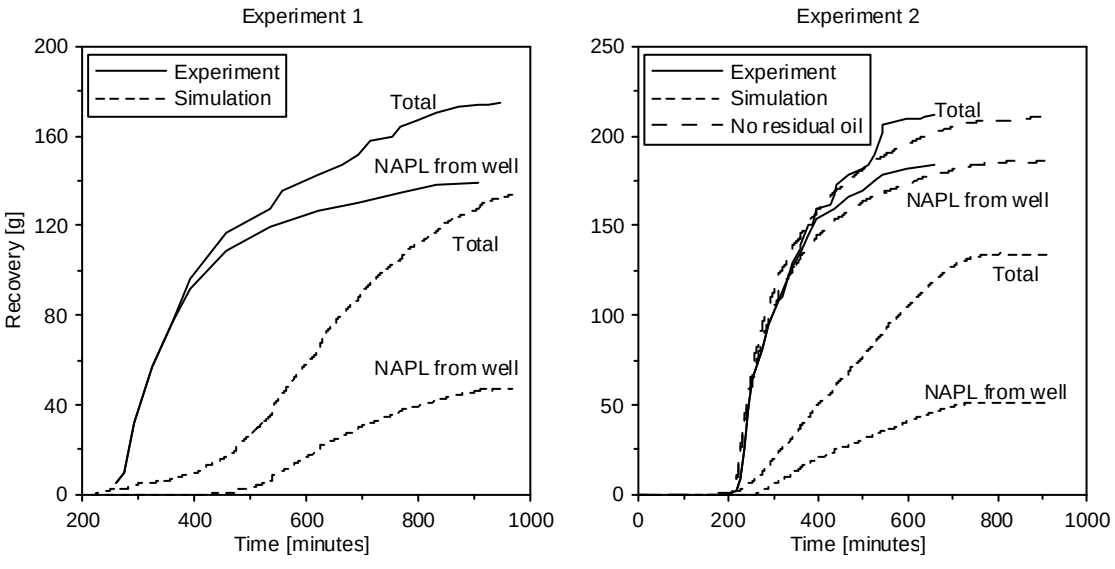

Fig. 13. Experimental and simulated recovery.

The simulations indicate that two different mechanisms are important in the NAPL transport. Initially, the steam zone moves up through the contaminated area and the NAPL is pushed ahead of the steam front. This occurs whether or not a NAPL residual saturation is included and therefore it cannot be a flow process. Instead it is caused by continuous vaporization and condensation as has been demonstrated in the 1-D experiments by Hunt et al. (1988). This is possible when the steam contacts the NAPL directly. After 3 hours the NAPL is located below the steam zone (Fig. 10) and steam flow through the NAPL contaminated area is limited. The simulation with residual NAPL included could not reproduce the observed results. Thus, during this period flow of NAPL is the most important transport process. If NAPL is not allowed to flow, removal will mainly occur through vaporization and transport in the gas phase. Gudbjerg et al. (2003a) showed how conduction from a steam zone could cause boiling of a NAPL phase; however, in the experiments this process is not dominating. In the late part of experiment 2, the NAPL recovery rate becomes very low in the simulation even though there is still a substantial mass left in the sand box. Due to the pumping in the well that lowered the water table the LNAPL has become trapped in the saturated zone when pumping ceased and the water table increased to 30 cm in the extraction well. Consequently, steam cannot contact the NAPL but it could be expected that the contaminated zone may eventually be heated to the common boiling point of xylene and water through heat conduction. However, continuing the simulation does not increase the recovery because the temperature has reached a steady-state where the heat transfer by conduction from the steam zone is balanced by the heat loss from the sand box. The common boiling point of xylene and water at atmospheric pressure is 94 °C, which is very close to steam temperature and therefore heat conduction and subsequent boiling will only be able to remove NAPL in the very vicinity of the steam zone. A simulation of experiment 2 has been performed where the pumping in the well is omitted to avoid entrapment of the NAPL and in that case the recovery continues after the NAPL has become immobile through vaporization until complete removal. At field-scale vaporization may be the dominant process when the NAPL is located in between the steam zone and the saturated zone, because NAPL flow will be relatively slower over the larger distance. Still, it will only have an effect in the very first few centimeters and a thick smearing zone cannot be remediated without ensuring a direct access of the steam to the NAPL. In the experiments this was ensured because steam displaced most of the water due to the high injection pressures compared to the dimensions of the sand box. This will not be the case at field-scale where the steam zone may move above the water table and only limited displacement will occur.

4. Conclusions

A problem was identified when simulating steam injection into a water saturated porous medium with spurious water flow and unphysical behavior that severely influenced the computation time. The problem was remedied by not allowing flow of cold water into the steam zone identified by the partial pressure of air. This prevented the spurious water flow and resulted in an overall more realistic behavior without introducing numerical convergence problems. It was shown how previously reported difficulties with a steam injection example could be overcome by this new approach.

Two sand box experiments where an LNAPL was remediated from variably saturated natural sand were simulated using the method to prevent unphysical behavior. The experiments proved difficult to model because of uncertainty concerning hysteresis and relative permeability models. The experiments showed almost complete recovery of the NAPL because the steam zone was able to access the entire contaminated zone directly. The simulations indicated that if this is not the case remediation might be very difficult. In a clean-up operation it will therefore be essential to enable the steam zone to target the contaminated zone.

Acknowledgements

The comments and suggestions of Karsten Pruess during the making of this manuscript are greatly acknowledged.

References

Adenekan, A. E., Patzek, T. W. and Pruess, K., 1993. Modeling of multiphase transport of multicomponent organic contaminants and heat in the subsurface: Numerical model formulation. Water Resource Research, 29: 3727-3740.

Adenekan, A. E. and Patzek, T. W., 1994. Cleanup of the gasoline spill area with steam: Compositional simulations. In Newmark R. and various authors, 1994. Dynamic underground stripping project. Lawrence Livermore National Laboratory, UCRL-ID-116964-V-1-4.

Brooks, R. H., and Corey, A. T., 1966. Properties of porous media affecting fluid flow. J. Irrigation Drainage Division, ASCE 92 (IR2), 61-88.

Burdine, N. T., 1953. Relative permeability calculations from pore-size distribution data. Petroleum Transactions of the American Institute of Mining Engineering, 198: 71-77.

Class, H., Helmig, R., and Bastian, P. 2002. Numerical simulation of non-isothermal multiphase multicomponent processes in porous media. 1. An efficient solution technique. Advances in Water Resources 25: 533-550.

Class, H. and Helmig, R. 2002. Numerical simulation of non-isothermal multiphase multicomponent processes in porous media. 2. Applications for the injection of steam and air. Advances in Water Resources 25: 551-564.

Falta, R. W., Pruess, K., Javandel, I., and Witherspoon, P. A., 1992a. Numerical modeling of steam injection for the removal of nonaqueous phase liquids from the subsurface 1. Numerical formulation. Water Resources Research. 28: 433-449.

Falta, R. W., Pruess, K., Javandel, I., and Witherspoon, P. A., 1992b. Numerical modeling of steam injection for the removal of nonaqueous phase liquids from the subsurface 2. Code validation and application. Water Resources Research. 28: 451-465.

Falta, R. W., Pruess, K., Finsterle, S. and Battistelli, A., 1995. T2VOC User's Guide. Lawrence Berkeley Laboratory Report, LBL-36400 University of California, Berkeley.

Forsyth, P. A. 1993. A positivity preserving method for simulation of steam injection for NAPL site remediation. Advances in Water Resources 16: 351-370.

Gudbjerg, J., Sonnenborg, T. O., and Jensen, K. H., 2003a. Remediation of NAPL below the water table by steam induced heat conduction. Submitted to Journal of Contaminant Hydrology.

Gudbjerg, J., Heron, T., Sonnenborg, T. O., and Jensen, K. H., 2003b. Three-dimensional numerical modeling of steam override observed at a full-scale remediation of an unconfined aquifer. Submitted to Ground Water Monitoring and Remediation.

Hunt, J. R., Sitar, N. and Udell, K. S., 1988. Nonaqueous phase liquid transport and cleanup, 2. Experimental studies. Water Resources Research, 24: 1259-1269.

Kuhlman, M. I., 2002. Analysis of the steam injection at the Visalia Superfund Project with fully compositional nonisothermal finite difference simulation. Journal of Hazardous Materials, 92: 1-19.

Lee, K. H., 1994. Predictive modeling using the STARS code. In Newmark R. and various authors, 1994. Dynamic underground stripping project. Lawrence Livermore National Laboratory, UCRL-ID-116964-V-1-4.

Lenhard, R. J. and Parker, J. C., 1987. Measurement and prediction of saturation-pressure relationships in three phase porous media systems. Journal of Contaminant Hydrology, 1: 407-424.

Luckner, L., Van Genuchten, M. Th. and Nielsen, D. R., 1989. A consistent set of parametric models for two-phase flow of immiscible fluids in the subsurface. Water Resources Research. 25: 2187-2193.

Mualem, Y., 1976. A new model for predicting the hydraulic conductivity of unsaturated porous media. Water Resources Research, 12: 513-522.

Ochs, S. O., Hodges, R. A., Falta, R. W., Kmetz, T. F., Kupar, J. J., Brown, N. N. and Parkinson, D. L., 2003. Predicted heating patterns during steam flooding of coastal plain sediments at the Savannah River site. Environmental & Engineering Geoscience, 9: 51-69.

Panday, S., Forsyth, P. A., Falta, R. W., Wu, Y. S. and Huyakorn, P. S., 1995. Considerations for robust compositional simulations of subsurface nonaqueous phase liquid contamination and remediation. Water Resources Research. 31: 1273-1289.

Pruess, K., 1987. TOUGH User's Guide. Lawrence Berkeley Laboratory Report, LBL-20700 University of California, Berkeley.

Pruess, K., 1991. TOUGH2 - A general purpose numerical simulator for multiphase fluid and heat flow. Lawrence Berkeley Laboratory Report, LBL-29400 University of California, Berkeley.

Pruess, K., Calore, C., Celati, R. and Wu, Y. S., 1987. An analytical solution for heat transfer at a boiling front moving through a porous medium. International Journal of Heat and Mass Transfer, 30: 2595-2602.

Reid, R. C., Prausnitz, J. M. and Poling, B. E., 1987. The properties of gases and liquids. McGraw-Hill, New York.

Schmidt, R., Gudbjerg, J., Sonnenborg, T. O. and Jensen, K. H., 2002. Removal of NAPLs from the unsaturated zone using steam: prevention of downward migration by injecting mixtures of steam and air. Journal of Contaminant Hydrology, 55: 233-260.

She, H. Y. and Sleep, B. E., 1998. The effect of temperature on capillary pressure-saturation relationships for air-water and perchloroethylene-water systems. Water Resources Research, 34: 2587-2597.

Trötschler, O., Weber, K., Koschitzky, H.-P., Färber, A., 2003. Simultaneous Remediation of the Saturated and Unsaturated Zone by Steam-Air Injection and Alcohol Flushing. Scientific Report 03/06(VEG04), Institut für Wasserbau, Universität Stuttgart.

White, M. D., and Oostrom, M., 1996. Subsurface Transport Over Multiple Phases. Theory Guide. Pacific Northwest National Laboratory.

Three-dimensional numerical modeling of steam override observed at a full-scale remediation of an unconfined aquifer

Gudbjerg, J. [a], Heron, T. [b], Sonnenborg, T. O. [a], Jensen, K. H. [c]

[a] Environment & Resources DTU, Technical University of Denmark
[b] NIRAS Consulting Engineers and Planners
[c] Geological Institute, University of Copenhagen

Submitted to Ground Water Monitoring and Remediation

Abstract

Steam injected below the water table tends to move upwards because of buoyancy. This limits the horizontal steam zone development, which determines the optimal spacing between injection wells. In this study, observations indicating steam override at a full-scale remediation of an unconfined aquifer are analyzed by numerical modeling using the code T2VOC. A simplified 3-D numerical model is set up, which qualitatively shows the same mechanisms as observed at the site. By means of the model it is found that it will be possible to achieve a larger horizontal extent of the steam zone in a layered geology compared to the homogeneous case. In the homogeneous case the steam injection rate increases dramatically when the injection pressure is increased, which is necessary to achieve a larger horizontal development. The development of the steam zone under unconfined conditions is found to be a complex function of the geologic layering, the ground water table at steady-state extraction and the injection/extraction system. Because of this complexity it will be difficult to predict steam behavior without 3-D numerical modeling.

1. Introduction

Steam injection is a promising remediation technology that has originally been developed in the petroleum industry for enhanced oil recovery. Hunt et al. (1988) presented experimental results showing complete removal of volatile organic compounds from a water-saturated column indicating that steam injection could be a very efficient remediation technology. These findings were further developed in two-dimensional studies where Itamura (1996) and She and Sleep (1999) showed that also heterogeneous porous media could be remediated when steam contacted the contaminant directly. Gudbjerg et al. (2003a) showed that even if a steam zone is not in direct contact with the NAPL rapid clean-up may still occur. A conclusion of these

laboratory studies was that a volatile NAPL would be removed from the area heated to the boiling point. Thus, one of the key issues when applying steam injection in the field is to ensure that the steam heats the contaminated zone and therefore it is crucial to understand the development of a steam zone.

Steam zone development is controlled by the energy required to heat the porous medium to steam temperature and the steam flow direction. In the unsaturated zone the steam flow direction is mainly controlled by pressure gradients and heterogeneities in permeability, whereas steam flow in the saturated zone is also strongly influenced by buoyancy. Because of the low density of steam compared to water, steam injected below the water table tends to move upwards. This phenomenon is termed steam override and has been addressed in the petroleum industry (van Lookeren, 1983; Lake, 1989) where steam is mostly injected in high permeable layers confined by low permeable layers. For a two-dimensional confined system Basel and Udell (1989) presented a theoretical analysis of the steam front angle verified by experimental results. They showed that increasing the injection rate and thereby the pressure would make the steam front more vertical. However, the results obtained for confined conditions are not applicable for unconfined conditions, which is often the case at contaminated sites.

The steam zone develops in the horizontal direction when the steam pressure is sufficiently high to displace water. This pressure will be the same under confined and unconfined conditions; however, it may be difficult to obtain in unconfined aquifers. Under confined conditions the steam zone can only develop in the vertical direction to a limited extent and with continuing injection the pressure will increase and the steam zone will be diverted in the horizontal direction. Contrarily, under unconfined conditions the pressure may not increase during constant injection and horizontal development may be minimal. This issue is further complicated by the pressure loss that occurs because of steam condensation and water flow. When designing an optimal steam injection scheme it is crucial to know the horizontal extent of the steam zone because that determines the maximum spacing between injection wells.

The movement of a steam zone below the water table is somewhat similar to the movement of air when applying air sparging. The behavior of the steady-state aerated zone in air sparging will be qualitatively similar to that of the steady-state steam zone. Lundegaard and Andersen (1996) used a multiphase model to predict the steady-state aerated zone from a single well in an axisymmetric system and found that the width increased with the injection pressure and anisotropy ratio. Furthermore, it was shown that the presence of low permeable zones significantly influenced the airflow. However, when considering steam injection the assumption of axisymmetry will rarely be valid because of aggressive extraction in both the water and the gas phase. Also, the injection rate used in steam injection is typically much higher and even at steady-state the condensation of steam may influence the pressure significantly. Still we believe that the lessons learned from air sparging may help to provide a qualitative understanding and intuition of the steam zone behavior below the water table.

To fully capture the steam zone behavior in the vicinity of the water table by numerical modeling it is necessary to use a 3-D model. Only five 3-D numerical studies of remediation by steam injection have been found in the literature even though steam injection is becoming a widely used technology. Adenekan and Patzek (1994) used the numerical code M2NOTS (Adenekan et al., 1993) to perform a 3-D predictive simulation of the remediation at the LLNL site (Newmark et al., 1994)

where a gasoline spill was cleaned up from a layered geology. By assuming symmetry they reduced the necessary model area to 1/12 of the total area and used 506 gridblocks. They concluded that the high permeable layers would be nearly cleaned up in less than 16 days and that the contaminants were mainly recovered in the gas phase. A sensitivity analysis revealed that the clean-up time was sensitive to the intrinsic permeability because the injection rate was pressure-constrained whereas the relative permeability was less important. Lee (1994) also performed a 3-D simulation of the LLNL remediation using the numerical code STARS (Rubin and Buchanan, 1985). This study considered the entire area but restricted the vertical extent to the confined aquifer and used 604 gridblocks. It was observed that inflow of cold water between two injection wells initially delayed steam breakthrough at the extraction well.

Kuhlmann (2002) used the STARS code to simulate the remediation performed at the Visalia, California Superfund Site (Newmark et al., 1998) where creosote was removed from an aquifer with a geology similar to the LLNL site. The complete area, involving 18 injection wells and a central extraction well, was considered and resolved by 6000 gridblocks. The simulation showed that the dominant removal mechanism was vaporization and that upwards spreading of contaminant to the vadose zone could occur. Furthermore, the simulations suggested a more optimal design by adding a central injection well.

Ochs et al. (2003) simulated steam zone development at the Savannah River Site using the T2VOC code. The model domain was resolved by 12096 active gridblocks and contained four steam injection wells. Steam was injected in the unsaturated zone and a confined saturated zone. Steam zone development was controlled by the layered geology and the simulated results compared reasonably well with observations.

Forsyth (1994) presented results for 3-D simulations (4000 finite element nodes) of a heterogeneous variably saturated medium where TCE was removed by injecting steam below the contaminant. It was concluded that steam injection would be relatively insensitive to the heterogeneities in the simulation.

Neither of these studies addressed steam override since they considered sites with a strongly layered geology or in the case of Forsyth (1994) injected steam below the contaminant. However, since most contaminations will be found in unconfined aquifers it is of interest to analyze the limitations and possibilities of steam injection under these conditions.

In this study temperature measurements from a field scale remediation are analyzed by numerical modeling with the numerical code T2VOC. By considering a simplified geometry a 3-D model is set up with a discretization fine enough to capture the steam override behavior and the model is used to analyze and identify the dominant parameters. The focus will be on the steam zone development and not on contaminant removal.

2. Site description and remediation scheme

The site is located in the city of Aalborg in Denmark. A dry cleaner and an auto repair shop had previously been located at the site and they are expected to have caused the contamination consisting of turpentine (LNAPL) on top of the water table and PCE (DNAPL) partly dissolved in the turpentine and partly pooled on a low permeable clay layer. Fig. 1 shows the estimated source area and a geological profile.

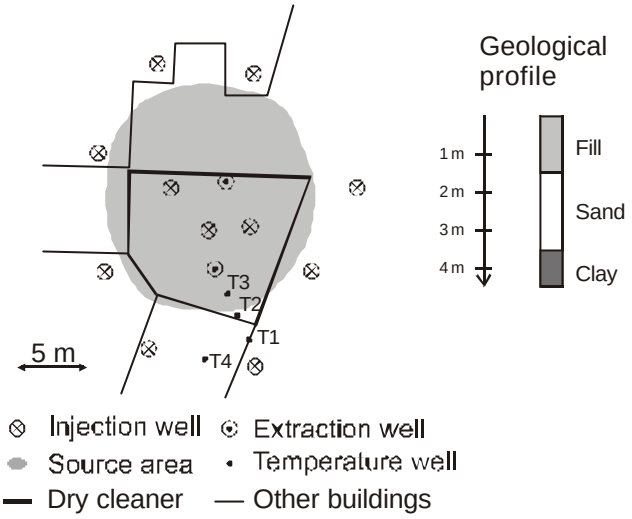

Fig. 1. Schematic of source area with location of wells and geological profile.

The geology of the site consisted of an upper fill layer down to 1.5 meters below surface (m.b.s). followed by a sand layer down to 3.5 m.b.s. where a low permeable, non-fractured clay layer was present. The ground water table was located at 1.7 m.b.s. but it was not possible to determine an overall flow direction from the piezometer measurements.

The remediation scheme consisted of steam injection in eight wells surrounding two central extraction wells and three central injection wells (Fig. 1) placed in a configuration that to some extent was constrained by the buildings at the site. The steam injection wells were screened from 3 to 3.5 m.b.s. and the extraction wells were screened from 1 m.b.s. to 4 m.b.s. with a ground water pump installed at the bottom and suction applied in the gas phase (Fig. 5c). The strategy was to create a surrounding steam zone that hindered ground water inflow and pushed the contaminant towards the extraction wells. Six automatically logged and several manually logged multilevel temperature monitoring wells were installed at the site. Only the results from the four temperature wells shown in Fig. 1 will be discussed as the same behavior was observed at the other wells.

2.1 Field observations

Fig. 2 shows the temperature at three different depths measured in the wells T1, T2 and T3 throughout the steam injection period. Due to technical problems steam injection was some times halted and this was reflected by the rapid temperature drops. Close to the injection well the steam zone extended to 3.5 m.b.s. whereas the steam zone never appeared to be deeper than 3 m.b.s. in T3. Thus, as the distance from the injection well increases the deepest point of the steam zone moved upwards indicating that steam override was occurring. Note that when the steam injection was halted the drops in temperature were markedly larger for depths lower than 2.25 m.b.s. indicating a rise in the water table providing a more rapid cooling than in the unsaturated zone.

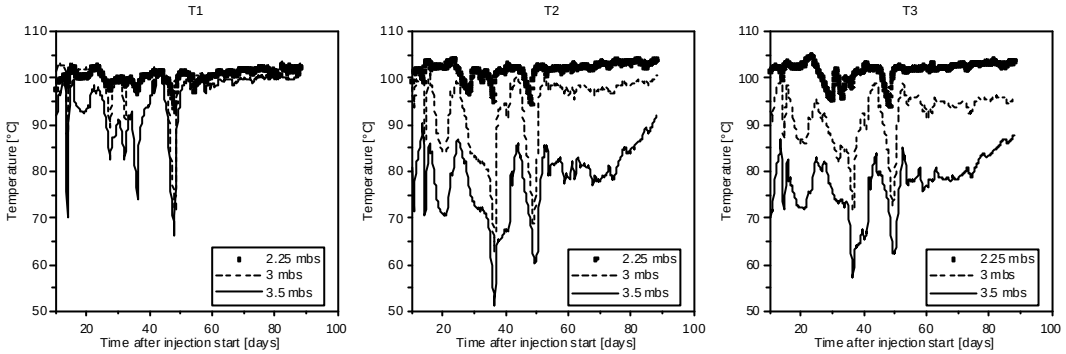

Fig. 2. Measured temperature at three continuously logged wells throughout the clean-up operation.

In Fig. 3 the temperature variation with depth after 60 days of steam injection is shown for all four temperature wells and again it is obvious that the steam zone had the largest extension with depth close to the injection well. Between injection wells (T4) the temperature was markedly lower than between the injection and extraction well even though the distance to the injection well was the same. Furthermore in T2 and T3 the temperature just above the clay layer seems affected by water flow since it was not as sharp as in T1, which more resembles the behavior expected when heat conduction dominates.

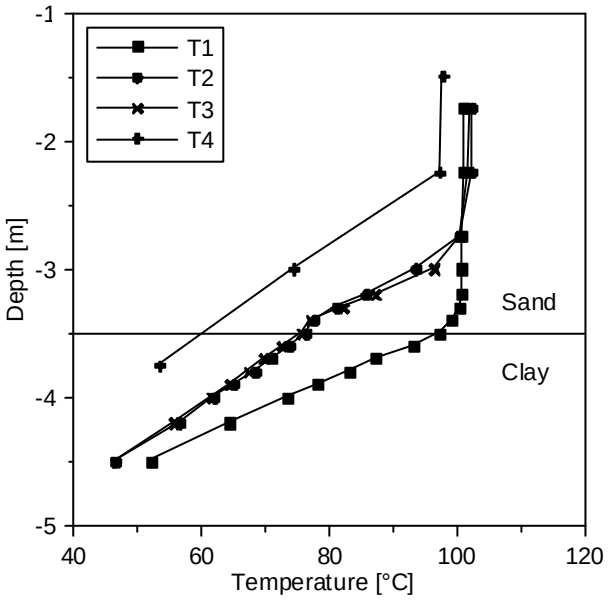

Fig. 3. Measured temperature with depth at four locations after 60 days of steam injection.

The steam injection rate varied during the clean-up operation as illustrated in Fig. 4a because of technical problems and because steam was distributed differently among the wells. The maximum injection rate for this well was 145 kg hour^{-1} and the maximum pressure was 150 kPa.

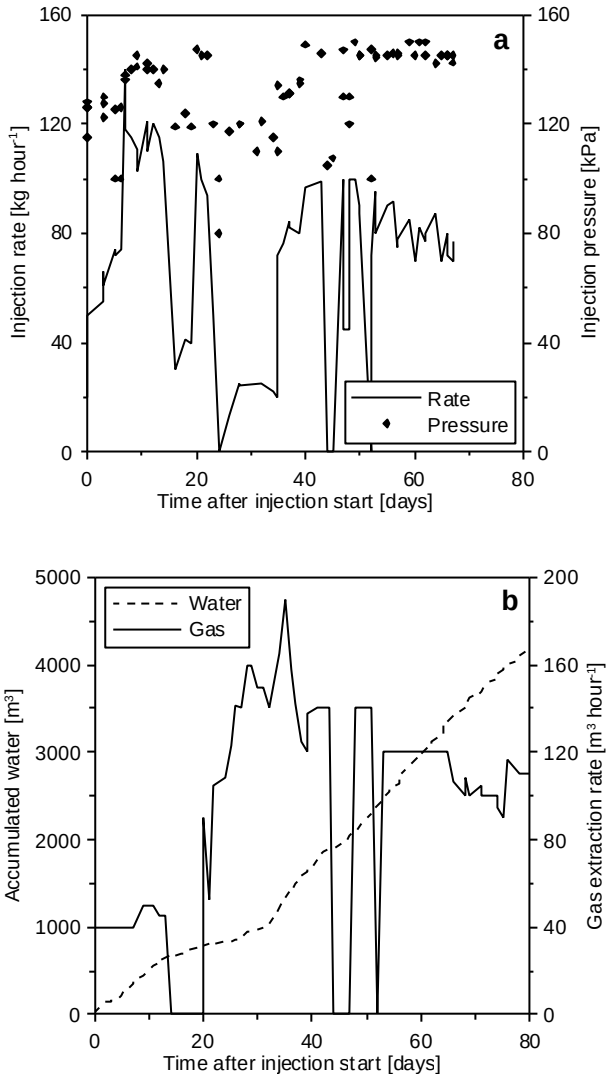

Fig. 4. (a) Steam injection rate/pressure for the injection well closest to the temperature wells, and (b) accumulated extracted water together with the gas extraction rate during clean-up operation.

Fig. 4b shows the accumulated extracted water and it is noted that the rate (2 m^3 $hour^{-1}$) is practically constant throughout the operation. The fluctuations in gas extraction rate were due to technical problems and the mean rate was approximately 100 m^3 $hour^{-1}$ at a temperature of 68 °C. The rate was measured after the condenser and corresponds to the atmospheric air extracted.

The temperature measurements and the continuous flow of ground water to the extraction wells suggest that the steam zone was not able to displace the water and prevent inflow. Consequently, it was necessary to maintain steam injection for a long period to ensure that all the cold spots had been sufficiently heated primarily by heat conduction. During the clean-up the pore volume of ground water in the contaminated zone was changed approximately 25 times, which removed a lot of energy and prolonged the clean-up time.

To further examine the behavior of the steam zone and the ground water flow a 3-D numerical model was applied. The numerical modeling analysis served the purpose of obtaining an understanding of the general processes occurring at the site rather than attempting to simulate the specific field conditions.

3. Numerical model

The simulations were performed using the numerical code T2VOC (Falta et al., 1995), which is a member of the TOUGH family of codes developed to simulate multidimensional, non-isothermal, multiphase flow and transport in porous media (Pruess, 1987; Pruess, 1991). The code considers simultaneous flow of up to three phases (water, gas and NAPL) according to a multiphase extension of Darcy's law. Hydrodynamic dispersion is neglected and only gas phase diffusion is included. Heat transfer occurs due to convection and conduction. Three components (water, air and contaminant) are partitioned among the phases according to the temperature dependent equilibrium equations except that water in the NAPL phase is neglected. To close the system of equations three mass balances (one for each component) and one energy balance are formulated. The set of equations are solved by integral finite difference techniques. The original code was slightly modified to account for the distinct entry pressure when using the Brooks and Corey formulation for the capillary pressure-saturation relationship. To avoid spurious pressure fluctuations the method proposed by Gudbjerg et al. (2003b) was applied. This method prevents unphysical flow of cold water into the steam zone, which would lead to pressure drops and dramatic reduction in timestep size. Without this method it was not practically possible to run the simulations.

3.1 Model setup

Due to computational constraints it was not possible to simulated the entire clean-up operation and account for all the wells. Instead a simplified configuration was designed (Fig. 5a) in which the model domain was reduced by symmetry considerations. The model domain was a cylinder section containing two wells (Fig. 5b), which contrarily to a planar 2-D model is able to capture the interaction between the steam zone and the ground water correctly.

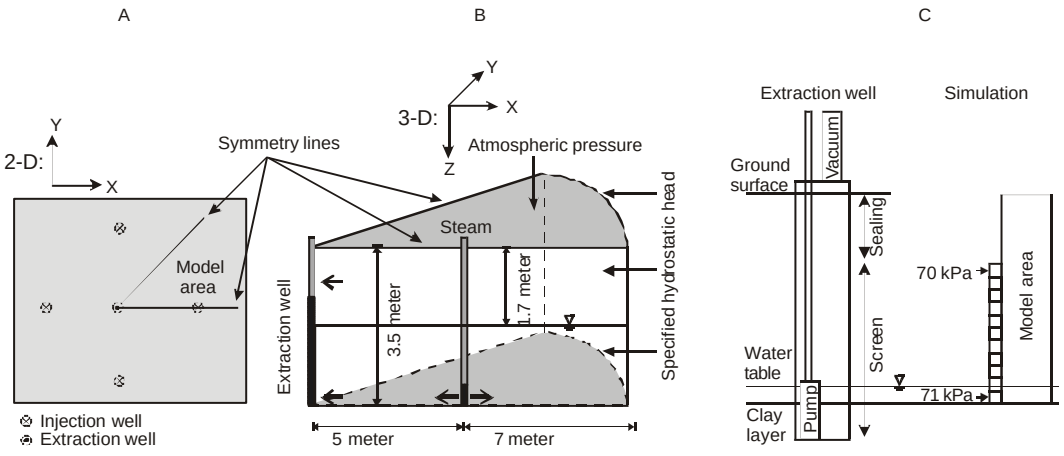

Fig. 5. Schematic of model setup.

Between the wells the gridblock dimensions were 0.2x0.2x0.2m and further away from the injection well the size increased to a maximum of 0.6x0.2x0.2m. In total, the domain was resolved by 17759 gridblocks. The outer circular edge was a constant head boundary in the gas and water phase derived from the initial hydrostatic conditions. To simulate the boundary to the atmosphere, the top layer of gridblocks were connected to a gridblock with constant pressure and temperature that allowed flow in the gas phase. The remaining boundaries were no-flow boundaries. The initial conditions were hydrostatic conditions with a water table 1.7 m.b.s. and a temperature of 10 °C. Saturated steam at 130 kPa was injected into three gridblocks (2.9 to 3.5 m.b.s) located 5.1 m from the extraction well. Thus, the injection well was not explicitly simulated but it corresponded to a well radius of approximately 10 cm. The extraction well was simulated with a column of high permeable gridblocks where extraction occurred at a total pressure of 70 kPa from the top and 71 kPa from the bottom, thus always maintaining a water table in the well mimicking the simultaneous extraction of gas and water (Fig. 5c).

As an initial reference case the porous medium was assumed to be homogeneous with a permeability of $4 \cdot 10^{-11}$ m^2 assessed from a pumping test and laboratory measurements on small, disturbed samples. A capillary pressure curve was measured on a disturbed sample from the sand layer using the syringe pump method (Wildenschild et al., 1997) and the capillary pressure/relative permeability-saturation relationship was described by the Brooks and Corey (1966) model. (See Table 1 for values). The computation time of the reference case was approximately 7 hours on a 2 GHz Pentium 4 PC.

Table 1. Soil properties.

Parameter	Value
Permeability	$4 \cdot 10^{-11}$ m^2
Porosity	0.41
Brooks and Corey pore distribution index, λ	2.6
Brooks and Corey entry pressure, P_e	24 cm
Residual water content, S_r	0.1
Heat capacity of soil grains	750 J kg^{-1} K^{-1}
Soil grain density	2650 kg m^{-3}
Heat conductivity coefficient, wet, Kh_{wet}	2.0 W m^{-1} K^{-1}
Heat conductivity coefficient, dry, Kh_{dry}	0.5 W m^{-1} K^{-1}

4. Results and discussion

After 72 hours of steam injection a quasi steady-state steam zone has developed. This is indicated in Fig. 6 that shows the temperature of the extracted fluids. The temperatures move towards constant values, indicating that further heating does not occur. The temperature response is seen earlier in the water phase than in the gas phase because steam is injected below the water table. Before steam breaks through to the unsaturated zone it cannot affect the temperature in the extracted gas phase.

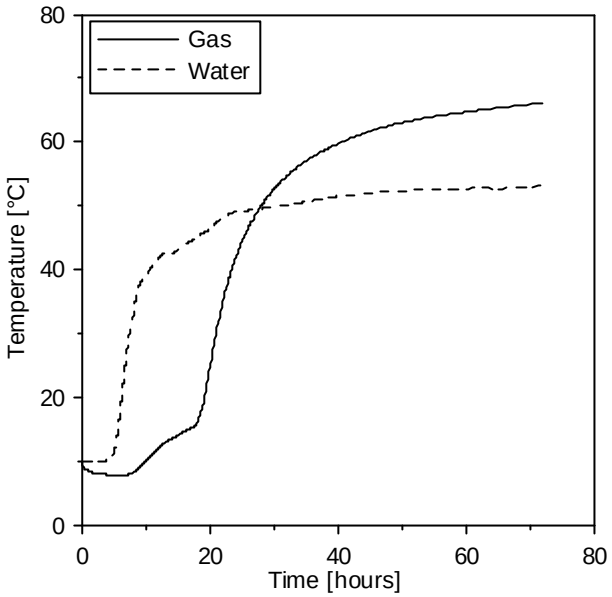

Fig. 6. Temperature in recovered fluids as a function of time.

Fig. 7 shows a 3-D plot of the quasi steady-state steam zone. Note that the plot is symmetric and have two injection wells, thus representing twice the simulated area. The steam zone rises above the saturated zone and has the largest horizontal extent in the unsaturated zone because of steam override. The individual steam zones from the two injection wells overlap in the unsaturated zone but not in the saturated zone. Due to the air flow induced by the soil vapor extraction there is a cold spot in the unsaturated zone around the extraction well. Around the injection wells, steam has broken through the soil surface to the atmosphere. From Table 2 it follows that only 76 % of the injected energy is extracted and the remaining is lost to the atmosphere. The steam zone has a complex shape compared to a steam zone created by injection in the unsaturated zone or under confined conditions. Consequently, a model that assumes a simple shape cannot be used to predict steam zone development under unconfined conditions. This emphasizes the need for fully 3-D models.

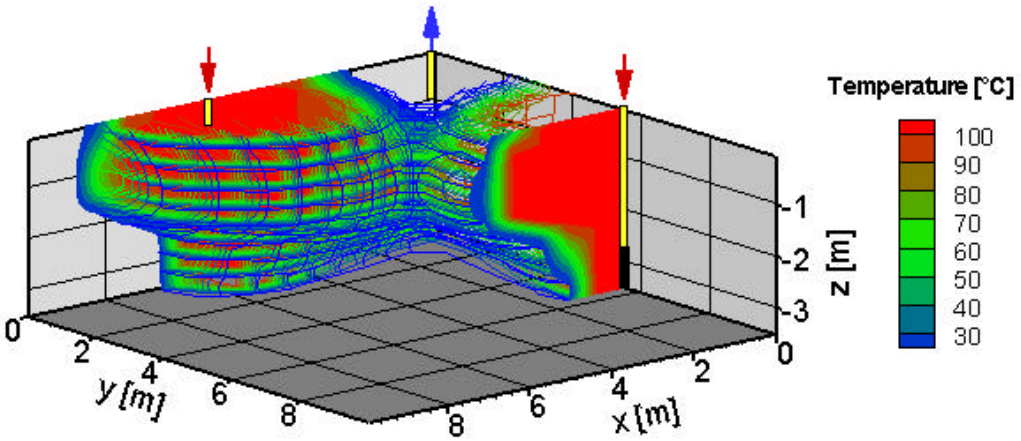

Fig. 7. 3-D plot of the simulated steady-state temperature viewed from the outer boundary towards the extraction well. The plot corresponds to twice the simulated volume and is symmetric around x = y. The temperature outside the contoured volume is below 20 °C. On the right the heated zone is cut through at the location of the injection well.

Table 2. Injection/extraction rates and temperatures at steady-state. Numbers in parentheses show the change in % from the reference case. Gray color indicates negative change. Numbers in brackets indicate energy extracted in percent of energy injected.

	Description	Injection rate, steam [kg hour^{-1}]	Extraction rate, water [m^3 hour^{-1}]	Extraction rate, gas [m^3 hour^{-1}]	Temperature water phase [°C]	Temperature gas phase [°C]
Reference case		263	10.1 [65]	699 [11]	53	66
Pumping test	No steam injection	0	6.9 (-32)	570 (-18)	10 (-81)	10 (-85)
Anisotropy (10)	Permeability reduced by 10 in vertical direction	199 (-24)	12.3 (22) [100]	280 (-60) [0]	51 (-4)	10 (-85)
High permeable bottom layer	Permeability increased by 2 from 2.5 to 3.5 m.b.s.	473 (80)	18.0 (78) [69]	814 (16) [9]	56 (6)	72 (9)
Low permeable top layer (100)	Permeability reduced by 100 down to 1.4 m.b.s.	276 (5)	11.8 (17) [74]	561 (-20) [20]	54 (2)	89 (35)
Lower permeability	Permeability reduced by 10	29 (-89)	1.1 (-89) [75]	77 (-89) [7]	59 (11)	54 (-18)
Confined conditions	Confining layer down to 2.8 m.b.s	140 (-47)	8.1 (-20) [97]	<1 (-100) [0]	52 (-2)	12 (-82)
Injection pressure 150 kPa	Injection pressure increased from 130 to 150 kPa	569 (116)	10.0 (-1) [43]	913 (31) [12]	71 (34)	82 (24)
Anisotropy (10) 150 kPa	Anisotropic with higher injection pressure	331 (26)	0.3 (-97) [3]	1167 (67) [37]	97 (83)	91 (38)
Confined 150 kPa	Confined with higher injection pressure	171 (-31)	0.1 (-99) [2]	541(-23) [33]	99 (87)	90 (36)
Lower extraction	Pressure increased to 90 kPa in extraction well	237 (-10)	7.5 (-25) [56]	175 (-75) [5]	54 (2)	78 (18)
Three injection wells	Three injection wells 5.1 m from extraction well	599 (128)	3.8 (-63) [17]	1129 (62) [15]	95 (79)	89 (35)
Two extraction wells	Extraction well added on symmetry line between injection wells	314 (20)	3.0 (-70) [28]	947 (36) [15]	86 (62)	70 (6)
Well on symmetry line			14.6 (45) [36]	1123 (61) [13]	30 (-43)	63 (-5)

Since the lower boundary is a no-flux boundary the model does not account for the heat loss by conduction to the low permeable clay layer. This heat loss can be evaluated by considering 1-D heat conduction of an infinite slap where the upper boundary is a constant temperature. Incropera and DeWitt (1996) presents an analytical solution to this problem and it is found that the rate of heat loss after 72 hours through the heated bottom area corresponds to the condensation of 0.28 kg hour^{-1} of steam. Compared to the injection rate of 263 kg hour^{-1} (Table 2) this is

negligible and the error introduced by not considering the clay layer in the simulation is insignificant.

The steam zone does not reach the outer boundary and consequently the small size of the model domain will not have a direct influence on the steam development. However, the ground water table during steady-state extraction will be affected by the distance to the hydrostatic boundary. From pumping tests it is known that increasing the distance to the boundary will be equivalent to lowering the fixed head at the boundary at steady-state. Thus, increasing the size of the model domain would have the same effect on the results as lowering the water table at the boundary.

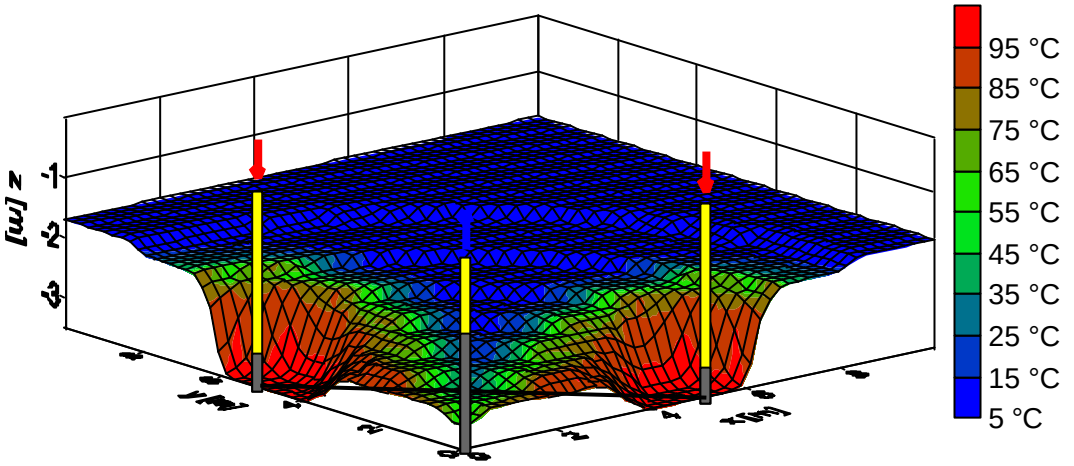

Fig. 8. Simulated boundary between saturated and unsaturated condition viewed from the extraction well towards the outer boundary. The plot corresponds to twice the simulated volume and is symmetric around x = y. The color scale indicates the temperature on the boundary.

Fig. 8 shows the boundary between saturated and unsaturated conditions. This is not the same as the piezometric water table since the pressure in the gas phase varies throughout the model area. Thus, the injection pressure would dominate the water table measured in a piezometer close to the injection well. The extraction well creates a cone of depression and close to the injection wells the saturated zone is further depressed due to the higher gas phase pressure in the steam zone. However, it is obvious that the injection of steam does not completely block the inflow of water to the contaminated area. This is also revealed by the continuous extraction of ground water. An interesting observation is that the ground water extraction rate is actually larger than during a steady-state pumping test with the same borehole pressure but without steam injection (Table 2). This intuitively appears strange since the steam zone blocks out part of the water flow. However, the high steam injection pressure increases the gradient towards the extraction well but more importantly the hydraulic conductivity increases with temperature because the viscosity of water decreases. A temperature increase from 10 °C to 50 °C increases the hydraulic conductivity by a factor 2.5. The effect has been verified by performing a simulation where the temperature effect on the viscosity was disabled and additionally pumping tests have been simulated at different temperatures. Thus, the extraction rate observed during a pumping test is not the maximum possible extraction rate during thermal remediation.

4.1 Comparison with field observations

To facilitate a comparison with the field observations in Fig. 3 the corresponding temperatures from the simulation are shown in Fig. 9. These figures show qualitatively the same pattern with lower temperatures away from the injection well indicating steam override. It is also noted how the temperature is lower between the injection wells (T4) than between the injection and the extraction well. This is more evident in the simulation where the distance between injection wells was larger. Because of this larger distance less heating is obtained, which is indicated by the lower extraction temperatures. As the extracted fluids integrate a large soil volume they are good indicators of the overall heating level.

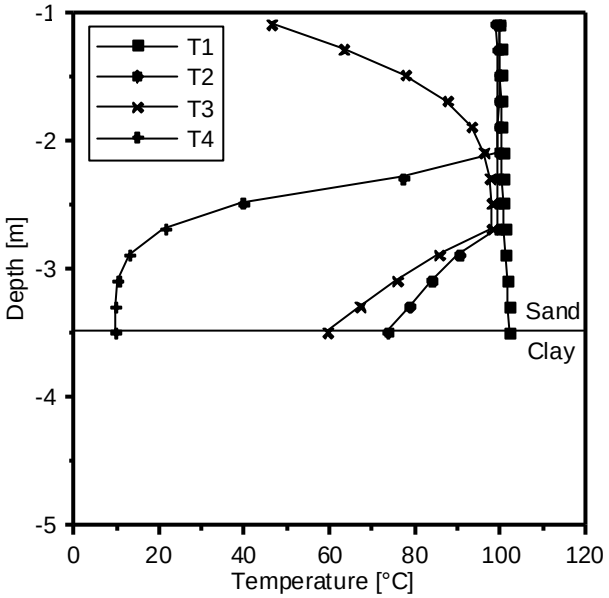

Fig. 9. Simulated temperature with depth at steady-state corresponding to the locations of the measurements in Fig. 3.

Steam did not penetrate the ground surface at the site, which may be explained by the lower permeability of the upper fill layer not accounted for in the simulation and the difference in injection rates. The large simulated ground water extraction rate indicates that the permeability may be too high; however, this will also be affected by the boundary conditions and the overall steam zone behavior.

The steam injection period at the site was much longer than the simulated time to reach steady-state. This was in part due to the forced shutdowns of the system, which prolonged the heating period. Furthermore, heating of the area outside the steam zone continues through conduction even though the steam zone appears to be at steady-state, which as shown by Gudbjerg et al. (2003a) can lead to further contaminant removal. This was indicated by the continuing extraction of contaminant at high rates after steam breakthrough. However, in this study we only address the steam zone behavior and consequently it is not necessary to simulate the entire clean-up period.

These differences between model and observations are not surprising since it was not the intention to directly simulate the field situation. However, it is evident

that the model captures the steam override mechanism observed at the site and it can therefore be used for a more detailed analysis of the steam zone behavior close to the water table at unconfined sites.

4.2 Individual impact of dominant parameters

Fig. 10 shows a symmetric contour plot of the temperature between the injection wells (the location is indicated by the black line in Fig. 8). This figure shows the cold areas at the bottom and at the top due to flow of water and air towards the extraction well. This type of figure will be used in the following to show the impact of the various dominant parameters and properties.

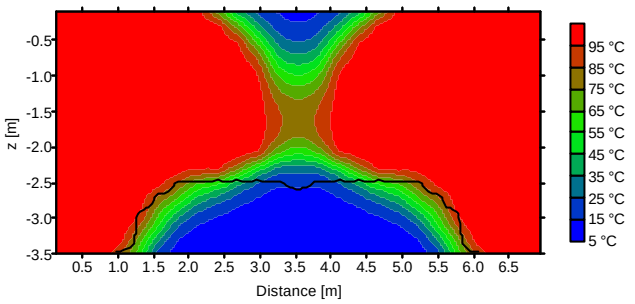

Fig. 10. Simulated temperature between injection wells at position indicated by the black line in Fig. 8. The black line in this figure indicates the boundary between saturated and unsaturated conditions.

The horizontal extent of the steam zone at the bottom is approximately 1 m. In this case the steam injection wells would therefore have to be placed 2 m apart to ensure overlapping steam zones at the bottom that prevented inflowing water. Since this distance will be one of the most important design parameters it is important to understand the mechanisms controlling it. At steady-state the location of the steam-water boundary below the water table is determined by a pressure balance. If the steam pressure were high enough to displace water, the steam zone would advance in the horizontal direction. The steam pressure is a function of the injection pressure, the shape of the steam zone and the condensation rate. The injection pressure is controllable whereas the shape of the steam zone and the condensation rate are complex functions of the geology, the boundary conditions and the extraction system. In the simulation 65 % of the injected steam condenses and gets extracted in the water phase at steady-state (Table 2). Thus, it seems that the cooling effect of the continuous ground water flow may have a significant influence on the steam pressure and thereby on the steam zone development. It is possible to increase the horizontal extent of the steam zone by increasing the injection pressure; however, that may prove problematic because it will increase the injection rate and furthermore the injection pressure can normally not be allowed to exceed the lithostatic pressure of the soil.

In the following a series of simulations are presented where at first the impact of the geology and then the impact of the injection/extraction scheme is investigated. In all cases the simulation is continued to steady-state as indicated by the extraction temperatures. The steam zones are illustrated by temperature contour plots between the injection wells similar to the plot in Fig. 10 except that only half of the plot is included. Furthermore, Table 2 lists the final values for injection rate (1 well),

extraction rate (1 well, entire area, volumetric rate at extraction temperature) and the temperature of the extracted fluids. Also shown is how much of the injected energy is extracted in the fluid phases. When the extracted energy is lower than the injected energy it is either because of energy loss to the atmosphere or because thermal steady-state has not yet been completely reached.

4.2.1 Anisotropy

In the field, horizontal layering is often observed, which introduces a large-scale anisotropy in permeability. When the scale of layering is smaller than the gridblock size it can be incorporated by reducing the vertical permeability within gridblocks. A simulation has been performed where the vertical permeability has been reduced by a factor 10. As seen in Fig. 11 this has a dramatic influence on the steam zone development. The steam zone does not reach the unsaturated zone and the horizontal extent below the water table is larger. This occurs because the decrease in vertical flow results in a lower pressure loss thereby making a larger horizontal development possible. Note that the low development in the vertical direction is not a result of a confining layer preventing steam flow. Steam flows in the vertical direction but not fast enough to overcome the removal of energy caused by the ground water flow above. Fig. 11 shows that there is a thin saturated zone just above the steam zone. In this case steady-state is reached when the energy removal rate with the ground water equals the steam injection rate. Thus, a dominant property will be the area of the steam-water boundary.

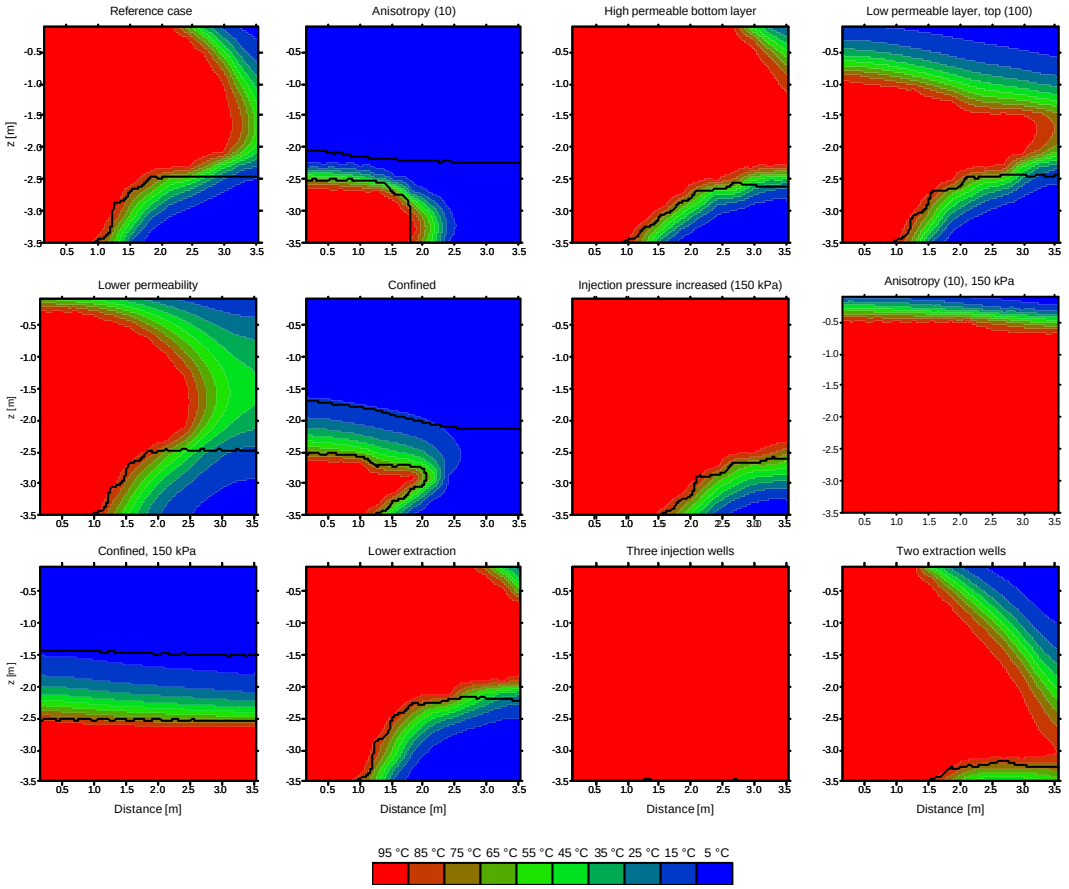

Fig. 11. Contour plots of temperature between injection wells. The black lines indicate the boundaries between saturated and unsaturated conditions.

4.2.2 High permeable bottom layer

From the borings at the site it was observed that the lower 1 m above the clay layer consisted of more coarse sand and the permeability could therefore be expected to be larger. To investigate how this will affect the steam zone development a simulation has been performed where the permeability in the lower 1 m of the model domain was increased by a factor 2. This results in larger injection and extraction rates and the steam zone is a little larger. The higher temperatures in the extracted fluids point to a more efficient heating. Thus, the larger flow of ground water and thereby cooling is countered by the increase in steam injection rate. This is only valid when steam is injected in the high permeable layer. If a more permeable layer had been present above the injection well this would have diminished the development of the steam zone.

4.2.3 Low permeable top layer

The upper fill layer at the site appeared to have a lower permeability and this could be expected to confine the steam zone in the vertical direction. A simulation has been performed where the permeability down to 1.4 m.b.s. has been decreased by a factor 100. This limits the steam zone propagation in the unsaturated zone and steam does not break through to the soil surface, which corresponds better with the field results. However, even though the steam zone is limited in the vertical direction more ground water displacement is not observed. Because of the low permeable layer the extraction well has a larger radius of influence and this balances the expected pressure increase due to the limitation in the vertical direction. The increase in water extraction rate also occurs because the vapor extraction well has a larger radius of influence. The higher temperature of the extracted gas is caused by a reduced amount of atmospheric air and is not an indication of an overall more efficient heating.

4.2.4 Lower permeability

To illustrate the effect of the total permeability it has been reduced by a factor 10. As Fig. 11 shows this has only a minor influence on the shape of the steam zone; however, the time to reach steady-state increases by a factor 10. This difference in time is also illustrated by the reduced injection and extraction rates. The small differences between the heated zones in the reference case and this case arise because heat conduction gets a larger significance since it is independent of permeability. Therefore a higher fraction of the energy is lost to the inflowing ground water resulting in a higher temperature in extracted water and less steam zone development in the unsaturated zone. This is also observed by the smoother temperature gradient on the steam front. Thus, as long as steam is injected at a fixed pressure the permeability does not influence the steady-state steam zone but only the time to reach steady-state. In cases where the removal depends on heat conduction from a steady-state steam zone it would actually be an advantage to have a low permeable media because this reduces the necessary steam injection rate. This is only true as long as the time to reach steady-state is not much larger than the necessary heat conduction time.

4.2.5 Confined conditions

This simulation illustrates the difference between confined and unconfined conditions. The permeability has been decreased three orders of magnitude from the soil surface to 2.8 m.b.s. The steam zone is now confined to the lower layer and heating of the confining layer takes place by conduction. The sloping steam front is

characteristic of steam injection under confined conditions showing steam override within the high permeable layer. The steam injection rate is reduced and practically no gas phase extraction occurs due to the low permeability of the unsaturated layers. Also the water extraction rate is reduced because only the lower layer contributes significantly. 97 % of the injected energy is extracted in the groundwater and the rest is lost by heat conduction to the low permeable layers. In contrast to the anisotropic case complete thermal equilibrium is not achieved but that does not affect the steam zone development. The horizontal extent of the steam zone immediately above the lower boundary is similar to the reference case and smaller than in the anisotropic case. As in the anisotropic case steady-state is reached when the extraction of energy in the water phase corresponds to the injection rate. In this case the area of the steam-water boundary becomes larger than in the anisotropic case because of the sloping steam front and therefore the volume of the steam zone is smaller at steady-state. This implies that it may not always be correct to include the effect of horizontal layering just by decreasing the vertical permeability as was done in the anisotropic example. Thus, incorporating an anisotropy ratio found by a large-scale pumping test may produce biased results because of steam override in between low permeable layers that will not be accounted for.

4.2.6 Higher injection pressure (150 kPa)

As previously stated a larger horizontal development of the steam zone can be achieved by increasing the injection pressure. However, the effect is strongly dependent on the geology as will be illustrated by increasing the injection pressure to 150 kPa for the reference, the anisotropic and the confined examples. Fig. 11 shows how this results in a larger steam zone in the reference case. The horizontal extent is now 1.5 m at the bottom and the cold saturated zone is diminished. Furthermore, the vapor extraction can no longer prevent the steam zone from penetrating all the way to the symmetry line in the unsaturated zone. The extraction temperatures increase, which also indicate that more of the contaminated area is heated. Even though more water is blocked out, the ground water extraction rate remains almost the same as with the lower injection pressure because of the higher ground water temperature and pressure drive. The benefits of the higher injection pressure, however, come at a high cost. The injection rate is more than doubled and a substantial amount of this energy is lost to the atmosphere. This can normally not be allowed in clean-up operations and therefore it may not be practically possible to achieve the high injection pressure.

In the anisotropic and the confined case the steam zones meet between the injection wells and water is blocked out. Very little water is extracted and the increase in vapor extraction rate occurs because steam flow directly into the well. The injection rates increase moderately. Only 35 – 40 % of the injected energy is recovered by the extraction system and the remaining part is lost through the outer boundary. When water is blocked out from the zone around the extraction well the pressure gradient in the water phase necessarily has to reverse. Thus, since condensation occurs at the steam front away from the extraction well the condensate will flow out through the outer boundary. There will be practically no condensation between the injection well and the extraction well since this area is already heated to steam temperature.

These simulations show the benefits of injecting steam in a layered geology where it is possible to achieve horizontal displacement without an unrealistic increase in the injection rate or steam breakthrough to the soil surface. Thus, in a layered geology the injection wells can be further apart provided that steam is injected in the most permeable layer.

It should again be emphasized that it might create fractures if the injection pressure exceeds the lithostatic pressure. Thus in many cases there will be an upper limit to the injection pressure determined by the depth to the injection well.

4.2.7 Lower extraction

The simulations show that the extraction well has a marked influence on the steam zone. A simulation has been performed where the pressure in the extraction well has been increased to 90 kPa. This allows the steam zone to develop more in the unsaturated zone; however, the steady-state water table is now higher and less water is displaced. It could have been expected that the decrease in water flow and thereby cooling would make the steam zone larger but this effect is countered by the higher water table. Additionally, the steam zone will propagate further in the direction away from the extraction well when the extraction is reduced.

4.2.8 Three injection wells

To illustrate the impact of a closer well spacing two injection wells have been added 5.1 m from the extraction well. This could also have been simulated by reducing the model area since new symmetry lines arise. Fig. 11 shows that the additional wells provide a much better horizontal sweep and the entire area between the injection wells is heated to steam temperature. The injection rate increases 128 %; however, the efficiency is much higher with this setup than with higher injection pressure in a single well where the rate increased 116%. This shows that it is possible to heat up the bottom layer in an unconfined aquifer if only the injection wells are spaced close enough.

4.2.9 Two extraction wells

A simulation has been performed where an additional extraction well has been placed on the symmetry line between the injection wells in the reference case. This significantly lowers the steady-state ground water table and makes it possible for the steam zone to fully develop in the area between the three wells. The steam injection rate is lower than in the case with three injection wells but the total ground water extraction rate increases. Whether or not this is more optimal will be an economic issue.

5. Conclusions and recommendations

Temperature measurements from a full-scale remediation by steam injection revealed that steam override occurred in the saturated zone. Consequently, there was a continuous flow of ground water into the contaminated area, which prolonged the clean-up. A 3-D numerical model was set up that qualitatively showed the same phenomenon with the steam zone predominantly developing in the unsaturated zone. The simulations have shown how steam override affects the horizontal extent of the steam zone under unconfined conditions. The horizontal extent will depend on the geologic layering, the ground water table at steady-state extraction, the steam injection pressure/rate and the extraction system. In a layered geology it will be easier to achieve a larger horizontal extent by increasing the injection pressure and the injection wells may therefore be spaced further apart. It is difficult to provide general predictions on steam zone development since so many coupled parameters are involved. Thus, it is not possible to suggest an optimal well spacing depending on

only a few easily measured parameters. It is therefore recommended to do a thorough characterization of the geology and the hydraulic properties at each particular site. This can be done by a combination of slug tests and pumping tests in the gas and water phases along with characterization of the geology. The obtained information could then be used to set up a site-specific numerical model that can be used to evaluate the steam zone development under different strategies. Furthermore, there may be various ways to heat the contaminated zone. Whether it is more optimal to install few injection wells and operate at high injection pressure or more wells at lower pressure will be an economical issue. It may also be more economical to install upstream pumping wells that could drain the contaminated area before steam injection. There are no general answers to these questions and they will have to be evaluated at every site.

Acknowledgements

This study was financed by the Danish Environmental Protection Agency, Programme for Development of Technology - Soil and Groundwater Contamination.The Danish Environmental protection Agency will, when opportunity offers, publish reports and contributions relating to environmental research and development project financed via the Danish EPA. Please note that publication does not signify that the contents of the reports necessarily reflect the views of the Danish EPA.

References

Adenekan, A. E., Patzek, T. W. and Pruess, K., 1993. Modeling of multiphase transport of multicomponent organic contaminants and heat in the subsurface: Numerical model formulation. Water Resource Research, 29: 3727-3740.

Adenekan, A. E. and Patzek, T. W., 1994. Cleanup of the gasoline spill area with steam: Compositional simulations. In Newmark et al. (1994).

Basel, M. D. and Udell, K. S., 1989. Two-dimensional study of steam injection into porous media. Multiphase transport in porous media. ASME-HTD-127. American Society of Mechanical Engineers, New York, N.Y, pp. 39-46.

Brooks, R. H. and Corey, A. T., 1966. Properties of porous media affecting fluid flow. J. Irrigation Drainage Division, ASCE 92 (IR2), 61-88.

Falta, R. W., Pruess, K., Finsterle, S. and Battistelli, A., 1995. T2VOC User's Guide. Lawrence Berkeley Laboratory Report, LBL-36400 University of California, Berkeley.

Forsyth, P. A., 1994. Three-dimensional modelling of steam flush for DNAPL site remediation. International Journal for Numerical Methods in Fluids, 19:1055-1081.

Gudbjerg, J., Sonnenborg, T. O. and Jensen, K. H., 2003a. Remediation of NAPL below the water table by steam induced heat conduction. Submitted to Journal of Contaminant Hydrology.

Gudbjerg, J., Trötschler, O., Färber, A., Sonnenborg, T. O. and Jensen, K. H., 2003b. On spurious water flow during numerical simulation of steam injection into water saturated soil. Submitted to Journal of Contaminant Hydrology.

Hunt, J. R., Sitar, N. and Udell, K. S., 1988. Nonaqueous phase liquid transport and cleanup, 2. Experimental studies. Water Resources Research, 24: 1259-1269.

Incropera, F. P. and DeWitt, D. P., 1996. Introduction to heat transfer. 3rd ed. John Wiley and Sons, New York.

Itamura, M. T., 1996. Removal of chlorinated hydrocarbons from homogeneous and heterogeneous porous media using steam. UMI Dissertation Services, Ann Arbor MI.

Kuhlman, M. I., 2002. Analysis of the steam injection at the Visalia Superfund Project with fully compositional nonisothermal finite difference simulation. Journal of Hazardous Materials, 92: 1-19.

Lake, L. W., 1989. Enhanced oil recovery. Prentice Hall, Englewood Cliffs, NJ.

Lee, K. H., 1994. Predictive modeling using the STARS code. In Newmark et al. (1994).

Lundegaard, P. D., and Andersen, G., 1996. Multiphase numerical simulation of air sparging performance. Ground Water, 34: 451-460.

Newmark R. and various authors, 1994. Dynamic underground stripping project. Lawrence Livermore National Laboratory, UCRL-ID-116964-V-1-4.

Newmark, R. L., Aines, R. D., Knauss, K. G., Leif, R. N., Chiarappa, M., Hudson, B., Carraigan, C., Tompson, A., Richards, J., Eaker, C., Wiedner, R. and Sciarotta, T., 1998. In situ destruction of contaminants via hydrous pyrolysis/oxidation: Visalia field test. Lawrence Livermore National Laboratory, UCRL-ID-132671.

Ochs, S. O., Hodges, R. A., Falta, R. W., Kmetz, T. F., Kupar, J. J., Brown, N. N. and Parkinson, D. L., 2003. Predicted heating patterns during steam flooding of coastal plain sediments at the Savannah River site. Environmental & Engineering Geoscience, 9: 51-69.

Pruess, K., 1987. TOUGH User's Guide. Lawrence Berkeley Laboratory Report, LBL-20700 University of California, Berkeley.

Pruess, K., 1991. TOUGH2 - A general purpose numerical simulator for multiphase fluid and heat flow. Lawrence Berkeley Laboratory Report, LBL-29400 University of California, Berkeley.

Rubin, B. and Buchanan, W. L., 1985. A general purpose thermal model. Society of Petroleum Engineers Journal, 25: 202-214.

She, H. Y. and Sleep, B. E., 1999. Removal of perchloroethylene from a layered soil system by steam flushing. Ground Water Monitoring and Remediation, 19: 70-77.

van Lookeren, J. 1983. Calculation methods for linear and radial steam flow in oil reservoirs. Society of Petroleum Engineers Journal, pp. 427-439.

Wildenschild, D., Høgh Jensen, K., Hollenbeck, K.J., Illangasekare, T.H., Znidarcic, D., Sonnenborg, T. and Butts, M.B., 1997. Two-stage procedure for determining unsaturated hydraulic characteristics using a syringe pump and outflow observations. Soil Science Society of America Journal, 61: 347-359.